Intramolecularly enhanced receptors with unusual binding and molecularly imprinted nanoparticles as nanoreactors and sensors

by

Xiaoyu Xing

A dissertation submitted to the graduate faculty

in partial fulfillment of the requirements for the degree of

DOCTOR OF PHILOSOPHY

Major: Organic Chemistry

Program of Study Committee:
Yan Zhao, Major Professor
Levi Stanley
Brett VanVeller
Arthur Winter
Keith Woo

The student author, whose presentation of the scholarship herein was approved by the program of study committee, is solely responsible for the content of this dissertation. The Graduate College will ensure this dissertation is globally accessible and will not permit alterations after a degree is conferred.

Iowa State University

Ames, Iowa

2018

DEDICATION

To my love and friend, Jiayue Li.

For our past, holding together and fighting together,

and in the unknown and attractive future.

TABLE OF CONTENTS

ACKNOWLEDGMENTS

First, I would like to give my sincere gratitude to Dr. Yan Zhao, my major professor, my research advisor, the committee chair, for his guidance and support throughout the course of the research in the past five years. Without him, this dissertation would not be possible.

I would also like to thank my program of study committee members, Dr. Levi Stanley, Dr. Brett VanVeller, Dr. Arthur Winter, and Dr. Keith Woo for their suggestions and support in my study. Special thanks to Dr. Robert Angelici, who shared with us his wisdom and experience in chemistry and life. Also, I really appreciate the support from the department of chemistry, Iowa State University. And many thanks to the members of the chemical instrumentation facility including Dr. Shu Xu, Dr. Sarah Cady, Dr. Kamel Harrata, and Mr. Steve Veysey for their technical assistance to my research.

I am really happy and grateful to work with other group members in Yan Zhao's group for collaborations, discussion, support, and having fun together. Among them, I want to give my special thanks to Shixin Fa and Roshan for mentoring me in experimental skills and life experience, as well as Lan Hu and Arif.

There is no need to say how important the support from my family is. Without the mental and financial support from my parents, I am not capable of finishing this.

In addition, I would also like to thank my friends, especially Jianwu Gong, with whom I had a lot of fun and dealt with a lot of difficulties together.

ABSTRACT

The conformational flexibility of a receptor is usually considered unfavorable to binding, due to the entropy loss upon binding. Inspired by the biological receptor with intra-receptor secondary binding sites which can strengthen guest binding, two series of artificial receptors with similar structures were constructed: pseudo crown ethers with aromatic donor/acceptor groups and aromatic tweezer molecules with carboxylic acids. When the guest binding was weakened by the solvents, i.e., pseudo crown ethers bound with cations in polar solvents and aromatic tweezers bound with counterparts in non-polar solvents, intra-receptor interactions became stronger and contributed to the guest binding. The overall binding showed a reversed solvent effect and unusually strong affinity.

Molecular imprinting with cross-linked micelles and functional templates created binding sites after removal of templates. The binding site complementary to the template can be used to study the chemical reactions in the confined nanospace, which can be different from those in homogeneous solution. Imine formation between amines and the aldehyde inside the binding site was studied. It was found the binding influenced reaction reactivity more than the electronic property of the amine. Besides the study of reaction reactivity, the binding site can be further functionalized with a fluorescent group to achieve sensitive and selective sensing.

CHAPTER 1.
GENERAL INTRODUCTION

Literature Review

Non-covalent interactions are the key to many important biological structures, such as DNA double helix structure,[1] and interactions, such as the enzyme-substrate complexation and further catalysis.[2-4] These interactions usually are surprisingly strong and selective. Biotin-streptavidin complex, which is one of the well-known cases of molecular recognition, has a surprising binding constant of $10^{13.4}$ M^{-1}.[5, 6] Chemists have put lots of efforts trying to synthesize artificial receptors with comparable binding property.[7] If such receptors can be made, they would lead to powerful sensors, catalysts, drug delivery systems, and binding-based separation systems.[7]

Chemists have achieved lots of artificial receptors with high affinity and selectivity by preorganization.[8-11] In the study of biotin-streptavidin binding, it was found that when the complex was formed, the melting point was raised by 37 °C and a large number of amide protons in backbone became resistant to H/D exchange.[6, 12-14] These findings indicates the stability of the protein upon binding is strengthened by other intramolecular interactions. Similarly, several artificial receptors with intramolecular interactions which can be triggered upon binding were reported.[15-18] Currently, there are still not enough examples to show how to design such biomimetic artificial receptors. In chapter 2 and 3 of this dissertation, two more artificial receptors with unusual binding affinities and solvent effects are presented. Chapter 2 is the research on aromatically functionalized pseudo crown ethers; chapter 3 is on hydrogen bonds enhanced molecular tweezers.

Molecularly imprinted polymers (MIPs) are highly cross-linked materials (including functional monomers and cross-linkers) with complementary binding sites to specific

templates.[19, 20] The complementarity is not limited to the shape and size but also regarding non-covalent interactions provided by functional monomers as well as cross-linkers.[21] Molecular imprinting is an easy and efficient way to create binding sites with strong affinity and high selectivity.[22] However, the heterogeneous distribution of binding sites could lower the binding efficiency, and it is difficult to functionalize the binding site after removal of the template, due to the poor solubility and relatively large size of the MIPs.[23-25]

Recently our group has prepared water-soluble molecularly imprinted nanoparticles (MINPs) with a relatively small diameter (~5 nm).[23] MINPs showed extraordinary properties, such as strong binding affinity and selectivity, sensing, and catalysis.[23, 26-34] Functionalization of the binding site after removal of the template would provide possibilities of achieving more applications. Previously, our group reported that binding sites could be functionalized by amide coupling between amine substrates and MINPs with carboxylic acid created inside binding site by using photo-cleavable templates.[26] The difficulty in this method is the cumbersome synthetic route to the template. However, imine is a readily formed, reversible covalent bond but with some stability, which makes it suitable as the building blocks of the template.[35, 36] Some imines, especially the ones between aldehydes with aromatic amines, could be stable during the preparation of MINPs and easily to be hydrolyzed under acidic condition. In chapter 4 of this dissertation, a method to create an aldehyde handle in the binding site after the template removal is presented, in which the aldehyde could be further reacted with aromatic amines. Therefore, the reaction reactivity of imine formation in the confined binding space was studied. A further application is presented in chapter 5, in which MINPs were linked with a fluorophore to the aldehyde handle in the binding site by reductive amination and achieved a direct "turn-on" fluorescence sensor.

References

1. E. Persch, O. Dumele and F. Diederich, *Angew. Chem. Int. Ed.*, 2015, **54**, 3290-3327.

2. J. A. McEvoy, *Molecular Recognition : Biotechnology, Chemical Engineering and Materials Applications*, Nova, Hauppauge, NY, USA, 2011.

3. E. A. Meyer, R. K. Castellano and F. Diederich, *Angew. Chem. Int. Ed.*, 2003, **42**, 1210-1250.

4. J. Cerny and P. Hobza, *Phys. Chem. Chem. Phys.*, 2007, **9**, 5291-5303.

5. P. C. Weber, D. Ohlendorf, J. Wendoloski and F. Salemme, *Science*, 1989, **243**, 85-88.

6. D. H. Williams, E. Stephens, D. P. O'Brien and M. Zhou, *Angew Chem Int Ed Engl*, 2004, **43**, 6596-6616.

7. Y. Zhao, *ChemPhysChem*, 2013, **14**, 3878-3885.

8. H.-J. Schneider, *Angew. Chem., Int. Ed.*, 2009, **48**, 3924-3977.

9. J. Rao, J. Lahiri, R. M. Weis and G. M. Whitesides, *J. Am. Chem. Soc.*, 2000, **122**, 2698-2710.

10. L. Cao, M. Sekutor, P. Y. Zavalij, K. Mlinaric-Majerski, R. Glaser and L. Isaacs, *Angew. Chem., Int. Ed.*, 2014, **53**, 988-993.

11. H. J. Hogben, J. K. Sprafke, M. Hoffmann, M. Pawlicki and H. L. Anderson, *J. Am. Chem. Soc.*, 2011, **133**, 20962-20969.

12. M. Gonzalez, L. A. Bagatolli, I. Echabe, J. L. R. Arrondo, C. E. Argarana, C. R. Cantor and G. D. Fidelio, *J. Biol. Chem.*, 1997, **272**, 11288-11294.

13. S. Meskers, J.-M. Ruysschaert and E. Goormaghtigh, *J. Am. Chem. Soc.*, 1999, **121**, 5115-5122.

14.   D. H. Williams, E. Stephens and M. Zhou, *J. Mol. Biol.*, 2003, **329**, 389-399.

15.   R. W. Gunasekara and Y. Zhao, *J. Am. Chem. Soc.*, 2015, **137**, 843-849.

16.   Z. Rodriguez-Docampo, S. I. Pascu, S. Kubik and S. Otto, *J. Am. Chem. Soc.*, 2006, **128**, 11206-11210.

17.   Z. Zhong, X. Li and Y. Zhao, *J. Am. Chem. Soc.*, 2011, **133**, 8862-8865.

18.   R. Carrillo, A. Feher-Voelger and T. Martin, *Angew. Chem., Int. Ed.*, 2011, **50**, 10616-10620, S10616/10611-S10616/10624.

19.   G. Wulff, *Angew. Chem. Int. Ed.*, 1995, **34**, 1812-1832.

20.   G. Wulff, T. Gross and R. Schönfeld, *Angew. Chem. Int. Ed. Engl.*, 1997, **36**, 1962-1964.

21.   K. Haupt and K. Mosbach, *Chem. Rev. (Washington, DC, U. S.)*, 2000, **100**, 2495-2504.

22.   C. Alexander, H. S. Andersson, L. I. Andersson, R. J. Ansell, N. Kirsch, I. A. Nicholls, J. O'Mahony and M. J. Whitcombe, *J. Mol. Recognit.*, 2006, **19**, 106-180.

23.   J. K. Awino and Y. Zhao, *J. Am. Chem. Soc.*, 2013, **135**, 12552-12555.

24.   W. Wan, M. Biyikal, R. Wagner, B. Sellergren and K. Rurack, *Angew. Chem. Int. Ed.*, 2013, **52**, 7023-7027.

25.   N. Murase, S.-i. Taniguchi, E. Takano, Y. Kitayama and T. Takeuchi, *Journal of Materials Chemistry B*, 2016, **4**, 1770-1777.

26.   J. K. Awino and Y. Zhao, *Chem. Eur. J.*, 2015, **21**, 655-661.

27.   J. K. Awino and Y. Zhao, *ACS Biomaterials Science & Engineering*, 2015, **1**, 425-430.

28.   J. K. Awino, L. Hu and Y. Zhao, *Org. Lett.*, 2016, **18**, 1650-1653.

29. J. K. Awino and Y. Zhao, *Org. Biomol. Chem.*, 2017, **15**, 4851-4858.

30. R. W. Gunasekara and Y. Zhao, *J. Am. Chem. Soc.*, 2017, **139**, 829-835.

31. J. K. Awino, R. W. Gunasekara and Y. Zhao, *J. Am. Chem. Soc.*, 2016, **138**, 9759-9762.

32. S. Fa and Y. Zhao, *Chem. Mater.*, 2017, **29**, 9284-9291.

33. S. Fa and Y. Zhao, *Chem. Eur. J.*, 2018, **24**, 150-158.

34. L. Hu and Y. Zhao, *Helv. Chim. Acta*, 2017, **100**, e1700147-n/a.

35. C. D. Meyer, C. S. Joiner and J. F. Stoddart, *Chem. Soc. Rev.*, 2007, **36**, 1705-1723.

36. A. Herrmann, *Org. Biomol. Chem.*, 2009, **7**, 3195-3204.

CHAPTER 2.
AROMATICALLY FUNCTIONALIZED PSEUDO CROWN ETHERS WITH UNUSUAL SOLVENT RESPONSE AND ENHANCED BINDING PROPERTIES

Xiaoyu Xing and Yan Zhao

Abstract

Conformational flexibility in the host's structure is often considered detrimental to its binding. Flexible pseudo crown ethers with aromatic donor/acceptor groups at the chain ends, however, displayed enhanced binding affinity and selectivity, particularly when the direct binding interactions were compromised by unfavorable solvents.

Introduction

Biopolymers such as proteins have rich conformational dynamics essential to their functions. Foldamers are synthetic mimics of these biopolymers with controlled conformational changes.[1-5] Foldamer-based supramolecular hosts differ from conventionally preorganized hosts because guest-induced conformational change is often an inherent property of the host,[6-9] sometimes leading to unusual molecular motions during binding.[10] Extreme sensitivity to the environment can be easily obtained from the conformational mobility.[11-14] Meanwhile, due to their highly programmable structures, foldamers can be designed to bind complex organic molecules with high structural precision.[15-18]

Guest-induced conformational change traditionally is considered detrimental to the binding affinity because the energetic cost associated with the change is assumed to be paid out of the binding energy.[19] Intuition also suggests that flexible hosts, being so accommodating, would be less selective in its binding. Although this has been the dominant view in

supramolecular chemistry, it is puzzling that conformationally mobile biofoldamers can obtain extremely high binding affinity and selectivity far better than rigid synthetic hosts.[20]

In recent years, an alternative strategy to achieve strong and selective binding has been proposed[21-23] and experimentally verified.[24-30] Representative examples include the anion-binding peptidic bismacrocycle by Kubik and Otto,[24] the crown ether-like receptor by Carrillo and co-workers,[25-27] and our glutamic acid-functionalized oligocholate foldamer.[28] Rational designs are also possible.[29, 30] In these hosts, disengaged noncovalent interactions within the host are "turned on" by the guest. Because these guest-triggered intrahost interactions (together with the solvation/desolvation changes) also contribute to the binding equilibrium, binding becomes stronger than what can be obtained from the direct binding interactions alone. As a result, binding in these receptors is delocalized over the entire host structure instead of being confined at the host–guest interface.[21]

Results and Discussion

Herein, we report two oligoether hosts with aromatic donor/acceptor (D/A) groups at the chain ends. The aromatic groups not only could preorganize the chain into a pseudo crown ether but also interacted more strongly in the presence of the guest. The result was usually strong binding for the guest, particularly in unfavorable solvents. Despite its conformational flexibility, such receptors could possess good binding selectivity.
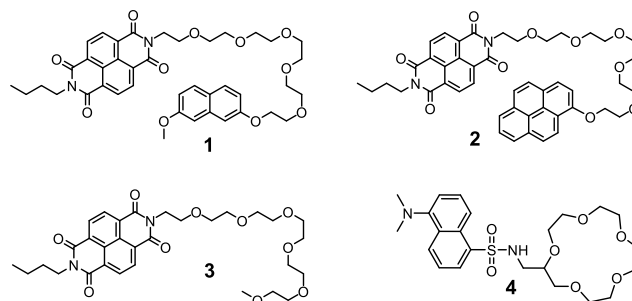
Scheme 1. Key compounds.

Our study involved four receptors (**1**–**4**). Receptors **1** and **2** are podands[31-35] with an electron-rich naphthyl and pyrenyl group, respectively, that can interact with the electron-deficient naphthalene diimide (NDI) on the other end of the chain. We chose aromatic rings as the intrahost-interacting groups because they can be tuned easily in strength and can be monitored spectroscopically.[36-39] The *direct* binding groups are oligo(ethylene oxide), akin to an open-chain crown ether that can bind a sodium ion through electrostatic interactions (vide infra for the binding of other alkali metal ions).[40, 41] Receptor **3** replaces the electron donor of **1** and **2** with a methyl group and thus is devoid of the aromatic interactions needed for the proposed intramolecular enhancement. Crown ether derivative **4** is a covalent control, preorganized in the conventional manner to bind sodium. Its dansyl group on the side chain makes it easy for us to study the binding by spectroscopy.
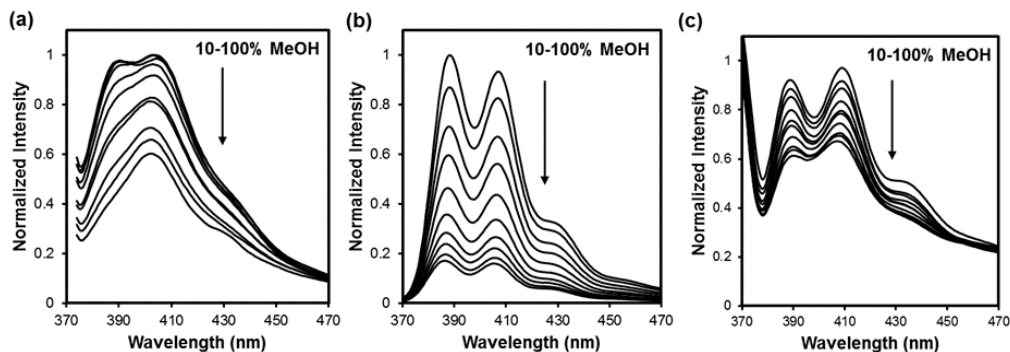
Figure 1. Normalized fluorescence emission spectra of compounds **1** (a), **2** (b), and **3** (c) in mixtures of methanol and DCM. [**1**] = 2.0 μM. [**2**] = 20 μM. [**3**] = 30 μM. λ_{ex} = 358 nm for compounds **1** and **3**. λ_{ex} = 278 nm for compound **2**.

Syntheses of **1**–**3** are reported for the first time and the details are given in the experimental section. Compound **4** was synthesized according to a literature procedure.[42]

Figure 1 shows the emission spectra of **1**–**3** in mixtures of methanol and dichloromethane (DCM).[43] Compounds **1** and **3** were excited at λ_{ex} = 358 nm, where naphthyl had no absorption. Although quenching was observed in both compounds, the emission peaks changed in shape in **1** but mostly decreased in intensity in **3**, presumably due to the NDI–naphthyl interactions in the former. When the emission intensity of NDI at ~390 nm was plotted against solvent polarity (Figure 2a), compound **1** afforded a sigmoidal curve (◆) but compound **3** a straight line (●). It is likely that the linear decrease in emission intensity in **3** was from a generic solvent effect on the NDI, as no other fluorophore was present in this compound. The sigmoidal transition in **1**, on the other hand, is a hallmark of cooperative conformational changes.[44]
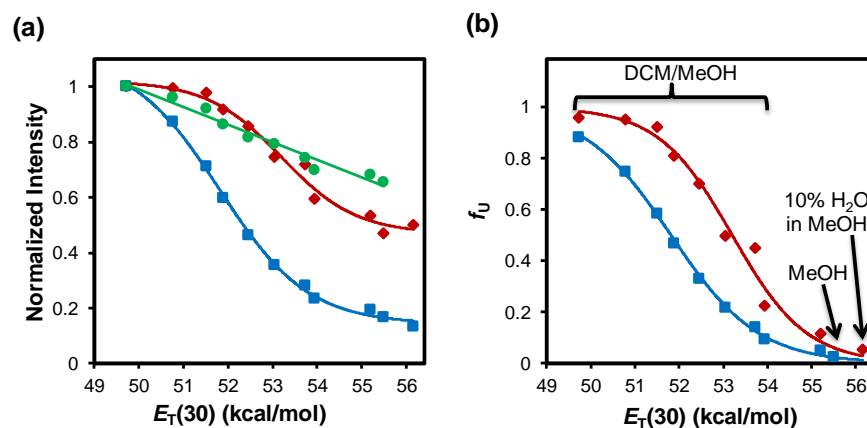
(a)

(b)

Figure 2. (a) Normalized fluorescence emission intensity at 390 nm as a function of solvent polarity for compounds **1** (◆), **2** (■), and **3** (●). The emission intensity of compound 3 fit well to a linear relationship with R = 0.995. (b) Unfolded fraction as a function of solvent polarity for compound 1 (◆) and 2 (■). Details of fitting are found in experimental section.

As shown in Figure 2, the fluorescence data for compound **1** (◆) fit well to the two-state transition model (unfolded ⇆ folded), which assumes the compound only exists in the folded or unfolded form and the free energy for the conformational change is linearly related to solvent polarity.[44] Two-state conformational changes are frequently observed in foldamers stabilized by solvophobic interactions.[12, 45-47] In our case, higher methanol in the solvent—i.e., larger $E_T(30)$—should strengthen the aromatic interactions between NDI and naphthyl[48-50] and thus help the compound fold. Intermolecular aggregation was ruled out by a dilution study (Figure 4 in experimental section).

Pyrene emits much more strongly than NDI and the emission spectrum of **2** is dominated by the pyrene emission (Figure 1b). Upon addition of methanol, significant quenching occurred and the quenching profile was a partial sigmoidal curve (Figure 2a, ■). The curve also fit well to the two-state model, which shows a higher population of folded conformer in **2** than in **1** at any given solvent composition (Figure 2b). Aromatic donors and acceptors tend to stack face-to-face and solvophobic interactions are known to be the major

contributor to the binding interactions, especially in polar solvents such as methanol.[48-50] Since the larger-sized pyrenyl group in **2** is expected to provide a stronger solvophobic driving force to the folding, better folding in **2** is expected.

The binding properties of compounds **1**–**3** were determined by UV titrations using sodium thiocyanate as the guest. The UV absorptions of these compounds displayed very little change during the solvent titration (in DCM/methanol mixtures) and thus better reflects the effect of binding than the changes in emission.[51] As shown by the titration curves (Figures Figure **5** and Figure **6**), the UV absorbance (at 358 nm for **1** and 382 nm for **2**) fit well to a 1:1 binding isotherm, from which the binding constant could be determined.

Figure 3a shows the relationship between log K_a of compounds **1**, **2**, and **4** and the solvent composition. The binding for sodium by **3** was hardly measurable in methanol/DCM mixtures and thus was not included.

The preorganized receptor (**4**, ▲) displayed a monotonous decrease in log K_a with increasing solvent polarity (larger $E_T(30)$)—this is the conventional solvent effect for the binding. Because methanol solvates both the binding functionalities (oxygen atoms on the ether chain) and the sodium guest, higher methanol in the solvent increases the desolvation cost of the binding. In addition, the higher dielectric constant of methanol over DCM screens the electrostatic interactions between the host and the guest and also weakens the binding.
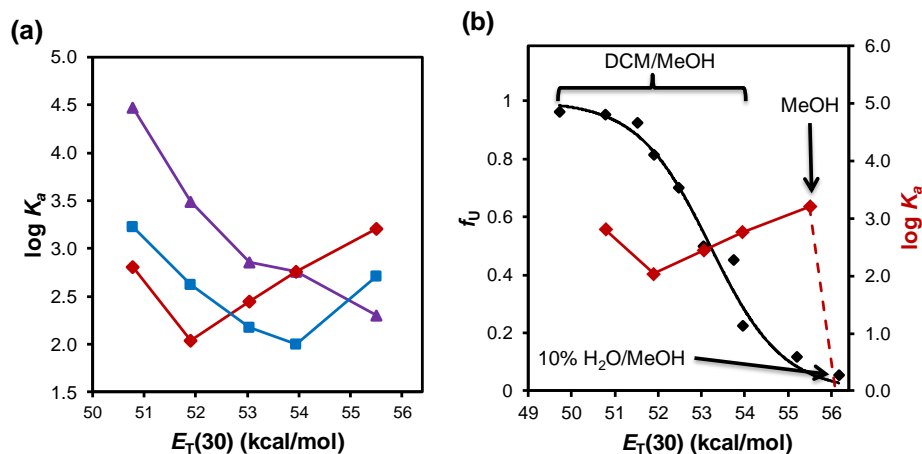
Figure 3. (a) Binding constant of compounds **1** (◆), **2** (■), and **4** (▲) for sodium determined by UV-vis titrations against solvent polarity in methanol/DCM mixtures. The binding constants were averages from triplicate titrations at 90% confidence level. Titrations curves are reported in the experimental section (Figures Figure **5**–Figure **8**) and binding constants in Table 1. Binding constants of hosts 1–4 in different solvents**.** All binding constants were averages of three titrations with 90% confidence.. (b) Unfolded fraction of **1** as a function of solvent polarity (black line) and log K_a of **1** for NaSCN (red line). The solid smooth curve was from nonlinear least-squares fitting of the intensity to the two-state transition model.

Both the naphthyl–NDI (**1**, ◆) and pyrenyl–NDI receptor (**2**, ■) behaved differently, showing a decrease in binding followed by an increase with increasing $E_T(30)$ (Figure 3a). In low-polarity solvents, log K_a followed the order of **4** > **2** > **1**. This trend supports the importance of preorganization in this solvent region. Receptor **4** has the best preorganization among the three, being covalently formed. The D–A aromatic interactions in **1** and **2** serve to preorganize the compound into a pseudo crown ether and the stronger D–A interactions in **2** makes it better preorganized for binding sodium.

The inflection points in the log K_a curves suggest that a different binding mechanism began to dominate in more polar solvents for **1** and **2** (Figure 3a). Several pieces of evidence support that the guest-triggered D–A interactions dominated after the inflection points.

First, since the direct binding force between oligo(ethylene oxide) and Na$^+$ was weakened continuously by polar solvents (evident from the weaker binding of the control

receptor **4**), the increase in log K_a for **1** and **2** beyond the inflection points must have other sources. Better preorganization by methanol to strengthen the D–A interactions *cannot* explain the trend, as the order of binding reversed for **1** and **2** after the inflection points. As mentioned above, the stronger D–A interactions in the pyrenyl receptor (**2**) should better preorganize the compound for binding. Interactions between the imide carbonyls and sodium could not explain the reversal either. (Besides, even with the imide carbonyls, **3** always displayed weak binding.)

Second, the key feature of intramolecular enhancement is that guest-triggered intramolecular interactions become part of the overall binding energy. Such enhancement is expected to occur only if the donor and acceptor are *not* fully engaged prior to the guest binding. Given that **2** folded almost fully in methanol (Figure 2b), it is quite likely that the pyrenyl and NDI were simply bound too well prior to guest-binding so that further improvement from the guest binding was minimal. Weaker naphthyl–NDI interactions in **1**, on the other hand, made it possible for the guest to strengthen the D–A interactions. Thus, the model of intramolecular enhancement correctly predicts the weaker binding of **2** than **1** after the inflection points.

Third, when 10% water was added to methanol, a precipitous drop in binding was observed for **1** ($K_a < 10$ M^{-1}, Figure 3b, red dashed line) while **4** was barely affected (K_a went from 200 to 180 M^{-1}). Thus, the small amount of water did not change the direct binding force significantly but completely shut down the intramolecular enhancement. Addition of water served to increase the solvophobic interactions between the donor and acceptor, evident from the enhanced charge-transfer band near 450 nm for **1** (Figure 9). Once the D–A pair became tightly bound before the guest binding, the very basis of intramolecular enhancement—guest-triggered strengthening of intrahost interactions—was removed. Similar observation was made in other intramolecularly enhanced receptors.[28-30]

Fourth, the sodium-enhanced D–A interaction was confirmed spectroscopically. As shown by UV-vis spectroscopy, when sodium was added to **1** in methanol, the charge-transfer band near 450 nm increased steadily, supporting a closer contact between the donor and acceptor induced by the guest (Figure 10). Receptor **1** displayed no NOE signals between the NDI and the naphthyl protons in methanol at 213 K, suggesting that the naphthyl and NDI are separated by a significant distance in the NMR sense (Figure 11). Addition of sodium significantly enhanced the naphthyl–NDI contact and numerous naphthyl–NDI cross peaks appeared (Figure 13). The NDI protons also became closer to the ethylene oxide protons, supporting the sodium-triggered "ring closure" in **1**. Our fluorescence data indicate that the population of folded 1 was over 90% in methanol (Figure 2b). The CT band in the UV-vis spectrum (Figure 9) indicates that some of the naphthyl and NDI groups were in reasonable proximity. Taken together, the spectroscopic data support a loosely bound donor–acceptor pair, hypothesized to be essential to the cooperatively enhanced binding.

Fifth, although by itself not conclusive, the extremely weak binding of **3** was consistent with the intramolecular enhancement. Without an appropriate donor, intramolecular D–A interactions do not exist in this compound. Without the D–A interactions, neither preorganization nor intramolecular enhancement could operate and the weak binding was an expected result.

Figure 3a also shows that the onset of intramolecular enhancement was earlier for **1** than for **2**. The most likely reason for this is the interplay between the preorganization and intramolecular enhancement. In general, very strong D–A interactions favor preorganization but a weakly bound D–A pair with "room for improvement" is best for intramolecular enhancement. In the case of **2**, the stronger pyrenyl–NDI interactions serve to better

preorganize the oligo(ethylene oxide) chain for binding, and thus can promote the principle of preorganization and make it last longer.

To be selective in binding, preorganized receptors typically are fairly rigid so that only the best-fitted guest can enter the binding site to engage the largest number of binding interactions possible. Intramolecularly enhanced receptors obtain their binding selectivity in a different way—by having the best guest turn on the largest number of intrareceptor interactions while maintaining as much direct binding interaction as possible.[29, 30]

Receptor **1** indeed displayed significant binding selectivity, despite its flexibility.[52, 53] In methanol, among common alkali metal ions, it showed insignificant binding for Li^+, bound Na^+ with $K_a = 1.6 \times 10^3 \, M^{-1}$, and bound K^+ with $K_a = 4.2 \times 10^2 \, M^{-1}$ (Figure 15). The Na/K ratio in the binding affinity was nearly 4:1. In contrast, the binding constants of 15-crown-5 for Na^+ and K^+ are reported to be 1.7×10^3 and $2.7 \times 10^3 \, M^{-1}$, respectively, with a Na/K ratio of 1:1.5—18-Crown-6 has a Na/K ratio of 1:54. [54] Therefore, at least in this example, the flexible intramolecularly enhanced receptor **1** actually displayed a higher binding selectivity for sodium than the traditionally preorganized crown ether.

Conclusion

In summary, flexible structures with intramolecular enhancement offer an interesting strategy to strong and selective receptors. As shown by Figure 3a, they become particularly competitive when the direct binding forces are weakened by unfavorable solvents. Binding selectivity, meanwhile, does not have to suffer. These are very useful properties and could help chemists design a new generation of biomimetic receptors.

Acknowledgement

Experimental Section

General Method

For spectroscopic purpose, methanol, and dichloromethane (DCM) were of HPLC grade. All other reagents and solvents were of ACS-certified grade or higher, and were used as received from commercial suppliers. Routine ^{1}H and ^{13}C NMR spectra were recorded on a Bruker DRX-400, on a Bruker AV II 600 or on a Varian VXR-400 spectrometer. Variable temperature ^{1}H NMR spectra, nuclear Overhauser effect spectroscopy (NOESY), and diffusion ordered spectroscopy (DOSY) were recorded on a Bruker AV II 600 spectrometer. UV-vis spectra were recorded at ambient temperature on a Cary 100 Bio UV-visible spectrophotometer. Fluorescence spectra were recorded at ambient temperature on a Varian Cary Eclipse Fluorescence spectrophotometer.

Syntheses

Syntheses of compounds **4**[55], **9**[56], **10**[57], and **11**[58] were previously reported.
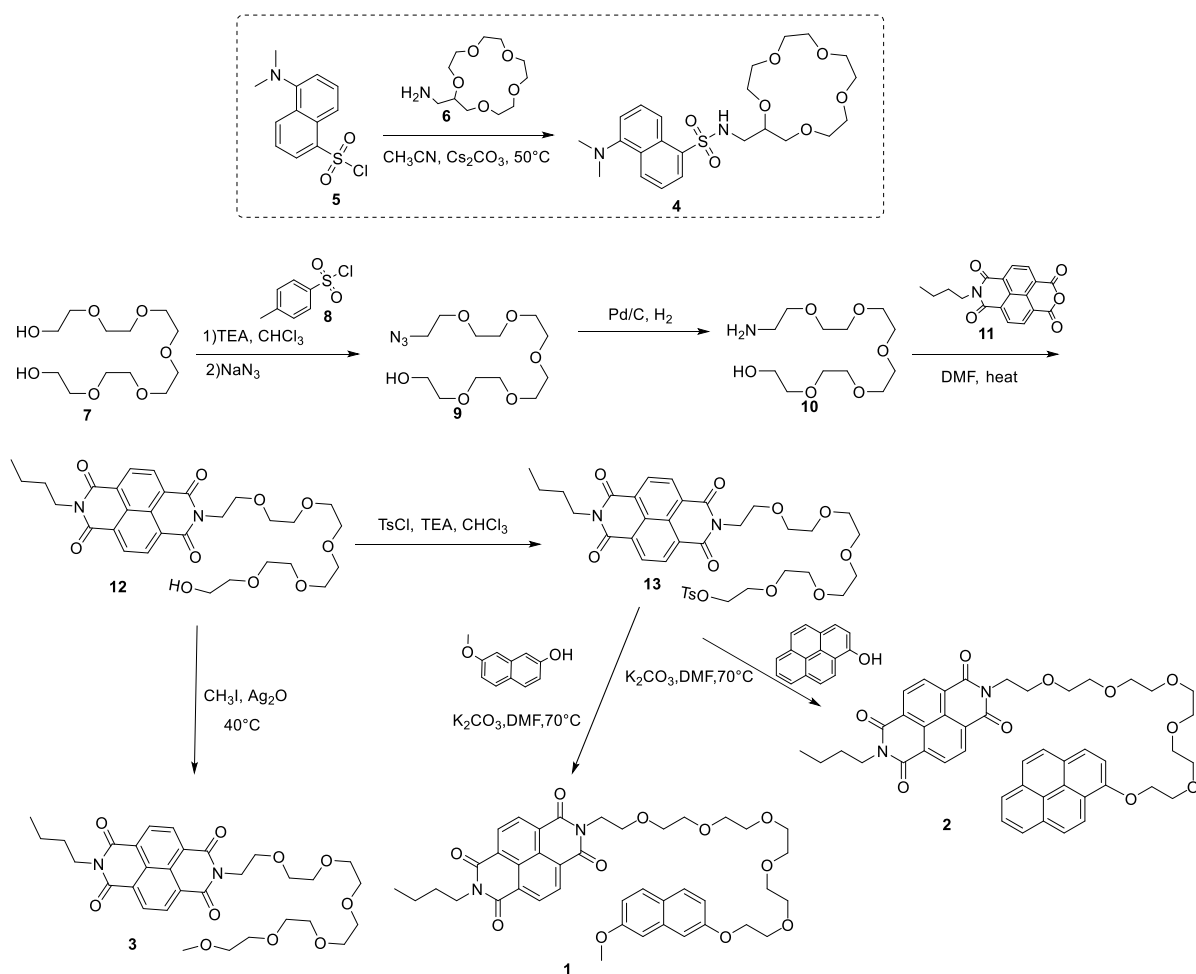
Scheme 2. Synthetic route.

Compound 12. Compound **10** (81.4 mg, 0.289 mmol) and compound **11** (98.2 mg, 0.304 mmol) were dissolved in DMF (5 mL). After the reaction mixture was stirred at 120 °C overnight, TLC showed completion of the reaction. The mixture was mixed with water (50 mL) and then extracted with ethyl acetate (3 × 30 mL). The organic phase was washed with brine (50 mL), dried with MgSO$_4$, concentrated by rotary evaporation. The residue was purified by flash column chromatography over silica gel with 15:1 dichloromethane/methanol as the eluent to give a brown solid (100 mg, 59%). ^{1}H NMR (600 MHz, CDCl$_3$, δ) 8.76 (s, 4H), 4.46 (t, J = 5.8 Hz, 2H), 4.21 (t, J = 7.5 Hz, 2H), 3.85 (t, J = 5.9 Hz, 2H), 3.73–3.54 (m, 20H), 1.74 (m,

2H), 1.47 (m, 2H), 1.00 (t, $J = 7.4$ Hz, 3H). ^{13}C NMR (151 MHz, CDCl$_3$, δ) 162.9, 162.8, 131.0, 130.9, 126.8, 126.7, 126.6, 77.2, 77.0, 76.8, 72.6, 70.6, 70.6, 70.6, 70.5, 70.5, 70.3, 70.0, 67.8, 61.7, 40.8, 39.6, 30.2, 20.4, 13.8. ESI-MS (*m/z*): [M+H] $^+$ cacld for C$_{30}$H$_{38}$N$_2$O$_{10}$, 587.2599; found, 587.2607.

Compound 13. Compound **12** (41.3 mg, 0.07 mmol), triethylamine (0.1 mL, 0.7 mmol), and 4-dimethylaminopyridine (catalytic amounts) were dissolved in anhydrous dichloromethane (5 mL). The reaction mixture was cooled with an ice bath. After the addition of 4-toluenesulfonyl chloride, the reaction mixture was stirred at room temperature overnight. The mixture was mixed with water (50 mL) and then extracted with dichloromethane (3×30 mL). The combined organic phase was washed with brine (50 mL) and dried with MgSO$_4$. After the solvent was removed by rotary evaporation, the crude product was used in the next step without further purification.

Compound 1. Compound **13** (20.4 mg, 0.0275 mmol), 7-methoxy-2-naphthol (9.6 mg, 0.0551mmol), and potassium carbonate (15.2 mg, 0.1102 mmol) was combined in DMF (5 mL). Then the reaction mixture was heated to 70 °C and stirred overnight. After TLC showed completion of the reaction, water (50 mL) was added to the reaction mixture. The mixture was extracted with ethyl acetate (3×30 mL), washed with brine (30 mL), and dried with MgSO$_4$. The solvent was removed by rotary evaporation, and the residue was purified by preparative TLC using 5:1 ethyl acetate/dichloromethane as the developing solvent to give a red powder (8.2 mg, 40%). ^{1}H NMR (600 MHz, CDCl$_3$, δ) 8.73 (s, 4H), 7.57 (d, $J = 8.5$ Hz, 2H), 6.98 (s, 2H), 6.95 (d, $J = 8.8$ Hz, 2H), 4.47 (t, $J = 5.9$ Hz, 2H), 4.23 (m, 4H), 3.95 (t, $J = 4.5$ Hz, 2H), 3.91 (s, 3H), 3.87 (t, $J = 5.9$ Hz, 2H), 3.80 (t, $J = 4.8$ Hz, 2H), 3.75–3.59 (m, 14H), 1.78 (m, 2H), 1.50 (m, 2H), 1.03 (t, $J = 7.4$ Hz, 3H). ^{13}C NMR (151 MHz, CDCl$_3$, δ) 162.9, 162.8, 158.0,

157.3, 135.7, 130.9, 130.8, 129.0, 126.6, 126.6, 126.6, 126.4, 124.2, 116.2, 116.0, 106.1, 105.1, 77.2, 77.0, 76.8, 70.9, 70.7, 70.6, 70.6, 70.6, 70.5, 70.1, 69.8, 67.8, 67.4, 55.2, 40.8, 39.6, 30.2, 29.7, 20.4, 13.8. ESI-MS (*m/z*): [M+Na]$^+$ cacld for $C_{41}H_{46}N_2O_{11}$, 765.2994; found, 765.2999.

Compound 2. Compound **13** (130 mg, 0.175 mmol), 1-hydroxypyrene (20 mg, 0.092 mmol), and potassium carbonate (64 mg, 0.46 mmol) was combined in DMF (10 mL). Then the reaction mixture was heated to 70 °C and stirred overnight. After TLC showed completion of the reaction, water (50 mL) was added to the reaction mixture. The mixture was extracted with ethyl acetate (3 × 30 mL), washed with brine (30 mL), and dried with $MgSO_4$. The solvent was removed by rotary evaporation, and the residue was purified by preparative TLC using 5:1 ethyl acetate/dichloromethane as the developing solvent to give a purple powder (68 mg, 94%). ^{1}H NMR (600 MHz, CDCl$_3$, δ) 8.17 (s, 4H), 8.10 (d, *J* = 9.1 Hz, 1H), 7.87 (t, *J* = 6.9 Hz, 2H), 7.82 (t, *J* = 7.3 Hz, 2H), 7.70 (d, *J* = 9.1 Hz, 1H), 7.65 (d, *J* = 8.9 Hz, 1H), 7.60 (d, *J* = 8.8 Hz, 1H), 7.36 (d, *J* = 8.4 Hz, 1H), 4.46 (t, *J* = 4.8 Hz, 2H), 4.39 (t, *J* = 6.0 Hz, 2H), 4.15–4.06 (m, 4H), 3.93–3.79 (m, 6H), 3.75–3.58 (m, 12H), 1.75 (m, 2H), 1.50 (m, 2H), 1.04 (t, *J* = 7.4 Hz, 3H). ^{13}C NMR (151 MHz, CDCl$_3$, δ) 162.6, 162.6, 152.7, 131.2, 131.1, 129.9, 129.8, 127.0, 126.1, 126.0, 125.5, 125.4, 125.4, 125.3, 124.8, 124.8, 124.2, 124.1, 123.9, 121.1, 109.0, 77.2, 77.0, 76.8, 71.2, 70.9, 70.8, 70.6, 70.2, 70.0, 68.6, 68.0, 40.6, 39.5, 30.2, 29.7, 20.4, 13.9. ESI-MS (*m/z*): [M+Na]$^+$ cacld for $C_{46}H_{46}N_2O_{10}$, 809.3045; found, 809.3062.

Compound 3. A mixture of compound **12** (100 mg, 0.17 mmol), methyl iodide (5 mL, 80.32 mmol), and silver oxide (78.8 mg, 0.34 mmol) was stirred at room temperature for three days. After the reaction mixture was concentrated by rotary evaporation, the residue was purified by flash column chromatography over silica gel with 25:1 ethyl acetate/methanol as the eluent to give a deep yellow solid (71.6 mg, 70%). ^{1}H NMR (600 MHz, CDCl$_3$, δ) 8.75 (s,

4H), 4.45 (t, J = 5.8 Hz, 2H), 4.20 (t, J = 7.6 Hz, 2H), 3.84 (t, J = 5.9 Hz, 2H), 3.69 (t, J = 4.6

Hz, 2H), 3.66 – 3.52 (m, 18H), 3.37 (s, 3H), 1.73 (m, 2H), 1.46 (m, 2H), 0.99 (t, J = 7.4 Hz,

3H). ^{13}C NMR (151 MHz, CDCl$_3$, δ) 162.9, 162.8, 131.0, 130.9, 126.8, 126.7, 126.7, 126.6,

77.2, 77.0, 76.8, 72.0, 70.6, 70.6, 70.5, 70.1, 67.81, 59.0, 40.8, 39.9, 30.2, 20.4, 13.8. ESI-MS

(m/z): [M+Na] [+] cacld for C$_{31}$H$_{40}$N$_2$O$_{10}$, 623.2575; found, 623.2577.

Fluorescence Solvent Study and Data Analysis Method

Stock solution of **1** (4.0 mM), **2** (4.0 mM), and **3** (4.0 mM) in DCM were prepared. For

the solvent titration, a typical procedure is as follows. An aliquot of the stock solution was

added to 2.00 mL of the appropriate solvent in a quartz cuvette. The sample was gently

vortexed for 30 s before the fluorescence spectrum was collected.

Literature method[59] was followed in the two-state curve fitting for the fluorescence data

for hosts **1** and **2**:
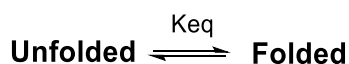
$$\text{Unfolded} \overset{Keq}{\rightleftharpoons} \text{Folded}$$

According to the two-state model, at any given concentration of the denaturant (i.e.,

MeOH), only the folded and unfolded conformations are present and their fractions are

represented by f_F and f_U. Fraction of the unfolded conformation can be calculated by:

$$K_{eq} = f_F/f_U$$

$$f_F = (I - I_U)/(I_F - I_U)$$

$$f_U = 1 - f_F$$

I is the fluorescence intensity at a certain solvent composition. I_U is the intensity at fully

unfolded state, and I_F is the state at fully folded state.

The equilibrium constant (K_{eq}) and the free energy ($\varDelta G$) for the folding reaction can be

calculated using:

$$\Delta G = -RT\ lnK_{eq} = -RT\ ln(f_F/f_U) = -RT\ ln[(1-f_U)/f_U]$$

In the two-state model, the free energies are linearly related to the concentration of denaturant and are assumed to have the same relationship to the $E_T(30)$ values of the solvent:

$$\Delta G = \Delta G_0 + m\ E_T(30)$$

Then we can obtain equations:

$$f_F = 1/(1+1/exp\ (-(\Delta G_0 + m\ E_T(30)\ /RT))$$

$$I = I_U + (I_F - I_U)/\ (1+1/exp(-(\Delta G_0 + m\ E_T(30)\ )/RT))$$

A nonlinear least-squares fitting of the experimental data to above equation affords the two-state folding-unfolding curves and f_U.

UV-Vis Titration and Data Analysis Method

Stock solution of **1** (4.0 mM), **2** (4.0 mM) and **3** (4.0 mM) in DCM were prepared. Stock solutions of the guest (LiSCN, NaSCN or KSCN) were prepared in the appropriate solvent mixture, in which titrations would be performed. For the titrations, a typical procedure is as follows. An aliquot of the host stock solution was added to 2.00 mL solvent in a quartz cuvette. The sample was gently vortexed for 30 s before its UV-vis spectrum was recorded. Aliquots of the guest was added and the UV-vis spectrum was recorded after each addition. The titration was continued until saturation was reached and the total volume of the guest solution added was kept below 100 μL. The binding constant was obtained by nonlinear least squares curving fitting of the absorbance data to the 1:1 binding isotherm.[60] Titrations were repeated three times and the reported binding constant was the average with 90% confidence using uncertainty calculation:

$$U = t\frac{1}{\sqrt{n}}\sqrt{\frac{\sum(\overline{K}-K_i)^2}{(n-1)}}$$

in which *U* is the uncertainty, *n* is the number of experiments, *t* is the student t-value, which

is 2.92 when n is 3 and 90% confidence for two sides.

Fluorescence Emission Spectroscopy Titration and Data Analysis Method

A stock solution of **4** (2.0 mM) in DCM prepared. Stock solutions of NaSCN were

prepared in the appropriate solvent mixture, in which titrations would be performed. For the

titrations, a typical procedure is as follows. An aliquot of the host stock solution was added to

2.00 mL solvent in a quartz cuvette. The sample was gently vortexed for 30 s before its

fluorescence spectrum was recorded. Aliquots of the guest was added and the fluorescence

spectrum was recorded after each addition. The titration was continued until saturation was

reached and the total volume of the guest solution added was kept below 100 µL. The binding

constant was obtained by nonlinear least squares curving fitting of the fluorescence data to the

1:1 binding isotherm. Titrations were repeated three times and the reported binding constant

was the average with 90% confidence.
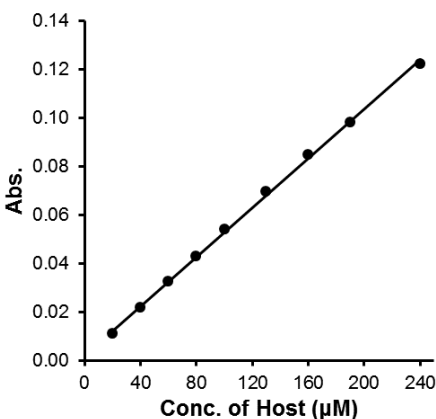
Figure 4. Charge transfer absorbance at 450 nm in MeOH as a function of the concentration of host **1**. A linear relationship was obtained with R^2 = 0.9972.
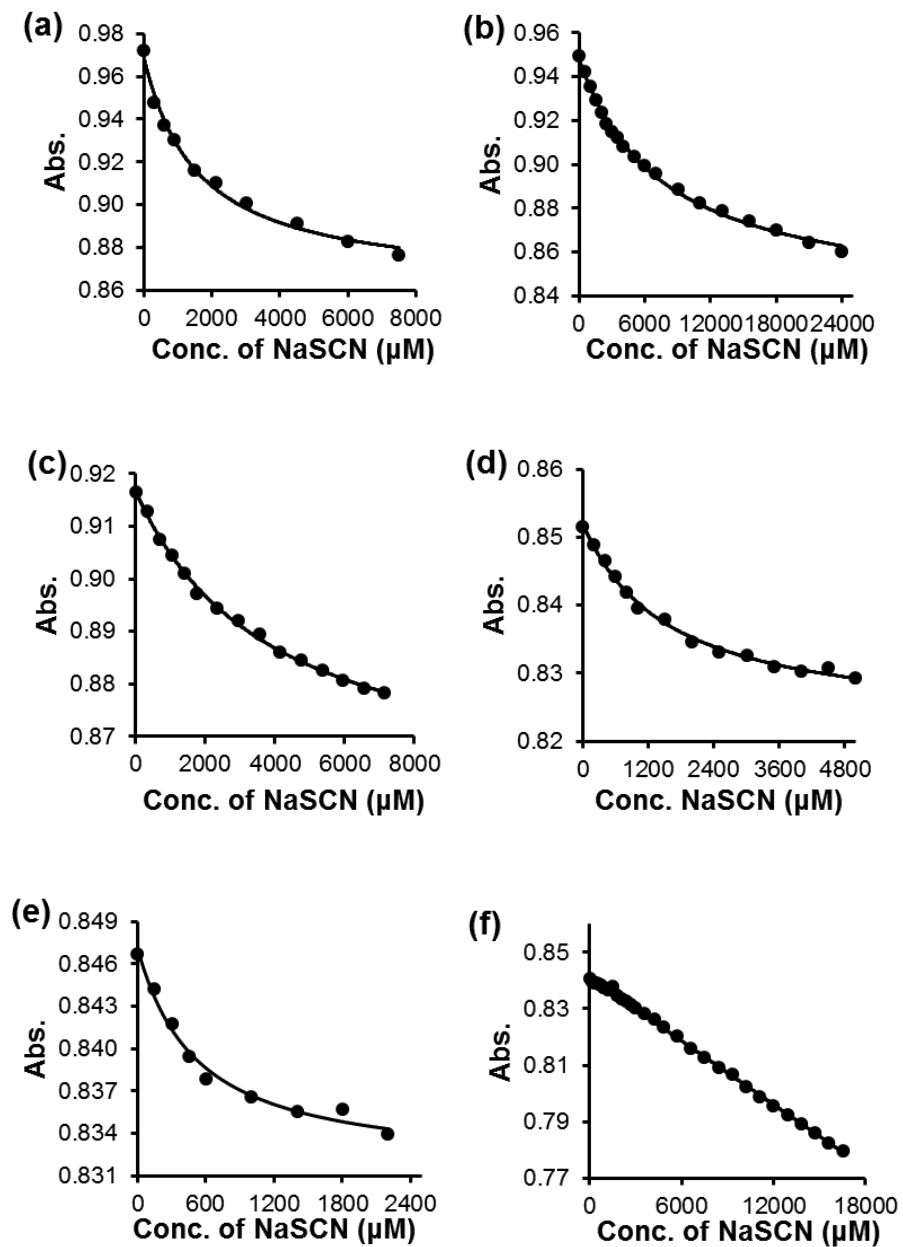
Figure 5. UV-vis titration curves of host **1** by sodium thiocyanate in (a) 4:1 DCM/MeOH (v/v), (b) 3:2 DCM/MeOH (v/v), (c) 2:3 DCM/MeOH (v/v), (d) 1:4 DCM/MeOH (v/v), (e) MeOH, and (f) 9:1 MeOH/H$_2$O (v/v). [**1**] = 50 μM. The UV absorbance at 358 nm was monitored and the smooth curve was from nonlinear least squares curving fitting to a 1:1 binding isotherm.
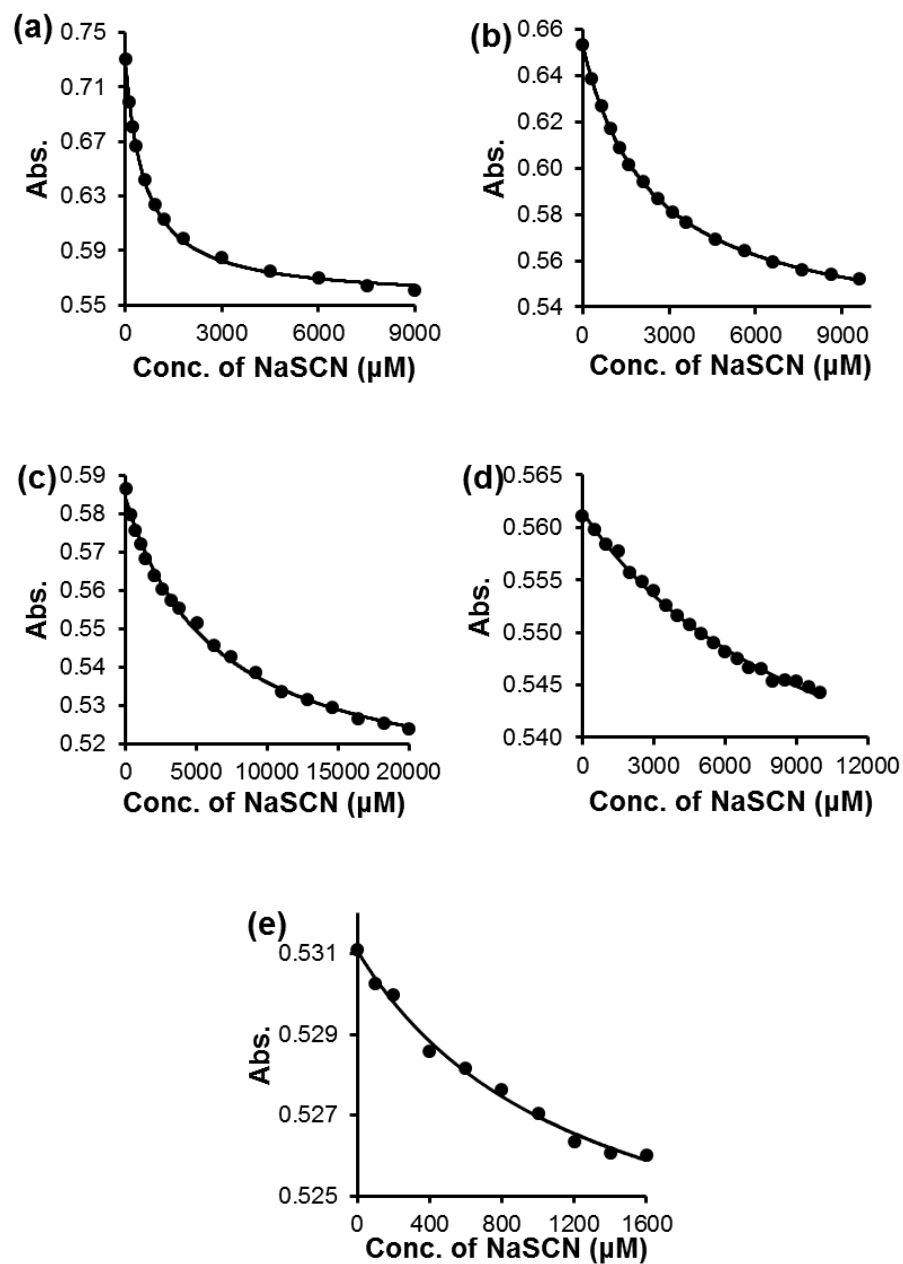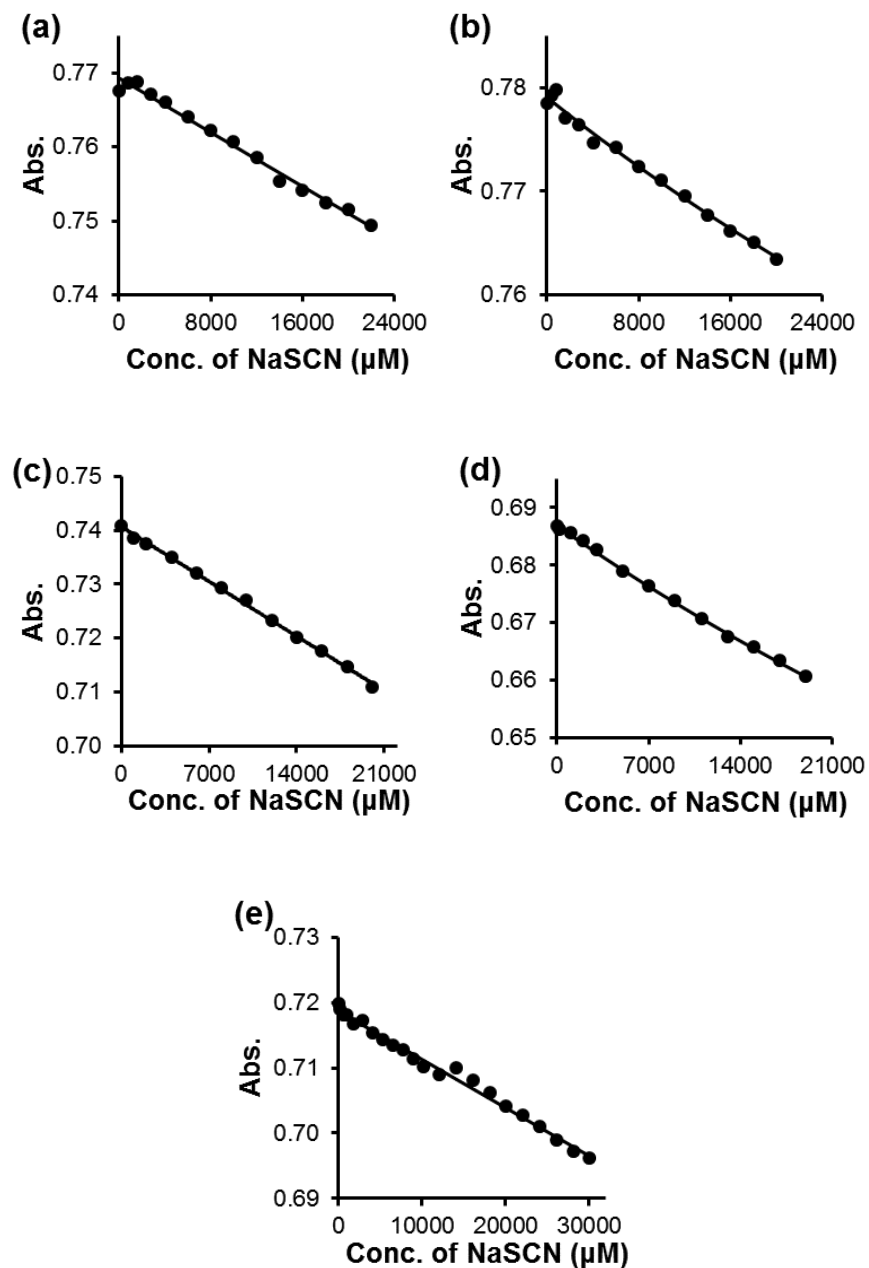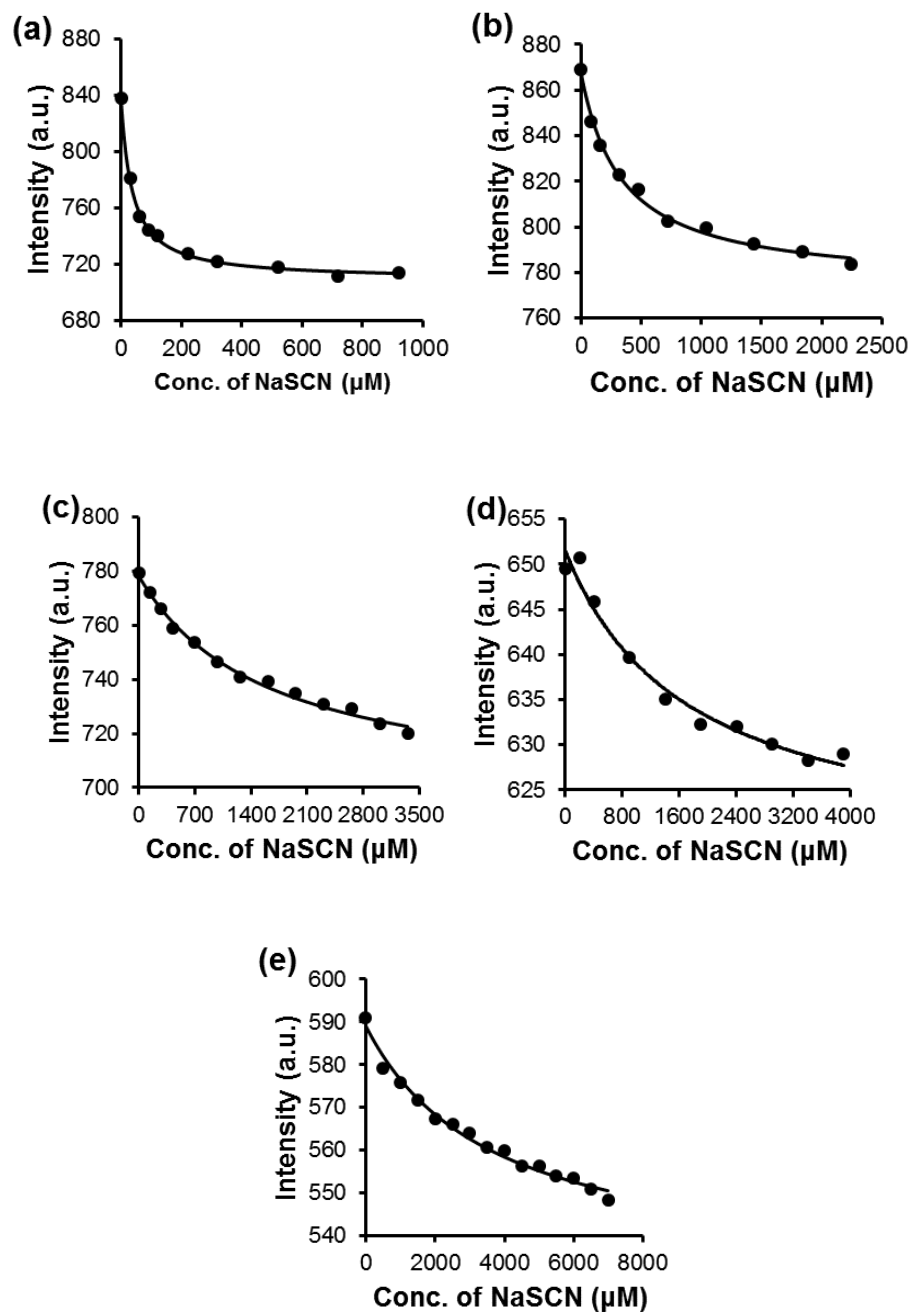
**Figure 6.** UV-vis titration curves of host **2** by sodium thiocyanate in (a) 4:1 DCM/MeOH (v/v), (b) 3:2 DCM/MeOH (v/v), (c) 2:3 DCM/MeOH (v/v), (d) 1:4 DCM/MeOH (v/v), and (e) MeOH. [**2**] = 20 μM. The UV absorbance at 382 nm was monitored and the smooth curve was from nonlinear least squares curving fitting to a 1:1 binding isotherm.

Figure 7. UV-vis titration curves of host **3** (40 μM) by sodium thiocyanate in (a) 4:1 DCM/MeOH (v/v), (b) 3:2 DCM/MeOH (v/v), (c) 2:3 DCM/MeOH (v/v), (d) 1:4 DCM/MeOH (v/v), and (e) MeOH. [**3**] = 40 μM. The UV absorbance at 358 nm was monitored and the smooth curve was from nonlinear least squares curving fitting to a 1:1 binding isotherm.

Figure 8. Fluorescence titration curves of host **4** by sodium thiocyanate in (a) 4:1 DCM/MeOH (v/v), (b) 3:2 DCM/MeOH (v/v), (c) 2:3 DCM/MeOH (v/v), (d) 1:4 DCM/MeOH (v/v), and (e) MeOH. [**4**] = 2.0 μM. The maximum emission intensity was monitored and the smooth curve was from nonlinear least squares curving fitting to a 1:1 binding isotherm.
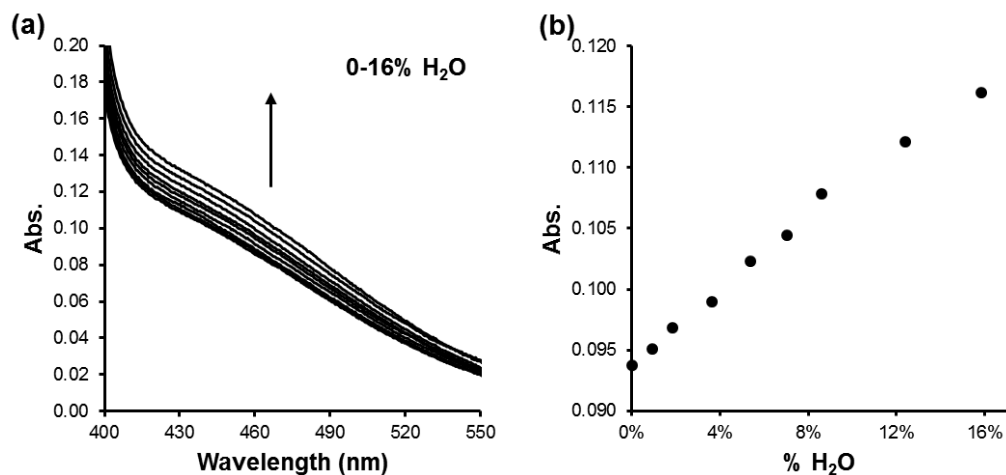
Figure 9. (a) UV-Vis spectra of host **1** with 0–16% H$_2$O. [**1**] = 180 μM in methanol. (b) Absorbance at 450 nm as a function of H$_2$O volume percentage.
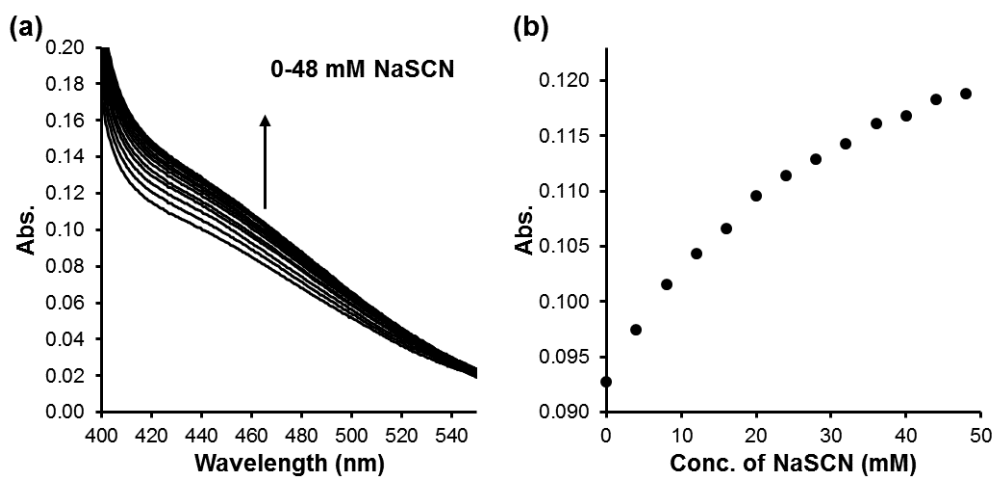
Figure 10. (a) UV-Vis spectra of host **1** with 0-48 mM sodium thiocyanate. [**1**] = 180 μM. (b) Absorbance at 450 nm as a function of concentration of NaSCN.
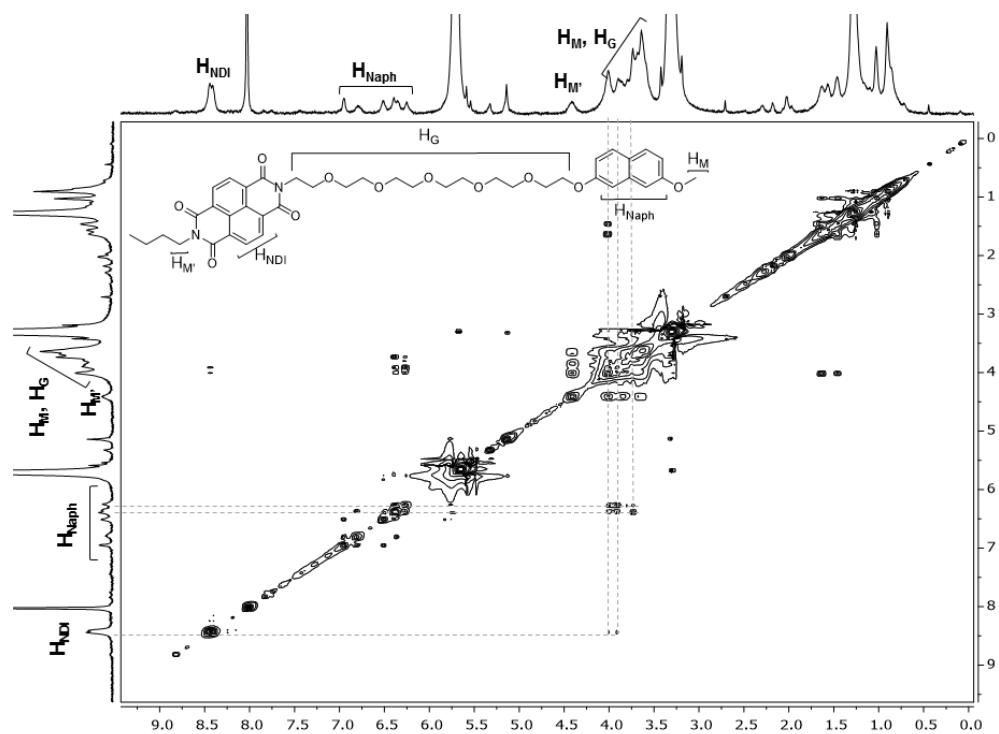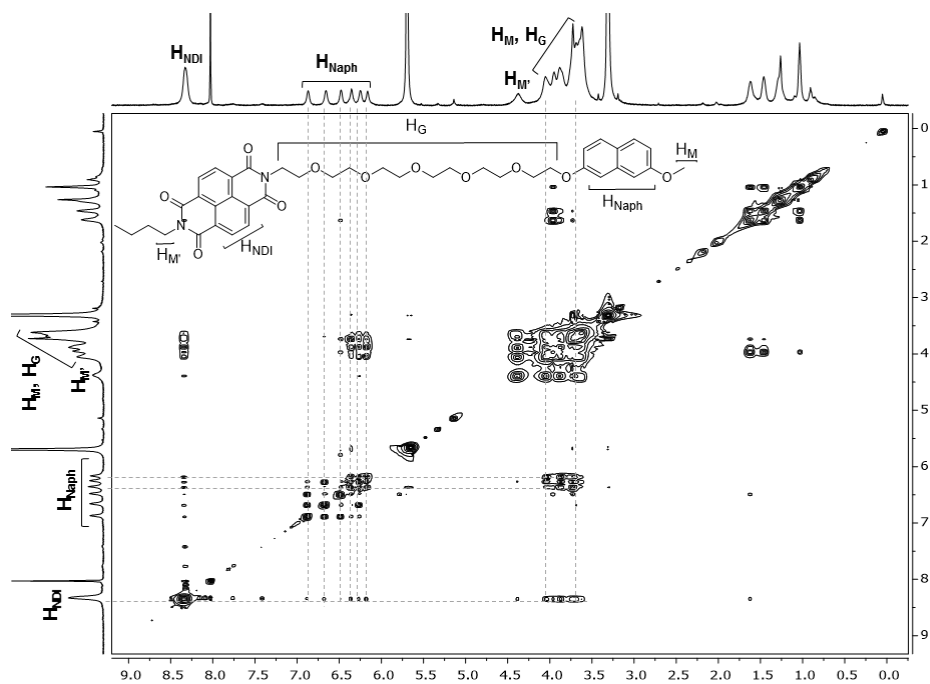
Figure 11. NOESY spectrum of 1 mM host **1** in CD₃OD (with 7% CDCl₃ to improve solubility) at 213 K.
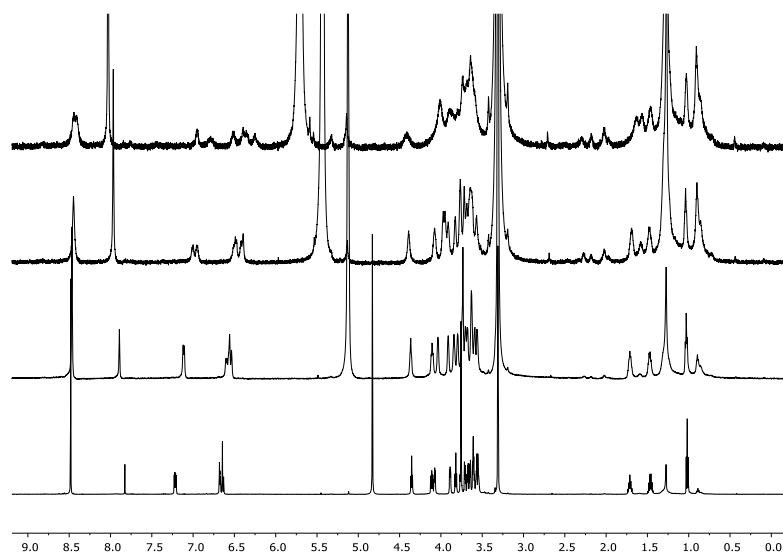
Figure 12. NMR spectra of 1 mM host **1** in CD₃OD (with 7% CDCl₃ to improve solubility) at different temperatures. Temperature from bottom to top was 298 K, 273 K, 243 K, and 213 K.

Figure 13. NOESY spectrum of 1 mM host **1** with 8 mM sodium thiocyanate in CD₃OD (with 7% CDCl₃ to improve solubility) at 213 K.
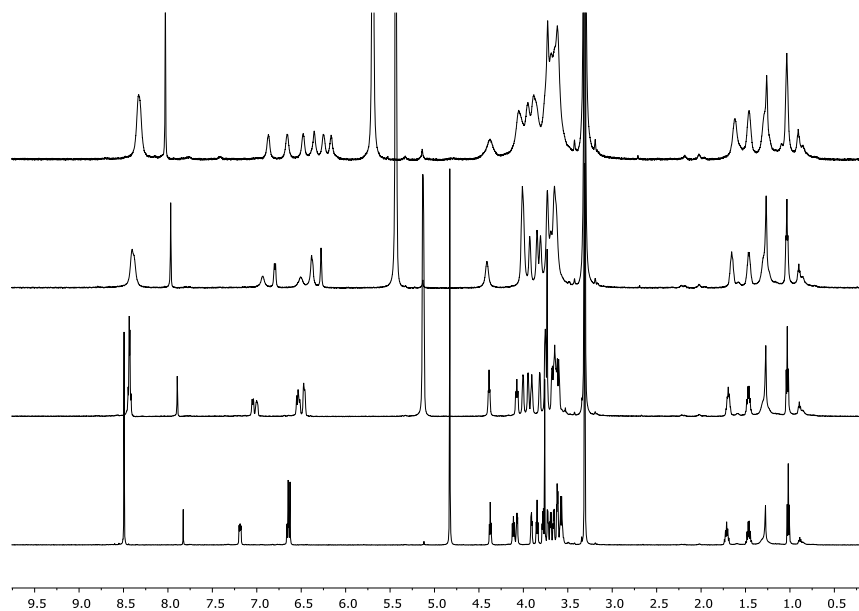

Figure 14. NMR spectra of 1 mM host **1** with 8 mM sodium thiocyanate in CD₃OD (with 7% CDCl₃ to improve solubility) at different temperatures. Temperature from bottom to top was 298 K, 273 K, 243 K, and 213 K.
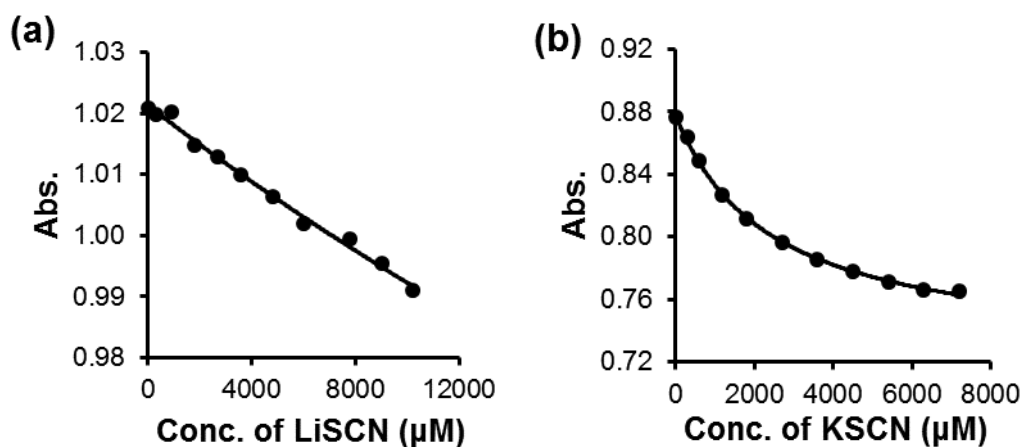
Figure 15. UV-vis titration curves of host **1** by (a) lithium thiocyanate and (b) potassium thiocyanate in methanol. [**1**] = 40 μM. The UV absorbance at 358 nm was monitored and the smooth curve was from nonlinear least squares curving fitting to a 1:1 binding isotherm.

Table 1. Binding constants of hosts **1**–**4** in different solvents. All binding constants were averages of three titrations with 90% confidence.

Entry	Host	Solvent(s)	K_a ($10^2\,M^{-1}$)
1	**1**	DCM/MeOH 4/1 (v/v)	6.5 ± 1.0
2	**1**	DCM/MeOH 3/2 (v/v)	1.4 ± 0.2
3	**1**	DCM/MeOH 2/3 (v/v)	2.8 ± 0.4
4	**1**	DCM/MeOH 1/4 (v/v)	5.8 ± 1.2
5	**1**	MeOH	16 ± 9
6[a]	**1**	MeOH/H_2O 9/1 (v/v)	-
7	**2**	DCM/MeOH 4/1 (v/v)	17 ± 2
8	**2**	DCM/MeOH 3/2 (v/v)	4.2 ± 0.1
9	**2**	DCM/MeOH 2/3 (v/v)	1.5 ± 0.2
10	**2**	DCM/MeOH 1/4 (v/v)	1.0 ± 0.4
11	**2**	MeOH	5.1 ± 4.6
12[a]	**3**	DCM/MeOH 4/1 (v/v)	-
13[a]	**3**	DCM/MeOH 3/2 (v/v)	-
14[a]	**3**	DCM/MeOH 2/3 (v/v)	-
15[a]	**3**	DCM/MeOH 1/4 (v/v)	-
16[a]	**3**	MeOH	-
17[b]	**4**	DCM/MeOH 4/1 (v/v)	300 ± 40
18[b]	**4**	DCM/MeOH 3/2 (v/v)	31 ± 17
19[b]	**4**	DCM/MeOH 2/3 (v/v)	7.2 ± 2.9
20[b]	**4**	DCM/MeOH 1/4 (v/v)	5.7 ± 2.9
21[b]	**4**	MeOH	2.0 ± 1.2
22[b]	**4**	MeOH/H_2O 9/1 (v/v)	1.8 ± 0.8
23[a][c]	**1**	MeOH	-

Table 1. continued.

24[d]	**1**	MeOH	4.22 ± 0.04

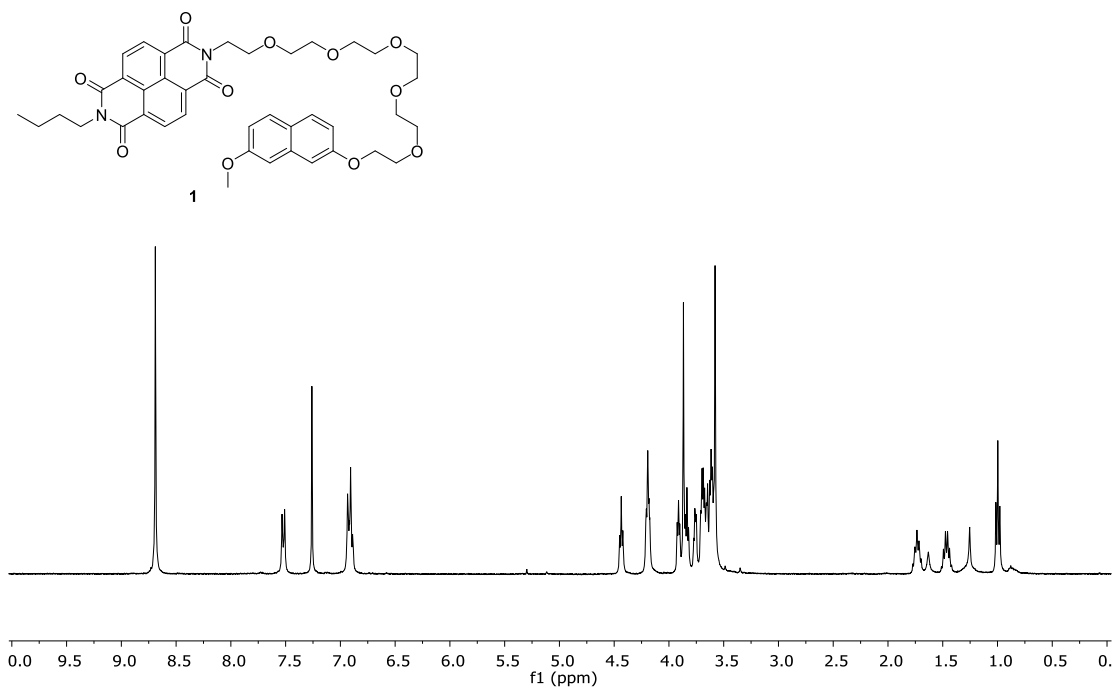[a] Saturation could not be reached even with high concentrations of guest. Binding was weak. [b] The binding constants were determined by fluorescence titration. [c] The guest was lithium thiocyanate. [d] The guest was potassium thiocyanate.
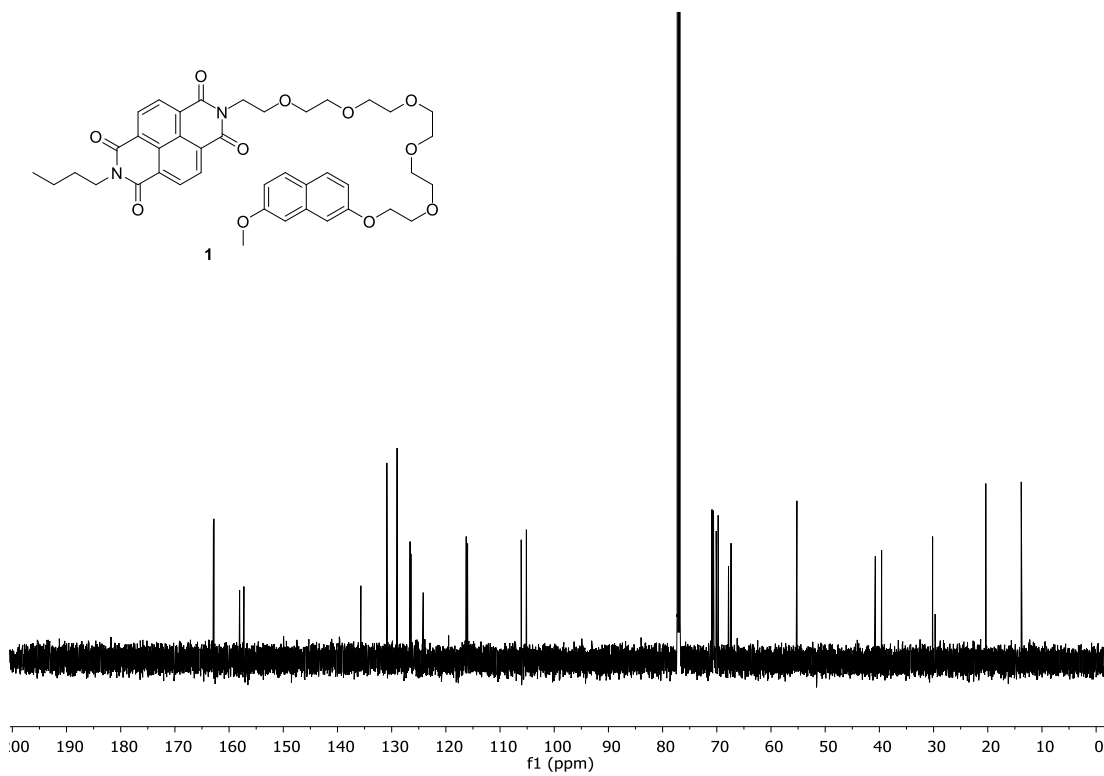
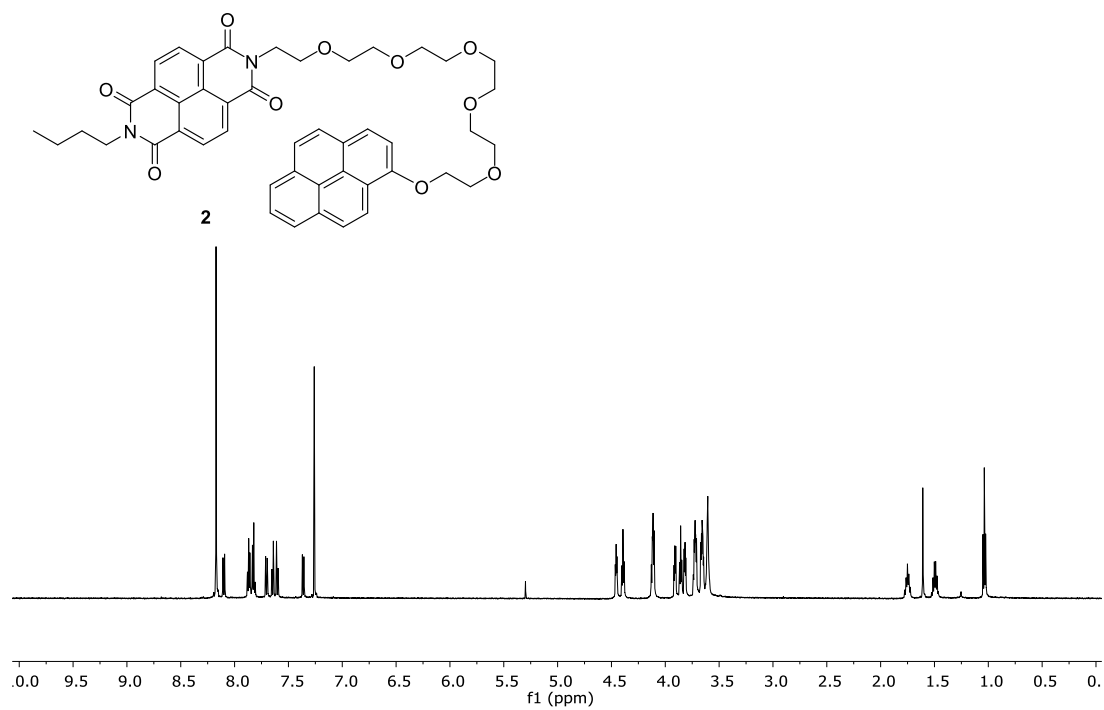## ^{1}H and ^{13}C NMR Spectra
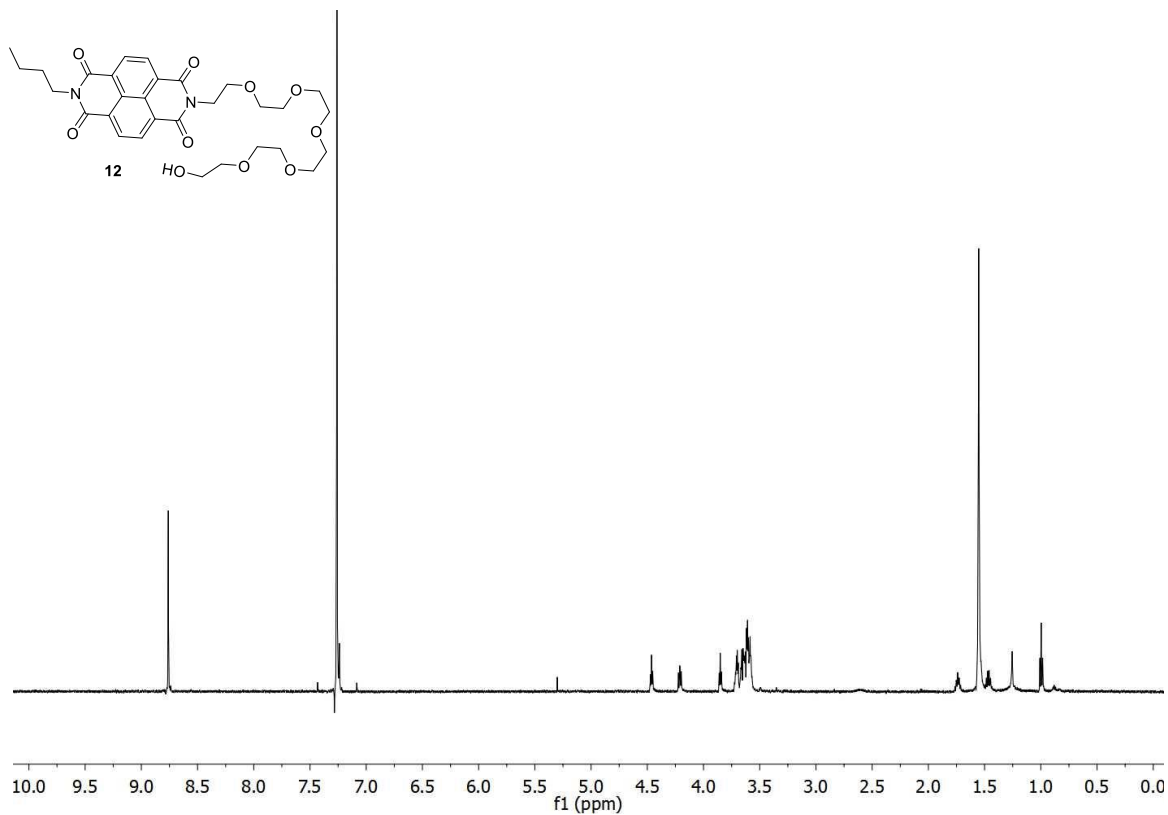
Scheme 3. ^{1}H NMR of **12**.
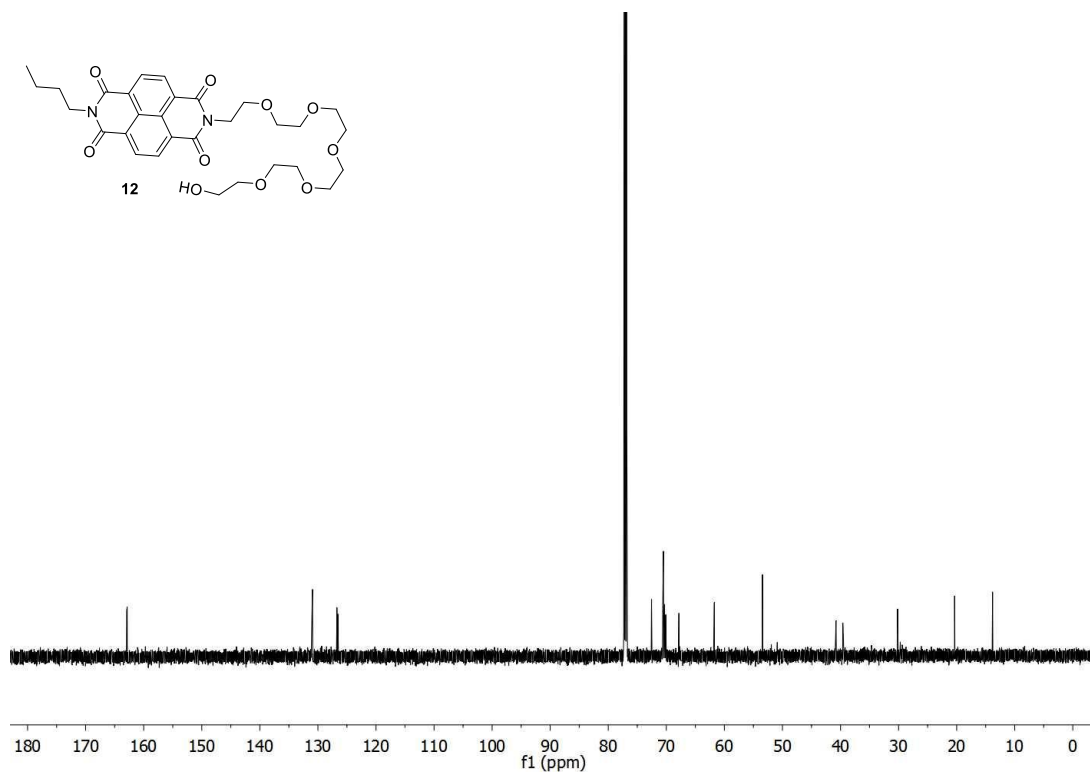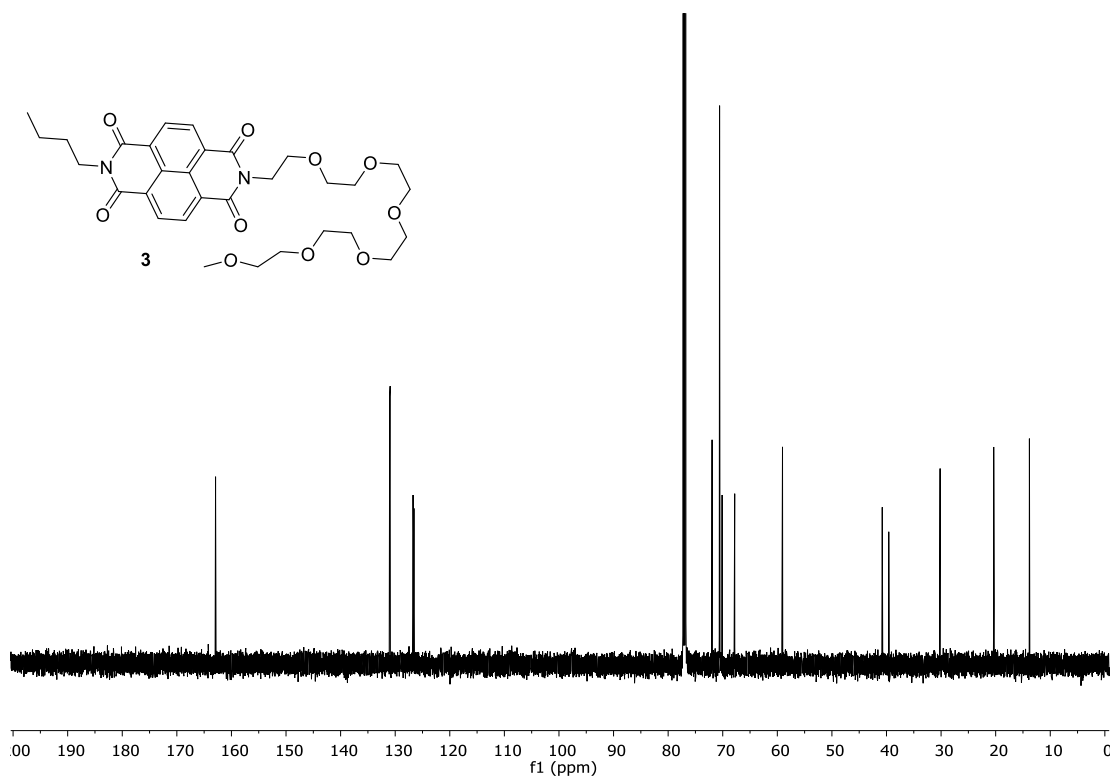
Scheme 4. ^{13}C NMR of **12**.

Scheme 5. ^{1}H NMR of **1**.

Scheme 6. ^{13}C NMR of **1**.

Scheme 7. ^{1}H NMR of **2**.

Scheme 8. ^{13}C NMR of **2**.

Scheme 9. ^{1}H NMR of **3**.

Scheme 10. ^{13}C NMR of **3**.

Notes and References

1. S. H. Gellman, *Acc. Chem. Res.*, 1998, **31**, 173-180.

2. D. J. Hill, M. J. Mio, R. B. Prince, T. S. Hughes and J. S. Moore, *Chem. Rev.*, 2001, **101**, 3893-4012.

3. S. Hecht and I. Huc, eds., *Foldamers: Structure, Properties, and Applications*, Wiley-VCH, Weinheim, 2007.

4. D.-W. Zhang, X. Zhao, J.-L. Hou and Z.-T. Li, *Chem. Rev.*, 2012, **112**, 5271-5316.

5. M. S. Cubberley and B. L. Iverson, *Curr. Opin. Chem. Biol.*, 2001, **5**, 650-653.

6. H. Juwarker, J. M. Suk and K. S. Jeong, *Chem. Soc. Rev.*, 2009, **38**, 3316-3325.

7. K. J. Chang, B. N. Kang, M. H. Lee and K. S. Jeong, *J. Am. Chem. Soc.*, 2005, **127**, 12214-12215.

8.   Y. Hua, Y. Liu, C.-H. Chen and A. H. Flood, *J. Am. Chem. Soc.*, 2013, **135**, 14401-14412.

9.   X. Chi, G. Yu, L. Shao, J. Chen and F. Huang, *J. Am. Chem. Soc.*, 2016, **138**, 3168-3174.

10.   Q. A. Gan, Y. Ferrand, C. Y. Bao, B. Kauffmann, A. Grelard, H. Jiang and I. Huc, *Science*, 2011, **331**, 1172-1175.

11.   Y. Zhao and Z. Zhong, *J. Am. Chem. Soc.*, 2006, **128**, 9988-9989.

12.   H. Cho and Y. Zhao, *J. Am. Chem. Soc.*, 2010, **132**, 9890-9899.

13.   S. Zhang and Y. Zhao, *Chem. -Eur. J.*, 2011, **17**, 12444-12451.

14.   E.-H. Ryu and Y. Zhao, *J. Org. Chem.*, 2006, **71**, 9491-9494.

15.   N. Chandramouli, Y. Ferrand, G. Lautrette, B. Kauffmann, C. D. Mackereth, M. Laguerre, D. Dubreuil and I. Huc, *Nat. Chem.*, 2015, **7**, 334-341.

16.   J. L. Hou, X. B. Shao, G. J. Chen, Y. X. Zhou, X. K. Jiang and Z. T. Li, *J. Am. Chem. Soc.*, 2004, **126**, 12386-12394.

17.   Z. T. Li, J. L. Hou and C. Li, *Acc. Chem. Res.*, 2008, **41**, 1343-1353.

18.   C. Li, Y. Y. Zhu, H. P. Yi, C. Z. Li, X. K. Jiang, Z. T. Li and Y. H. Yu, *Chem. -Eur. J.*, 2007, **13**, 9990-9998.

19.   D. J. Cram, *Angew. Chem. Int. Ed. Engl.*, 1986, **25**, 1039-1057.

20.   K. N. Houk, A. G. Leach, S. P. Kim and X. Y. Zhang, *Angew. Chem. Int. Ed.*, 2003, **42**, 4872-4897.

21.   D. H. Williams, E. Stephens, D. P. O'Brien and M. Zhou, *Angew. Chem. Int. Ed.*, 2004, **43**, 6596-6616.

22.   S. Otto, *Dalton transactions*, 2006, 2861-2864.

23. Y. Zhao, *ChemPhysChem*, 2013, **14**, 3878-3885.

24. Z. Rodriguez-Docampo, S. I. Pascu, S. Kubik and S. Otto, *J. Am. Chem. Soc.*, 2006, **128**, 11206-11210.

25. R. Carrillo, A. Feher-Voelger and T. Martín, *Angew. Chem. Int. Ed.*, 2011, **50**, 10616-10620.

26. R. Carrillo, E. Q. Morales, V. S. Martín and T. Martín, *Chem. -Eur. J.*, 2013, **19**, 7042-7048.

27. R. Carrillo, E. Q. Morales, V. S. Martín and T. Martín, *J. Org. Chem.*, 2013, **78**, 7785-7795.

28. Z. Zhong, X. Li and Y. Zhao, *J. Am. Chem. Soc.*, 2011, **133**, 8862-8865.

29. R. W. Gunasekara and Y. Zhao, *J. Am. Chem. Soc.*, 2015, **137**, 843-849.

30. R. W. Gunasekara and Y. Zhao, *Chem. Commun.*, 2016, **52**, 4345-4348.

31. A. N. Swinburne and J. W. Steed, in *Supramolecular Chemistry: From Molecules to Nanomaterials*, eds. J. W. Steed and P. A. Gale, Wiley, Online, 2012.

32. T. Iimori, W. C. Still, A. L. Rheingold and D. L. Staley, *J. Am. Chem. Soc.*, 1989, **111**, 3439-3440.

33. V. P. Solov'ev, V. E. Baulin, N. N. Strakhova, V. P. Kazachenko, V. K. Belsky, A. A. Varnek, T. A. Volkova and G. Wipff, *J. Chem. Soc., Perkin Trans. 2*, 1998, 1489-1498.

34. S.-G. Kim, K.-H. Kim, J. Jung, S. K. Shin and K. H. Ahn, *J. Am. Chem. Soc.*, 2002, **124**, 591-596.

35. M. H. Filby and J. W. Steed, *Coord. Chem. Rev.*, 2006, **250**, 3200-3218.

36. C. A. Hunter, K. R. Lawson, J. Perkins and C. J. Urch, *J. Chem. Soc. Perkin Trans. 2*, 2001, 651-669.

37.   M. L. Waters, *Curr. Opin. Chem. Biol.*, 2002, **6**, 736-741.

38.   R. Scott Lokey and B. L. Iverson, *Nature*, 1995, **375**, 303-305.

39.   G. J. Gabriel, S. Sorey and B. L. Iverson, *J. Am. Chem. Soc.*, 2005, **127**, 2637-2640.

40.   S. Ghosh and S. Ramakrishnan, *Angew. Chem. Int. Ed.*, 2004, **43**, 3264-3268.

41.   S. Ghosh and S. Ramakrishnan, *Angew. Chem. Int. Ed.*, 2005, **44**, 5441-5447.

42.   H. Sulowska, W. Wiczk, J. Młodzianowski, M. Przyborowska and T. Ossowski, *J. Photochem. Photobiol. A*, 2002, **150**, 249-255.

43.   The absorption spectra of the compounds did not show a signficant change with the solvent change.

44.   T. E. Creighton, *Protein Structure: A Practical Approach, 2nd Ed.*, IRL Press, Oxford, 1997.

45.   R. B. Prince, J. G. Saven, P. G. Wolynes and J. S. Moore, *J. Am. Chem. Soc.*, 1999, **121**, 3114-3121.

46.   Y. Zhao, *J. Org. Chem.*, 2009, **74**, 834-843.

47.   Y. Zhao, Z. Zhong and E.-H. Ryu, *J. Am. Chem. Soc.*, 2007, **129**, 218-225.

48.   D. B. Smithrud and F. Diederich, *J. Am. Chem. Soc.*, 1990, **112**, 339-343.

49.   M. S. Cubberley and B. L. Iverson, *J. Am. Chem. Soc.*, 2001, **123**, 7560-7563.

50.   H. J. Schneider, *Angew. Chem. Int. Ed.*, 2009, **48**, 3924-3977.

51.   Changes in emission could come from both the binding and the conformational change, as demonstrated by the solvent titration shown in Figures Figure **1** and Figure **2**.

52.   H. M. Sun, C. A. Hunter and E. M. Llamas, *Chem. Sci.*, 2015, **6**, 1444-1453.

53.   L. K. S. von Krbek, A. J. Achazi, S. Schoder, M. Gaedke, T. Biberger, B. Paulus and C. A. Schalley, *Chem.-Eur. J.*, 2017, **23**, 2877-2883.

54.   G. W. Gokel, D. M. Goli, C. Minganti and L. Echegoyen, *J. Am. Chem. Soc.*, 1983, **105**, 6786-6788.

55.   H. Sulowska, W. Wiczk, J. Młodzianowski, M. Przyborowska, T. Ossowski, *Journal of Photochemistry and Photobiology A: Chemistry* **2002**, *150*, 249-255.

56.   M. J. Hynes, J. A. Maurer, *Angewandte Chemie International Edition* **2012**, *51*, 2151-2154.

57.   M. K. Muller, K. Petkau, L. Brunsveld, *Chem. Commun. (Cambridge, U. K.)* **2011**, *47*, 310-312.

58.   S. Zhang, Y. Zhao, *Chemistry – A European Journal* **2011**, *17*, 12444-12451.

59.   Y. Zhao, Z. Zhong, *J. Am. Chem. Soc.* **2005**, *127*, 17894-17901.

60.   H. J. Schneider, A. K. Yatsimirsky, *Principles and methods in supramolecular chemistry*; New York: J. Wiley, **2000**, p 137-146.

CHAPTER 3.
INTRAMOLECULARLY ENHANCED MOLECULAR TWEEZERS WITH UNUSUALLY STRONG BINDING FOR AROMATIC GUESTS IN UNFAVORABLE SOLVENTS

Manuscript submitted.

Xiaoyu Xing and Yan Zhao

Abstract

Molecular tweezers using aromatic interactions for binding normally work best in polar instead of nonpolar solvents due to the strong solvophobic effect in the binding. Inspired by biological receptors that utilize "*delocalized binding interactions*" remote from the binding interface to strengthen guest-binding, we constructed molecular tweezers that have a reversed solvent effect. As the direct aromatic binding interactions were weakened by nonpolar solvent, guest-triggered intrahost interactions between two strategically placed carboxylic acids became stronger and contributed to the binding. This type of intramolecular enhancement of binding had a specific operating window.

Introduction

Molecular tweezers are commonly receptors with two cofacial aromatic arms linked by a rigid spacer. They are designed to "pick out" or bind aromatic guests with opposite electronic properties. This type of supramolecular hosts was first reported by Whitlock[1] and then popularized by Zimmerman.[2] Due to their unique topology and binding properties, molecular tweezers and analogues (e.g., molecular clips) have found wide applications in molecular recognition, chromatographic separation, and biology.[1-3]

The aromatic interactions involved in the binding of molecular tweezers have several contributions including electrostatics, van der Waals interactions, and a very strong solvophobic effect.[4] Iverson and co-workers reported that the binding constant (K_a) for a 1,5-

dialkoxynaphthalene (DAN) and a 1,4,5,8-naphthalenetetracarboxylic diimide (NDI) derivative increased from ~2 M^{-1} in chloroform to 30 M^{-1} in methanol and to >2000 M^{-1} in water.[5] The binding free energy was found to correlate roughly in a linear relationship to the $E_T(30)$ value of the solvent, which measures the solvent polarity.[6] The increase of binding with solvent polarity has been previously observed by Smithrud and Diederich between pyrene and its cyclophanes host as well, and was attributed to the low polarizability and high cohesive energy density of polar solvent that enhances the solvophobic interactions.[7]

Results and Discussion

In this work, we report a molecular tweezer displaying the opposite solvent effect in comparison to traditional tweezers. Although the unusual solvent effect had a certain window of operation, our method illustrates a strategy to overcome unfavorable solvation, which is frequently the cause of dissociation for desired supramolecular complexes in challenging solvent conditions.

$$\left[R' = (CH_2CH_2O)_nCH_3 \right]$$

1a, R = H; **1b**, (R = t-Bu)
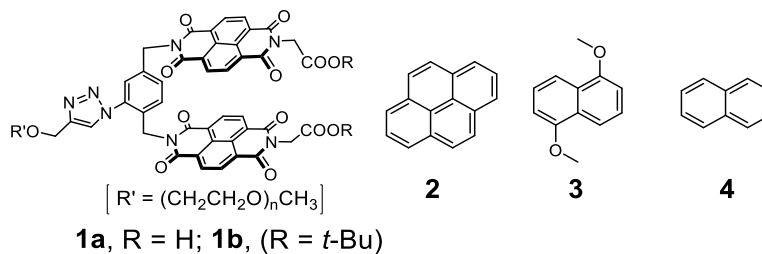
Scheme 1. Key compounds.

Receptor **1a** consists of two electron-deficient NDI groups joined by a *p*-xylylene spacer. The NDI arms are expected to bind electron-rich aromatic guests of appropriate size (e.g., **2**–**4**) through donor–acceptor (D–A) aromatic interactions. The receptor contains a poly(ethylene glycol) (PEG) chain for solubility in both polar and nonpolar solvents. In addition, the compound has two carboxylic acid groups that could hydrogen-bond

intramolecularly through the carboxylic acid dimer. Compound **1b** has two *tert*-butyl esters instead of the acids, and thus serves as the control receptor to understand the effect of the acids in the binding.

The design of **1a** was inspired by biological receptors with "*delocalized binding interactions*".[8] In these receptors, binding of the guest triggers partially or completely disengaged noncovalent interactions *within* the host. Because the *extra* intrahost interactions only occur upon the guest binding, they become part of the change in free energy during the binding process and contribute to the binding equilibrium. In this way, even though these intrahost interactions are remote from the binding interface, they help the binding indirectly and can be considered the "hidden binding interactions" of the host. Although still few and far between, such intramolecularly enhanced receptors have been synthesized.[9]
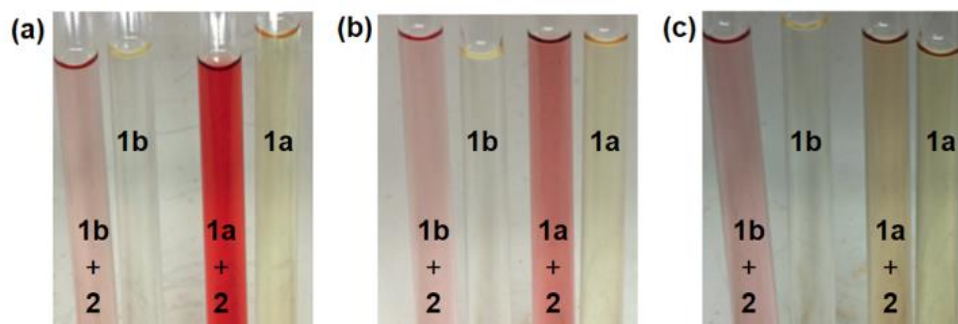
Figure 1. Photographs of receptors **1b** and **1a** in CDCl$_3$ in the presence and absence of pyrene **2** at 298 K with (a) 0 mM, (b) 4.6 mM, and (c) 42 mM NH$_3$. [**1a**] = [**1b**] = 2.0 mM. [**2**] = 8.0 mM.

Figure 1a shows the photographs of **1a** and **1b** in the presence and absence of pyrene (**2**) in CDCl$_3$. At 2 mM, **1a** was slightly yellow and **1b** colorless. Addition of 4 equiv pyrene turned the solution of **1b** pink and that of **1a** intense red. The pink/red color comes from the pyrene–NDI charge-transfer band. The more intense color of **1a**/pyrene in comparison to **1b**/pyrene indicates that the acids promoted the binding.

The importance of acids to the binding was verified further by the addition of a base such as ammonia or diisopropylethylamine (DIPEA). As shown by Figure 1b,c, the color of **1b**/pyrene stayed unchanged but the intense red color of **1a**/pyrene faded away when ammonia was added, indicating the dissociation of the complex. Not only did the experiment confirm the importance of the carboxylic acids in the binding, it also showed that the effect of ammonia was neither generic not related to other parts of the receptor, as it only affected **1a**/pyrene but not **1a**, **1b**, or **1b**/pyrene.

NOESY showed similar results. Figure 4 shows a 1:4 mixture of **1a** and pyrene (**4**) in CDCl$_3$ at 253 K. Significant cross peaks were observed between the NDI and the pyrenyl protons. The close distance between NDI and pyrene supports the insertion of pyrene in between the two NDI units, in agreement with the "tweezer" binding motif. Once the acids were converted into the *tert*-butyl esters, these cross peaks disappeared (Figure 5), confirming the dissociation of the complex. Addition of ammonia had the same effect (Figure 6).

The stronger binding of **1a** for pyrene was further confirmed by diffusion-ordered spectroscopy (DOSY). At 253 K, the NDI protons of **1a** at 8.56–8.85 ppm showed a diffusion coefficient of 2.063×10^{-9} m^2/s in CDCl$_3$ at ambient temperature (Figure 7). In the presence of 4 equiv pyrene, the diffusion coefficient decreased to $7.017–7.585 \times 10^{-10}$ m^2/s for NDI protons (Figure 8), indicating the formation of a species with a larger hydrodynamic radius.[10] For the *tert*-butyl ester derivative (**1b**), addition of the same amount of pyrene had little effect, with the diffusion coefficient of the NDI protons about $\sim 3 \times 10^{-9}$ m^2/s (Figures 9–10).

At this point, it is clear that the carboxylic acids helped tweezer **1a** to bind its guest. The question is how were they able to do so. One possibility is that the intramolecular carboxylic acid dimer preorganizes the receptor into a pseudo cyclophane, which has a better

formed binding pocket than an open tweezer. Although the suggestion seems reasonable, additional experiments showed that a more complex mechanism might be operating.
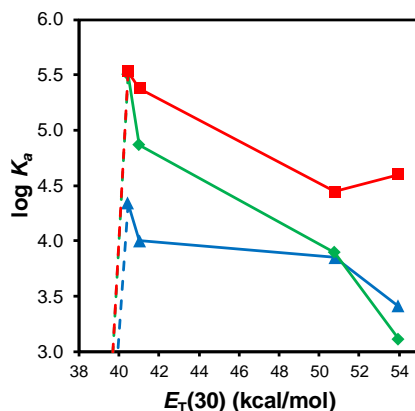

Figure 2. Binding constant of **2**(■), **3** (◆), and **4** (▲) by host **1a** as a function solvent polarity. The actual binding constants are reported in Table 2 in experimental section). The data points are connected to guide the eye. Binding in 3:2 hexane/DCM was too weak to be measured accurately.

Figure 2 shows the log K_a values between **1a** and **2**–**4** as a function of the $E_T(30)$ value of the solvent. The binding was studied in five solvents of varying polarity: 3:2 hexane/dichloromethane (DCM) ($E_T(30)$ value: 38.80), 1:4 hexane/DCM ($E_T(30)$ value: 40.44), DCM ($E_T(30)$ value: 41.02), 4:1 DCM/MeOH ($E_T(30)$ value: 50.78), and 1:4 DCM/MeOH ($E_T(30)$ value: 53.95) (Figure 11–13). The receptor started having solubility problems if solvents less polar than 3:2 hexane/DCM were used. Self-association of the host was ruled out by a dilution study (Figure 16). Large aggregation between the host and the guest was ruled out by dynamic light scattering (Figures 17–18 and Table 1 in experimental section).

The "normal" feature of Figure 2 is the overall positive correlation between the size/electron density of the guest and the binding affinity, i.e., **2** > **3** > **4** on average. This is fully expected for aromatic D–A interactions and results from the stronger van der Walls interactions and solvophobic effect with a larger binding interface.[4]

What is "abnormal" is the opposite solvent effect for the binding: instead of increasing with solvent polarity, log K_a showed an overall decrease for all three guests, in all solvents studied except 3:2 hexane/DCM, in which the binding plummeted.

Compound **1a** is by no means an optimized molecular tweezer, with multiple rotatable bonds in between the two NDI groups. In the literature, preorganization, either through covalent construction[2a, 2b] or metal complexation,[3c] is essential to the binding of molecular tweezers. Even for optimized tweezers, the binding constant was generally $<10^4$ M^{-1} for similarly sized aromatic guests in $CDCl_3$.[2a, 2b, 3c] For bis-NDI-based molecular tweezers with similar structures (with a meta linkage), their binding constant with pyrene was only ~130 M^{-1} in $CDCl_3$.[11] Another "abnormality" of **1a**, therefore, was its unusually strong binding, e.g., $K_a>10^5$ M^{-1} in 1:4 in hexane/DCM for **2** and **3**.[12] As shown earlier, once the acids were replaced by *t*-butyl esters (as in **1b**) or deprotonated by a base (Figure 1), only weak binding (which is normal in chloroform) was observed. The results were confirmed in UV titration (Table 2 in experimental section).

Taken together, our data— including the unusually strong binding of **1a**, the unconventional solvent effect, and the sudden drop of binding in the most nonpolar solvent— seem most consistent with intramolecular enhancement mentioned above.
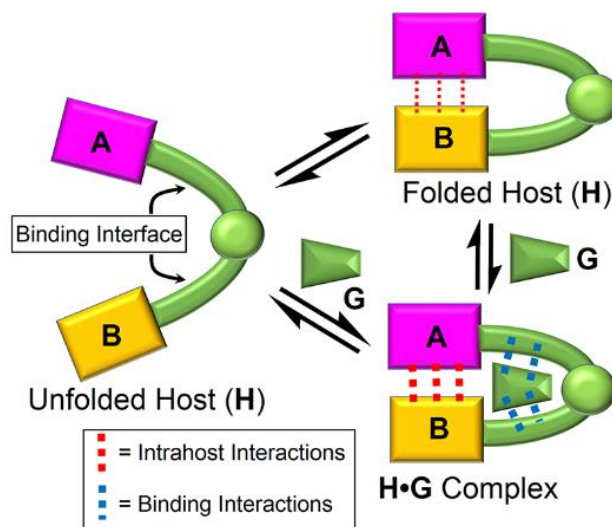
Scheme 2. Schematic representation of an intramolecularly enhanced receptor with guest-triggered intrahost interactions.

As shown in Scheme 2, an intramolecularly enhanced foldamer-like receptor could adopt a folded or unfolded conformation, depending on the solvent condition. The folded conformation is helped by the intrahost **A**–**B** interactions (i.e., the carboxylic acid dimer for **1a**) and should dominate in low-polarity solvents for **1a**.

The direct binding force between the host and the guest is the D–A aromatic interactions and is the strongest in methanol, the most polar solvent studied. The carboxylic acid dimer is weakened by solvent competition in methanol. Binding under this condition probably mainly derives from the strong aromatic D–A interactions.

As the solvent polarity decreases, the direct D–A binding force becomes weaker, the carboxylic acid dimer becomes stronger (a normal effect for hydrogen-bond-based interactions). The stronger **A**–**B** interaction can help the binding in two ways. First, it can better organize the binding site of tweezer **1a** by making it into a pseudo cyclophane. However, this cannot be the only effect involved, as a continued decrease of solvent polarity led to a precipitous drop of log K_a (Figure 2). The second reason, which could be more important, is

the dominance of intramolecular enhancement. Essentially, the **A**–**B** interaction is either completely disengaged (in the unfolded host) or weakly engaged (in the folded host). When the guest binds, the binding between the aromatic donor and the two NDI groups helps the receptor to fold and could help the formation of the carboxylic dimer. The guest-triggered, extra **A**–**B** interaction—shown by the bolder red dotted lines—becomes part of the free energy change in the binding and promotes the binding, as discussed earlier

As shown by Figure 19a, **1a** displayed characteristic changes in the UV-vis spectrum when different solvents (hexane/DCM and DCM/methanol) were used, consistent with large-scale conformational changes induced by the solvents. In contrast, **1b**, the *t*-butyl ester control, showed no change under the same conditions (Figure 19b).
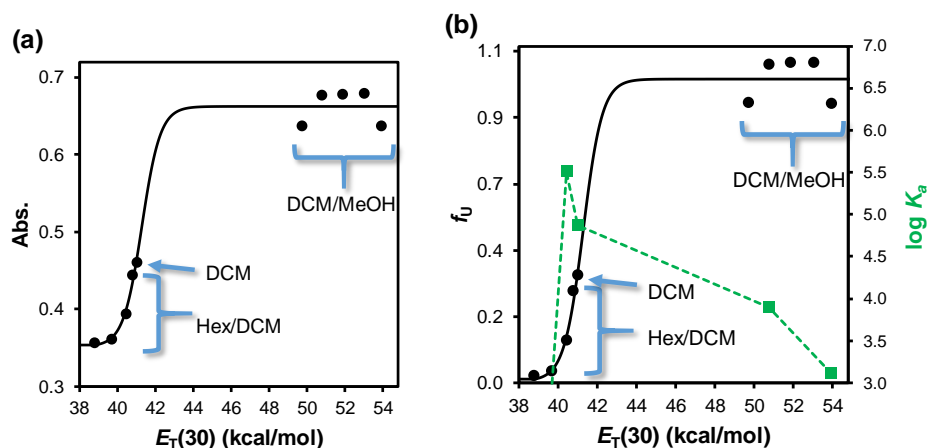
Figure 3. (a) Absorbance **1a** at 383 nm as a function of solvent polarity. [**1a**] = 15 μM. (b) Unfolded fraction as a function of solvent polarity. The smooth curve was from nonlinear least-squares fitting of the absorbance to the two-state transition model. The data points connected by the green dashed line correspond to log K_a of **1a** for **3**.

Our previous work shows that intramolecularly enhanced receptors often display a correlation between the receptor's conformation and its binding ability.[9f, 9g] As shown by Figure 3a, the absorbance of **1a** at 383 nm fit reasonably to a two-state transition model (folded ⇆ unfolded). Note that the clustering of the DCM/MeOH data points on the right happened

because even a small amount of methanol in DCM/MeOH mixtures increased the $E_T(30)$ value of the solvent dramatically. The two-state model is frequently used to understand the conformational transition of proteins[13] and solvophobic foldamers.[14] The hallmark of a two-state transition is a sigmoidal titration curve, when a denaturing solvent is added to the medium to unfold the chain.[13-14] The two-state fitting suggests that **1a** was unfolded in methanol/DCM mixtures and fully folded in solvents less polar than 3:2 hexane/DCM ($E_T(30) \approx 40$ in Figure 3b).

When the log K_a curve of **1a**/**3** is overlaid with the folding/unfolding curve, the binding is the strongest when the host was in the conformational transition but decreases when the receptor moves in the fully folded or unfolded regions. This trend is similar to the previously reported receptors with guest-triggered intrahost interactions. [9f, 9g] The rationale for this trend is that, when the receptor is too far in the unfolded region, binding (which occurs in the folded receptor) needs to first overcome an unfavorable folding equilibrium and is disfavored. On the other hand, in the most nonpolar solvents—i.e., with $E_T(30) < 40$ or in 3:2 hexane/DCM—the receptor is completely folded and possibly with the carboxylic acids fully engaged in the intramolecular dimer prior to binding due to the strength of hydrogen bonds. Under such a condition, the direct binding force (aromatic interactions) is very weak in nonpolar solvents,[5, 7] and intramolecular enhancement is not possible, because the guest binding cannot strengthen the already strong carboxylic acid dimer. Weak binding is fully expected as a result.

Conclusion

Traditional receptors rely on direct host–guest binding forces to achieve strong binding. The inevitable drawback of such receptors is their compromise by competitive solvents which could involve similar noncovalent interactions as the host–guest complex. This is frequently encountered by hydrogen-bonded systems in aqueous solution or aromatic receptors as

discussed in this work in nonpolar solvents. This work illustrates that, by equipping the host with appropriate guest-triggered intramolecular interactions, we can reverse the conventional solvent effect of the direct binding force. The net result is the ability for the receptor to operate under unfavorable solvent conditions and enhancement of the binding constant. We believe the design principle is general and can be very useful when unfriendly medium effects are the key impediment to a supramolecular process.

Acknowledgement

Experimental Section

General Method

For spectroscopic purpose, methanol, and dichloromethane (DCM) were of HPLC grade. All other reagents and solvents were of ACS-certified grade or higher, and were used as received from commercial suppliers. Routine ^{1}H and ^{13}C NMR spectra were recorded on a Bruker DRX-400, on a Bruker AV II 600 or on a Varian VXR-400 spectrometer. Variable temperature ^{1}H NMR spectra, nuclear Overhauser effect spectroscopy (NOESY), and diffusion ordered spectroscopy (DOSY) were recorded on a Bruker AV II 600 spectrometer. UV-vis spectra were recorded at ambient temperature on a Cary 100 Bio UV-visible spectrophotometer. Dynamic light scattering (DLS) data were recorded at 25 °C using PDDLS/ CoolBatch 90T with PD2000DLS instrument.

Syntheses

Syntheses of compounds **9**[15], **11**[16], **13**[17] and **14**[18] were previously reported.
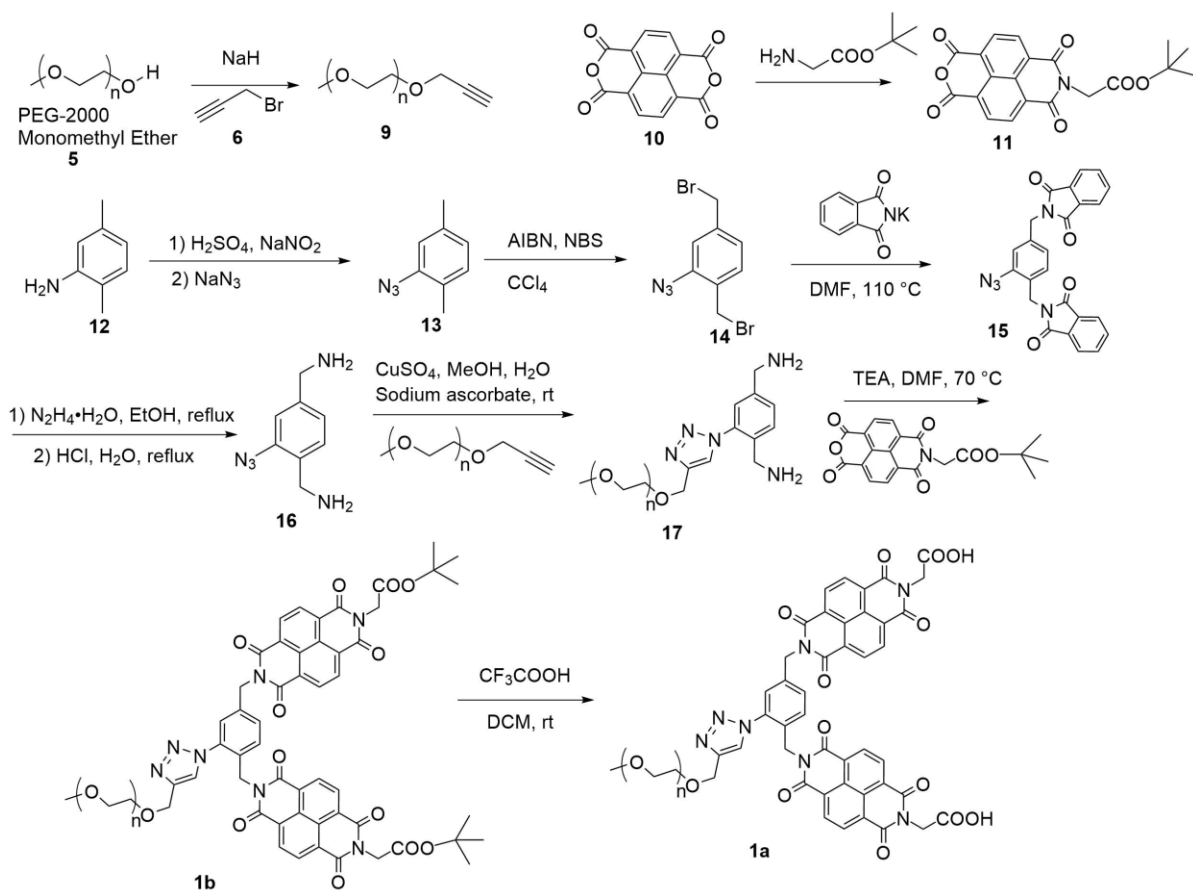
Scheme 3. Synthetic routhe.

Compound 15. Compound **14** (2.29 g, 7.52 mmol) and potassium phthalimide (3.06 g, 16.6 mmol) were dissolved in DMF (50 mL). After the reaction mixture was stirred at 110 °C overnight, TLC showed completion of the reaction. The mixture was cooled down to room temperature. The precipitate was filtered and washed with cold dichloromethane (3×15 mL) to give a white powder (2.36 g, 72%). The product was used in the next step without further purification.

Compound 16. Compound **15** (355 mg, 0.812 mmol) and hydrazine monohydrate (101 mg, 2.01 mmol) were combined in ethanol (30 mL). The reaction mixture was heated to reflux and stirred overnight. After TLC showed completion of the reaction, the mixture was concentrated by rotary evaporation. Aqueous hydrochloric acid (3M, 50 mL) was added and

the reaction mixture was heated to reflux overnight. After the reaction mixture was cooled down to room temperature, sodium hydroxide pellets were added slowly until pH = 12. The mixture was extracted with dichloromethane (3×30 mL). The combined organic layer was washed with brine (30 mL) and dried with $MgSO_4$. The solvent was removed by rotary evaporation to give a green oil (131 mg, 91%). ^{1}H NMR (600 MHz, $CDCl_3$, δ) 7.24 (d, $J = 7.7$ Hz, 1H), 7.14 (s, 1H), 7.05 (d, $J = 7.2$ Hz, 1H), 3.89 (s, 2H), 3.76 (s, 2H). ^{13}C NMR (151 MHz, $CDCl_3$, δ) 143.9, 138.1, 133.2, 129.5, 123.8, 117.0, 46.1, 42.7. ESI-MS (*m/z*): [M+H][+] cacld for $C_8H_{11}N_5$, 178.1087; found, 178.1090.

Compound 17. To a solution of **16** (91.8 mg, 0.518 mmol) in a1:1 water/methanol mixture (20 mL), copper sulfate hydrate (11.0 mg, 0.0441 mmol), sodium ascorbate (103 mg, 0.520 mmol), and **6** (1.06 g, 0.520 mmol) were added. After being stirred at room temperature for 12 h, the reaction mixture was concentrated by rotary evaporation. The resulting solution was diluted with water (30 mL) and extracted with dichloromethane (3×40 mL). The combined organic layer was washed with brine (30 mL). The dichloromethane solution was filtered through a layer of celite and the celite was washed with methanol (3×50 mL). The organic solvents were removed by rotary evaporation to give a yellow-green solid, which was used in the next step without further purification.

Compound 1b. To a solution of **17** (424 mg, 0.191 mmol) and **11** (219 mg, 0.574 mmol) in DMF (20 mL), triethylamine (508 mg, 5.02 mmol) was added. After being stirred at 70 °C overnight, the reaction mixture was concentrated by rotary evaporation. The residue was purified by flash column chromatography over silica gel with 10:1 dichloromethane/methanol as the eluent to give a brown solid (132 mg, 27%). ^{1}H NMR (600 MHz, $CDCl_3$, δ) 8.75 (dd, $J = 9.2, 4.8$ Hz, 6H), 8.69 (d, $J = 7.6$ Hz, 2H), 8.08 (s, 1H), 7.65 (d, $J = 8.3$ Hz, 1H), 7.56 (s, 1H),

7.38 (d, $J = 8.1$ Hz, 1H), 5.39 (s, 2H), 5.27 (s, 2H), 4.84 (s, 4H), 4.80 (s, 2H), 3.80-3.52 (series of m, multiple H), 3.37 (s, 3H), 1.49 (s, 18H). ^{13}C NMR (151 MHz, CDCl$_3$, δ) 166.5, 166.4, 162.7, 162.5, 162.3, 162.3, 145.1, 137.1, 136.1, 132.2, 131.29, 131.27, 131.2, 128.7, 127.0, 126.85, 126.82, 126.7, 126.51, 126.46, 126.44, 126.38, 124.9, 82.7, 77.4, 71.9, 70.53, 70.47, 69.9, 64.6, 59.0, 55.9, 50.6, 43.0, 42.3, 39.7, 28.0. ESI-MS (*m/z*): [M+3H]$^{3+}$ multiple peaks centered at 978.7941 and separated by 14.6775 from the PEG chain.

Compound 1a. To a solution of **1b** (29.6 mg, 0.0101 mmol) in dichloromethane (5 mL), trifluoroacetic acid (5 mL) was added. After being stirred at room temperature overnight, the reaction mixture was concentrated by rotary evaporation. The residue was purified by flash column chromatography over silica gel with 7:1 dichloromethane/methanol as the eluent to give a brown gel (21.1 mg, 74%). ^{1}H NMR (600 MHz, CDCl$_3$, δ) 8.71 (d, $J = 14.5$ Hz, 6H), 8.65 (d, $J = 7.5$ Hz, 2H), 8.06 (s, 1H), 7.67 (d, $J = 8.3$ Hz, 1H), 7.49 (s, 1H), 7.47 (s, 1H), 5.40 (s, 2H), 5.28 (s, 2H), 4.93 (s, 4H), 4.78 (s, 2H), 4.49 (t, $J = 4.5$ Hz, 3H), 3.87-3.36 (series of m, multiple H). ^{13}C NMR (151 MHz, CDCl$_3$, δ) 168.7, 162.6, 162.4, 162.0, 144.3, 137.1, 135.2, 131.0, 130.8, 130.60, 130.56, 129.4, 127.9, 126.7, 126.5, 126.4, 126.01, 125.99, 125.6, 125.5, 125.4, 125.3, 72.3, 71.2, 69.74, 69.71, 69.67, 69.6, 69.5, 69.1, 67.5, 67.4, 63.4, 60.2, 57.9, 42.7, 41.4. ESI-MS (*m/z*): [M+3H]$^{3+}$ multiple peaks centered at 970.7478 and separated by 14.6739 from the PEG chain.

Solvent Study by UV-Vis Spectroscopy and Data Analysis Method

Stock solution of **1a** (4.0 mM) and **1b** (4.0 mM) in DCM were prepared. For the solvent titration, a typical procedure is as follows. An aliquot of the stock solution was added to 2.00 mL of the appropriate solvent in a quartz cuvette. Concentration of the receptors was15 μM. The sample was gently vortexed for 30 s before the absorbance spectrum was collected at 298 K.

Literature method[19] was followed in the two-state curve fitting for the absorbance data for hosts **1a**:
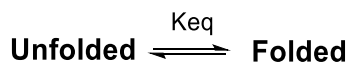
$$\text{Unfolded} \underset{}{\overset{Keq}{\rightleftharpoons}} \text{Folded}$$

According to the two-state model, at any given concentration of the denaturant (i.e., MeOH), only the folded and unfolded conformations are present and their fractions are represented by f_F and f_U. Fraction of the unfolded conformation can be calculated by:

$$K_{eq} = f_F/f_U$$

$$f_F = (I-I_U)/(I_F-I_U)$$

$$f_U = 1-f_F$$

I is the absorbance at a certain solvent composition. I_U is the absorbance at fully unfolded state, and I_F is that at fully folded state.

The equilibrium constant (K_{eq}) and the free energy (ΔG) for the folding reaction can be calculated using:

$$\Delta G = -RT \ln K_{eq} = -RT \ln(f_F/f_U) = -RT \ln[(1-f_U)/f_U]$$

In the two-state model, the free energies are linearly related to the concentration of denaturant and are assumed to have the same relationship to the $E_T(30)$ values of the solvent:

$$\Delta G = \Delta G_0 + m E_T(30)$$

Then we can obtain equations:

$$f_F = 1/(1+1/\exp(-(\Delta G_0 + m E_T(30)/RT)))$$

$$I = I_U + (I_F-I_U)/(1+1/\exp(-(\Delta G_0 + m E_T(30))/RT))$$

A nonlinear least-squares fitting of the experimental data to above equation affords the two-state folding-unfolding curves and f_U.

Titration by UV-Vis Spectroscopy and Data Analysis Method

Stock solution of **1a** (4.0 mM) and **1b** (4.0 mM) in DCM were prepared. Stock solutions of the guest (**2-4**) were prepared in the appropriate solvent mixture, in which titrations would be performed. For the titrations, a typical procedure is as follows. An aliquot of the host stock solution was added to 2.00 mL solvent in a quartz cuvette. Concentration of the receptors varies from 15 μM to 30 μM based on signal strength. The sample was gently vortexed for 30 s before its UV-vis spectrum was recorded. Aliquots of the guest was added and the spectrum was recorded after each addition. The titration was continued until saturation was reached and the total volume of the guest solution added was kept below 100 μL. The binding constant was obtained by nonlinear least squares curving fitting of the absorbance values to the 1:1 binding isotherm.[20] Titrations were repeated at least twice. The average with standard deviation as uncertainty was reported as final value.
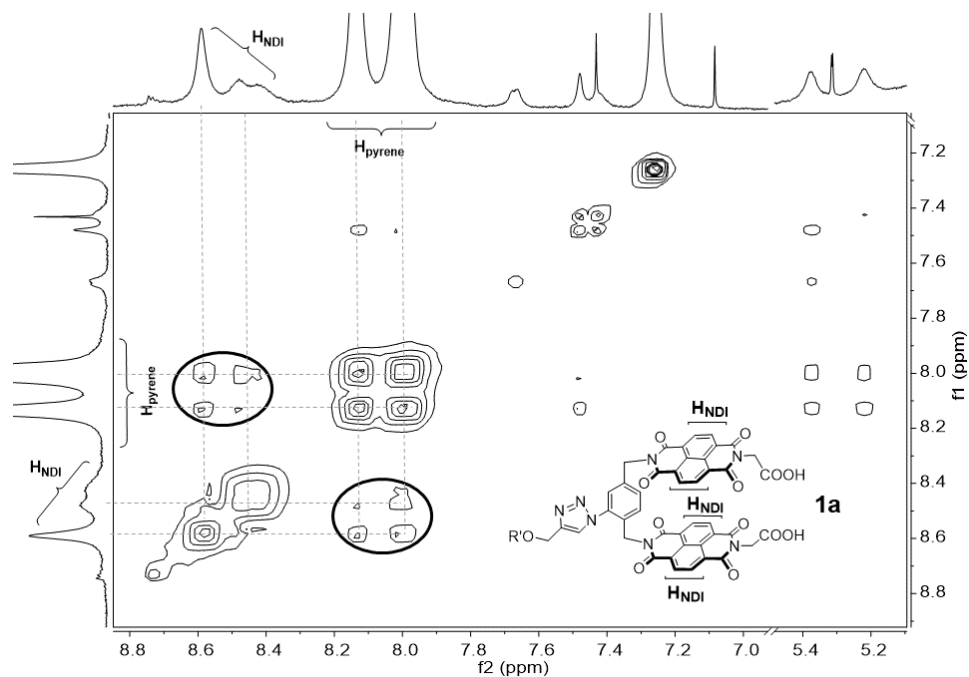
Figure 4. NOESY spectrum of 0.6 mM host **1a** with 2.5 mM pyrene in CDCl$_3$ at 253 K. Low temperature was used to enhance the binding and the cross-peaks. The NDI peaks were sharp at room temperature but became broad at 253 K, especially in the presence of pyrene (Figures 14–15). The cross peaks in the circles were between the NDI protons of host **1a** and pyrene.
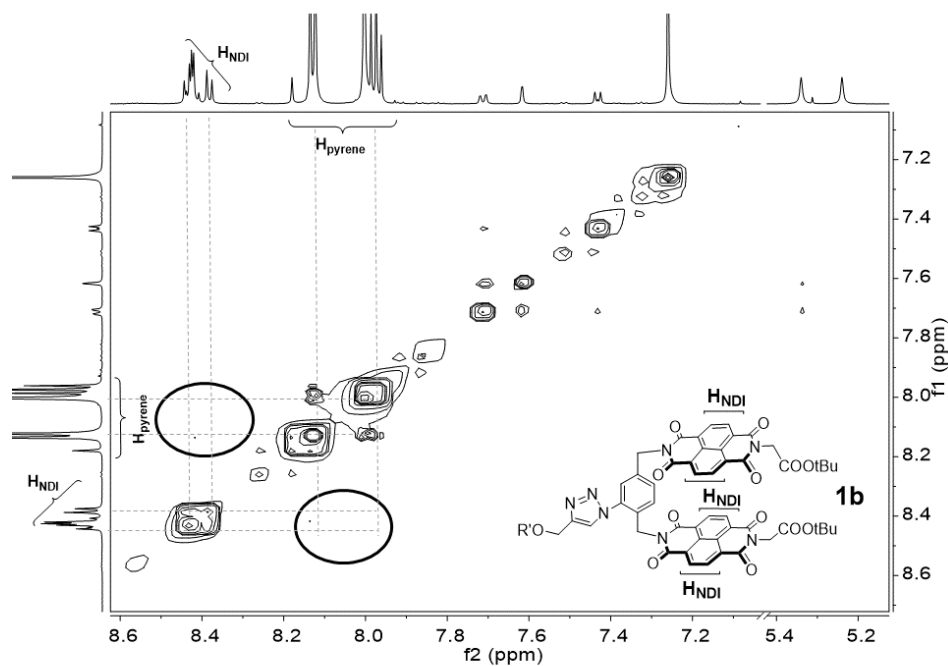
Figure 5. NOESY spectrum of 2 mM host **1b** with 8 mM pyrene in CDCl$_3$ at 253 K. Insignificant coupling was found between the NDI protons of host **1b** and pyrene.
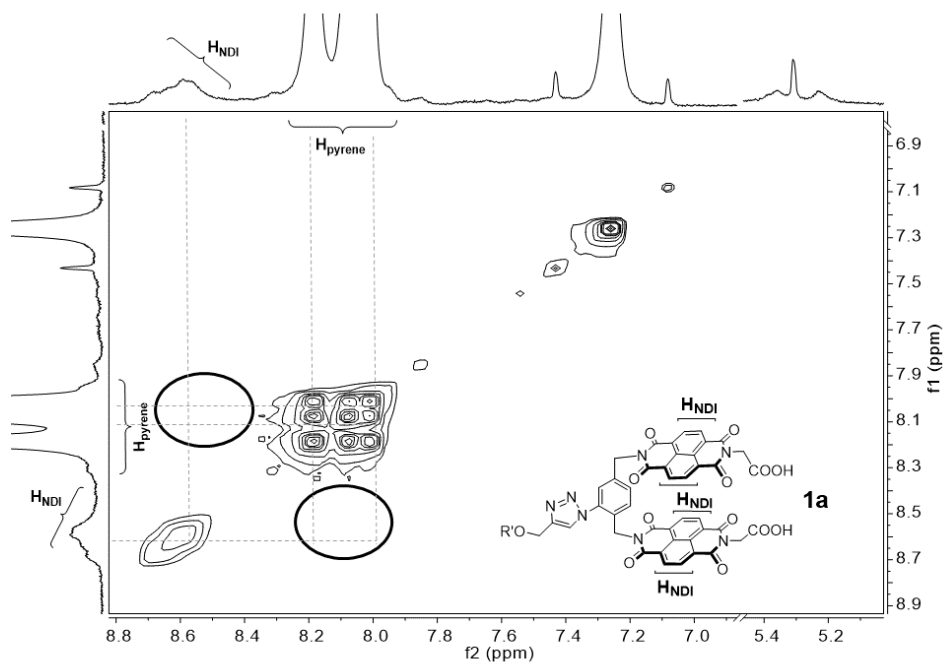
Figure 6. NOESY spectrum of 0.6 mM host **1a** with 2.5 mM pyrene and 11.4 mM ammonia in CDCl$_3$ at 253 K.
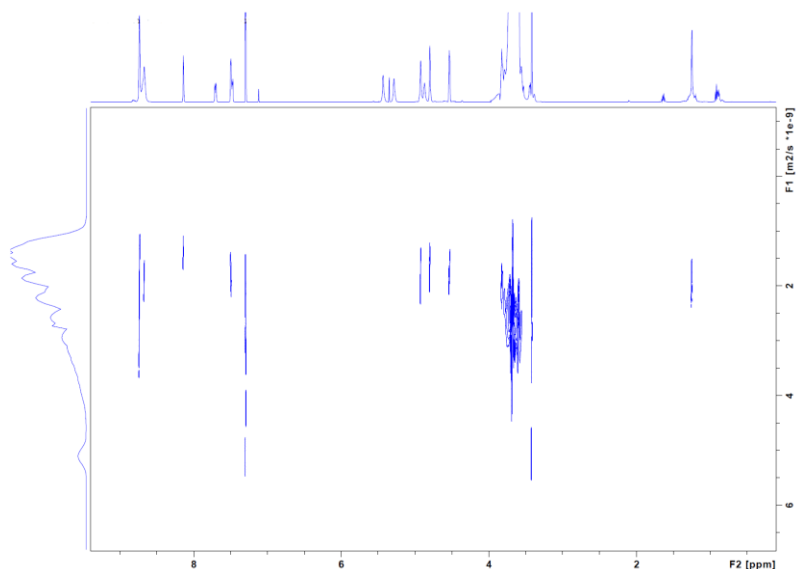
Figure 7. DOSY spectrum of 0.6 mM host **1a** in CDCl$_3$ at 253 K with diffusion coefficients of 2.063×10^{-9} m^2/s at 8.85-8.56 ppm (protons on NDI moieties), 1.964×10^{-9} m^2/s at 8.20-8.07 ppm.
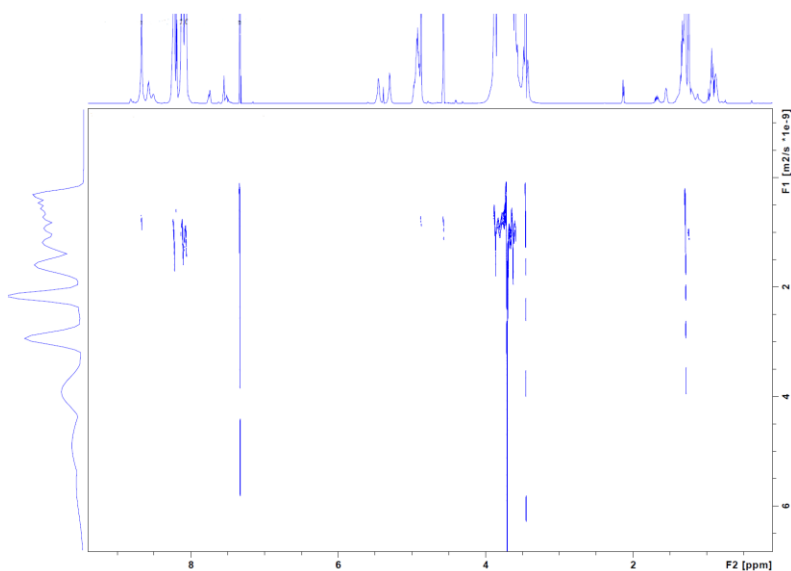
Figure 8. DOSY spectrum of 0.6 mM host **1a** with 2.5 mM pyrene in CDCl$_3$ at 253 K with diffusion coefficients of 7.017×10^{-10} m^2/s at 8.73-8.62 ppm and 7.585×10^{-10} m^2/s at 8.62-8.45 ppm (protons on NDI moieties), 1.105×10^{-9} m^2/s at 8.32-8.16 ppm and 1.149×10^{-9} m^2/s at 8.16-7.99 ppm (protons on pyrene).
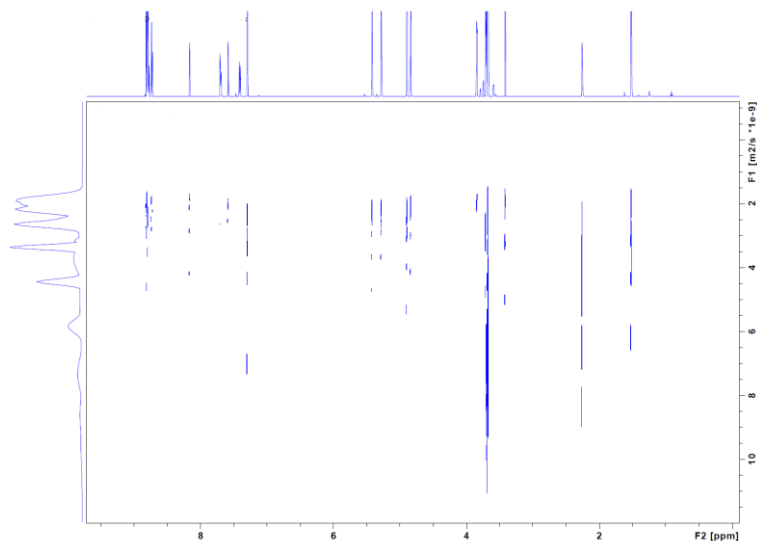
Figure 9. DOSY spectrum of 2 mM host **1b** in CDCl$_3$ at 253 K with diffusion coefficients of 3.351×10^{-9} m^2/s at 8.85-8.76 ppm, 3.634×10^{-9} m^2/s at 8.76-8.71 ppm (protons on NDI moieties), 3.146×10^{-9} m^2/s at 8.19-8.14 ppm.
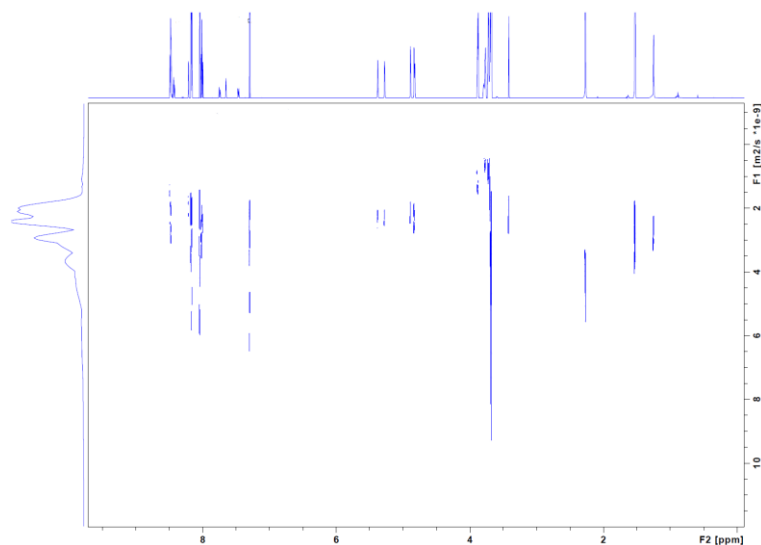
Figure 10. DOSY spectrum of 2 mM host **1b** with 8 mM pyrene in CDCl$_3$ at 253 K with diffusion coefficients of 2.820×10^{-9} m^2/s at 8.51-8.45 ppm and 3.573×10^{-9} m^2/s at 8.45-8.41 ppm (protons on NDI moieties), 1.430×10^{-9} m^2/s at 8.23-8.20 ppm, 3.550×10^{-9} m^2/s at 8.20-8.13 ppm and 3.812×10^{-9} m^2/s at 8.07-7.98 ppm (protons on pyrene).
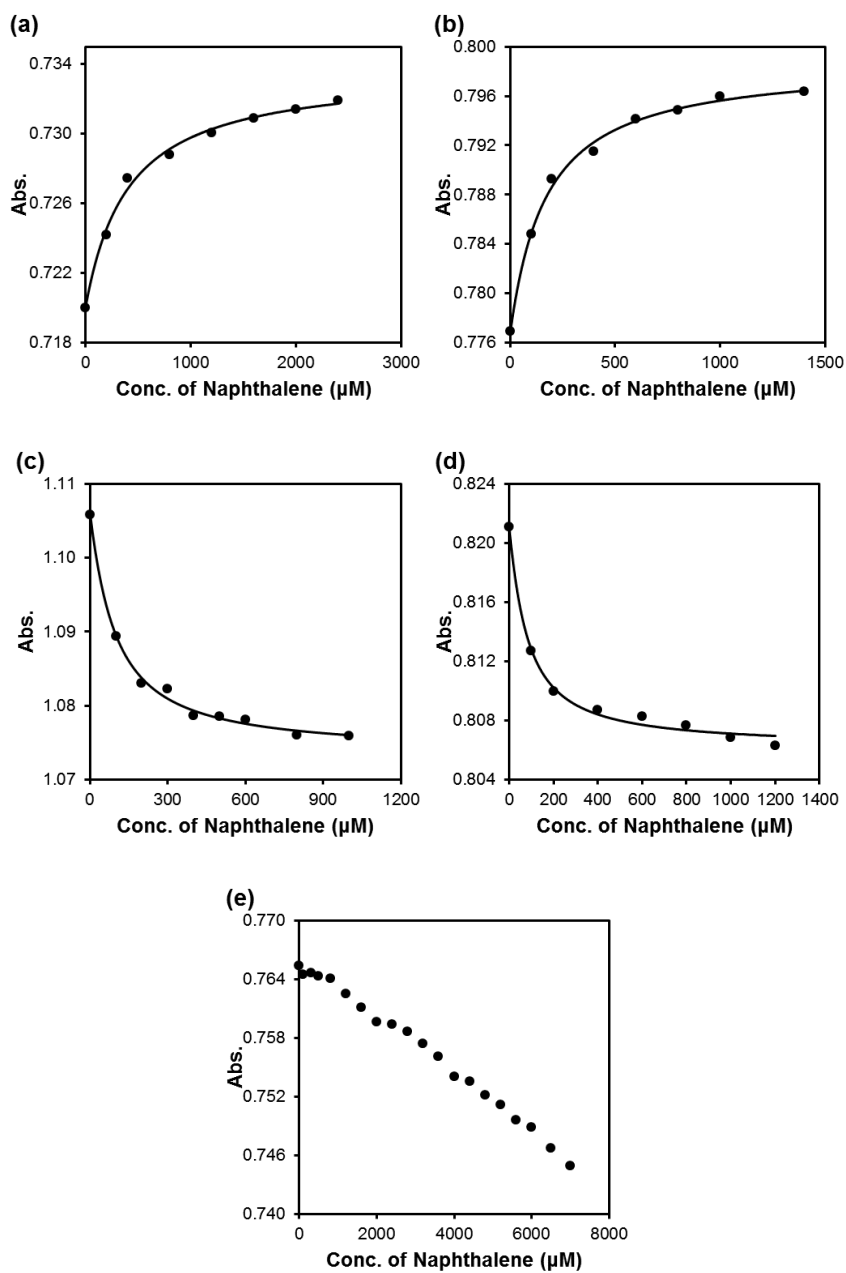
Figure 11. UV-vis titration curves of compound **1a** by naphthalene in (a) 1:4 DCM/MeOH (v/v), [**1a**] = 15 μM, (b) 4:1 DCM/MeOH (v/v), [**1a**] = 15 μM, (c) DCM, [**1a**] = 30 μM, (d) 1:4 Hexane/DCM (v/v), [**1a**] = 30 μM and (e) 3:2 Hexane/DCM (v/v), [**1a**] = 30 μM. The UV absorbance at 382 nm was monitored and the smooth curve was from nonlinear least squares curving fitting to a 1:1 binding isotherm.
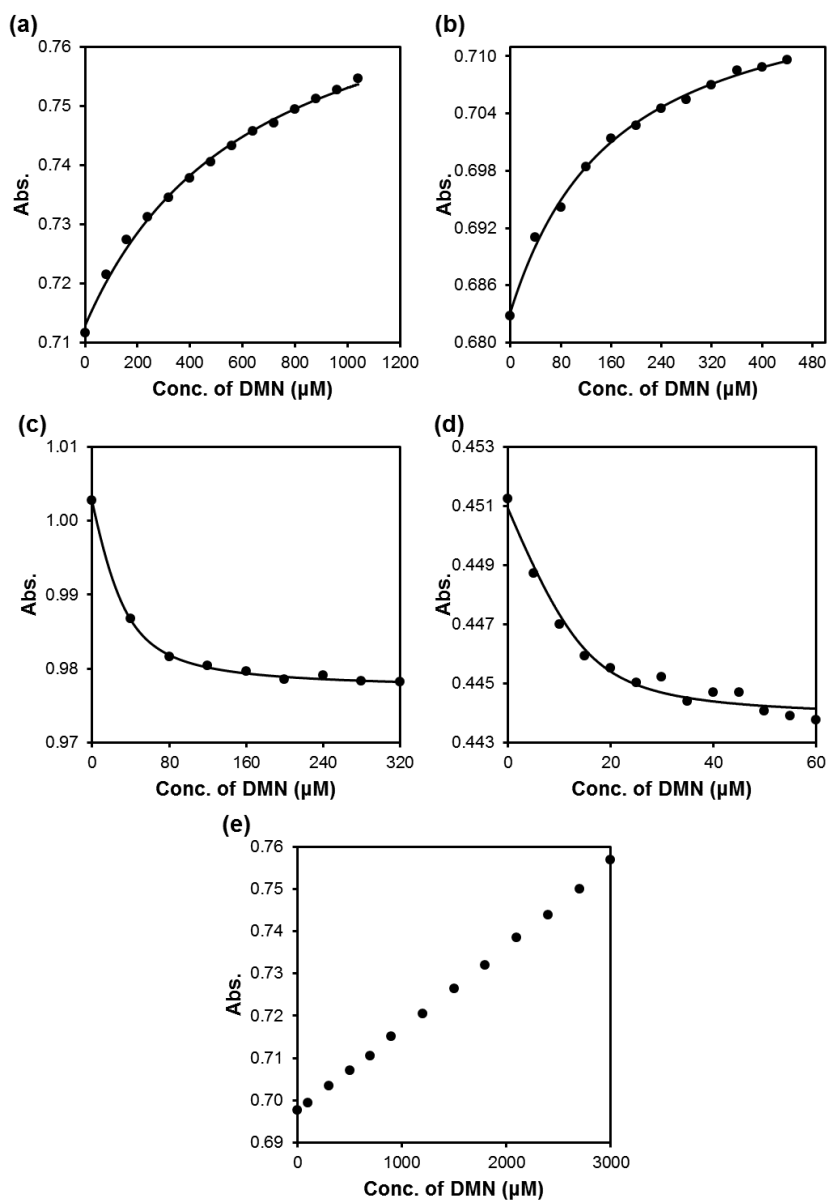
Figure 12. UV-vis titration curves of compound **1a** by 1,5-dimethoxynaphthalene in (a) 1:4 DCM/MeOH (v/v), [**1a**] = 15 μM, (b) 4:1 DCM/MeOH (v/v), [**1a**] = 15 μM, (c) DCM, [**1a**] = 30 μM, (d) 1:4 Hexane/DCM (v/v), [**1a**] = 15 μM and (e) 3:2 Hexane/DCM (v/v), [**1a**] = 30 μM. The UV absorbance at 382 nm was monitored and the smooth curve was from nonlinear least squares curving fitting to a 1:1 binding isotherm.
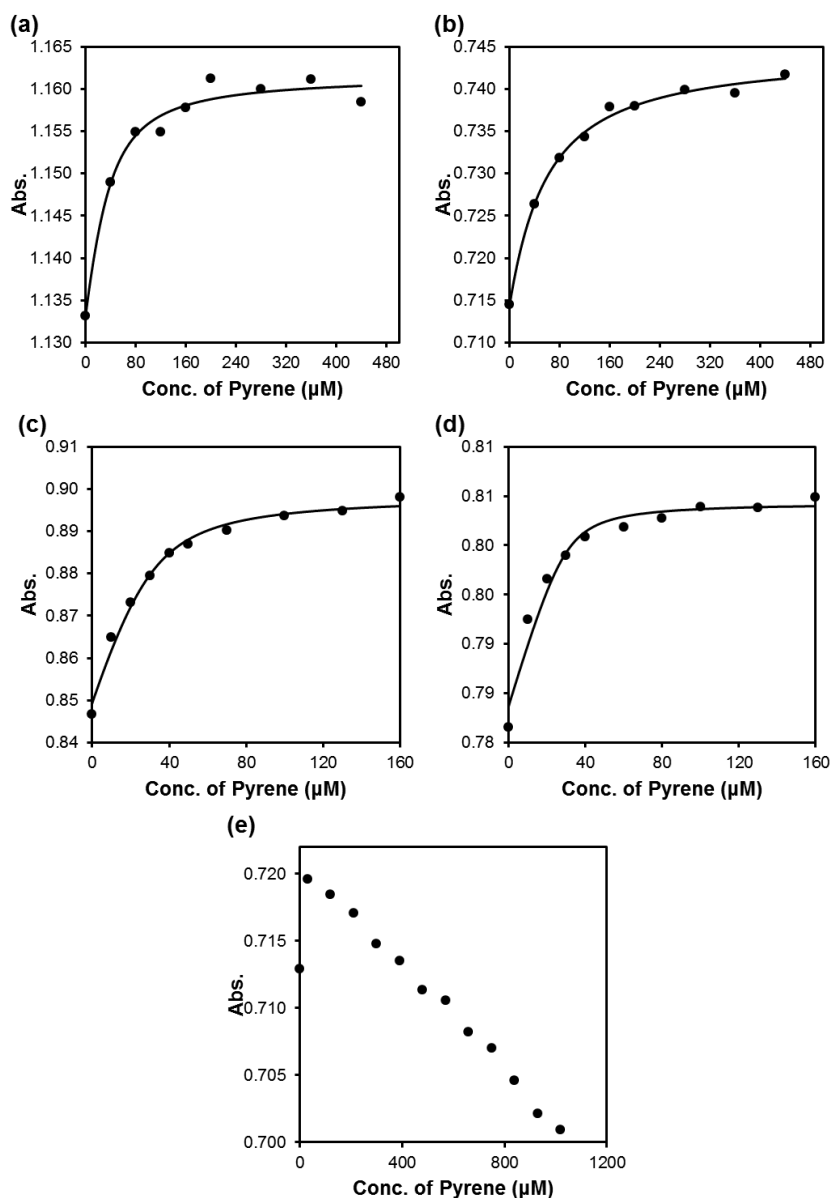
Figure 13. UV-vis titration curves of compound **1a** by pyrene in (a) 1:4 DCM/MeOH (v/v), [**1**] = 30 μM, (b) 4:1 DCM/MeOH (v/v), [**1a**] = 15 μM, (c) DCM, [**1a**] = 30 μM, (d) 1:4 Hexane/DCM (v/v), [**1a**] = 30 μM and (e) 3:2 Hexane/DCM (v/v), [**1a**] = 30 μM. The UV absorbance at 382 nm was monitored and the smooth curve was from nonlinear least squares curving fitting to a 1:1 binding isotherm.
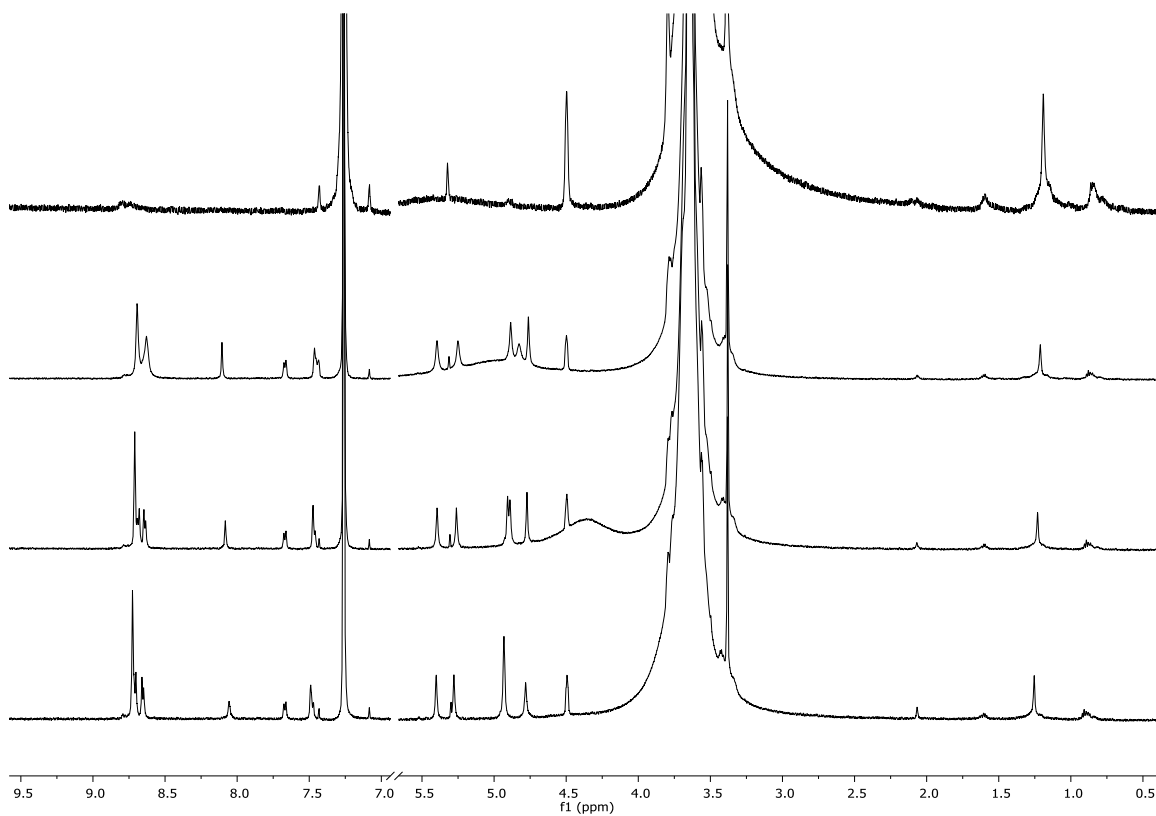
Figure 14. NMR spectra of 2 mM host **1a** in CDCl₃ at different temperatures. Temperature from bottom to top was 298 K, 273 K, 253 K, and 233 K.
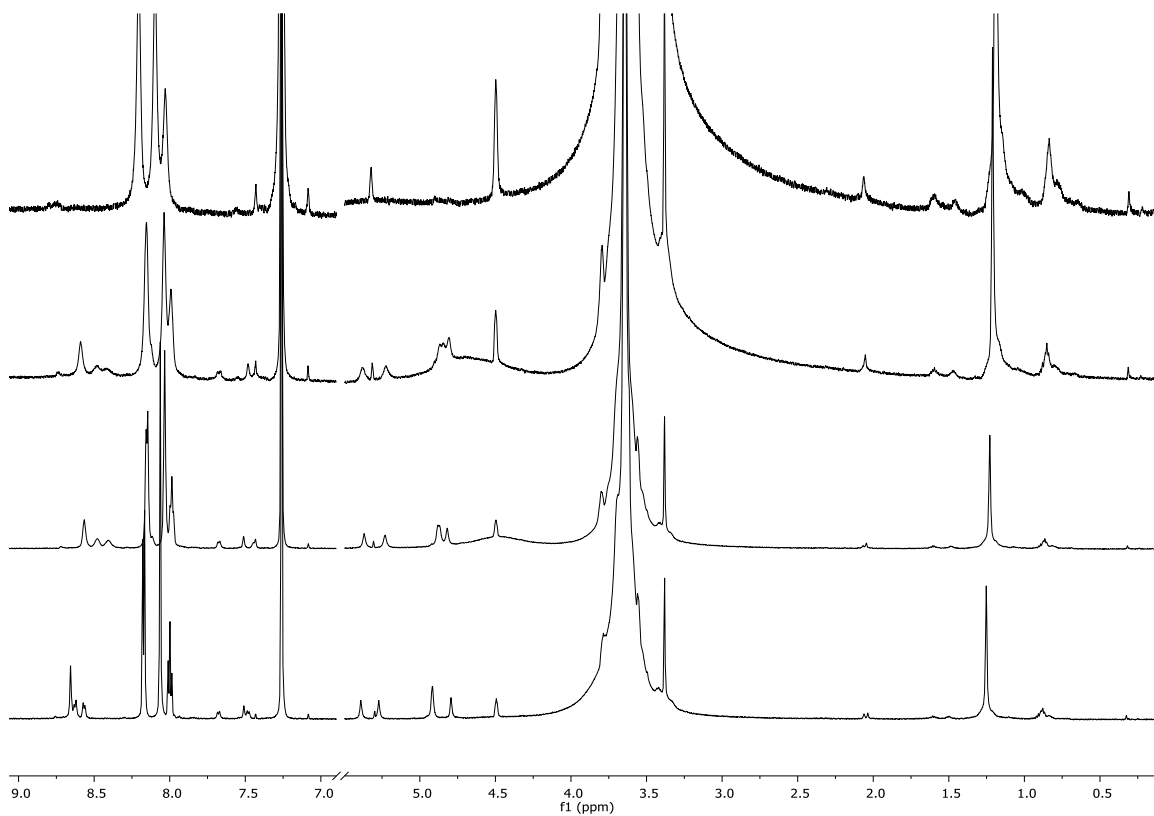
Figure 15. NMR spectra of 2 mM host **1a** with 3 mM pyrene in CDCl$_3$ at different temperatures. Temperature from bottom to top was 298 K, 273 K, 253 K, and 233 K.
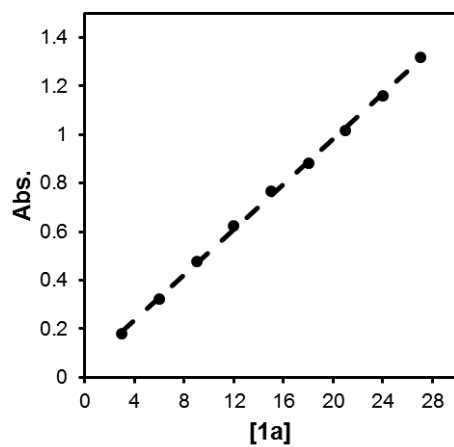
Figure 16. UV-vis absorbance as a function of [1a] in μM with linear trend line of R2=0.9991.
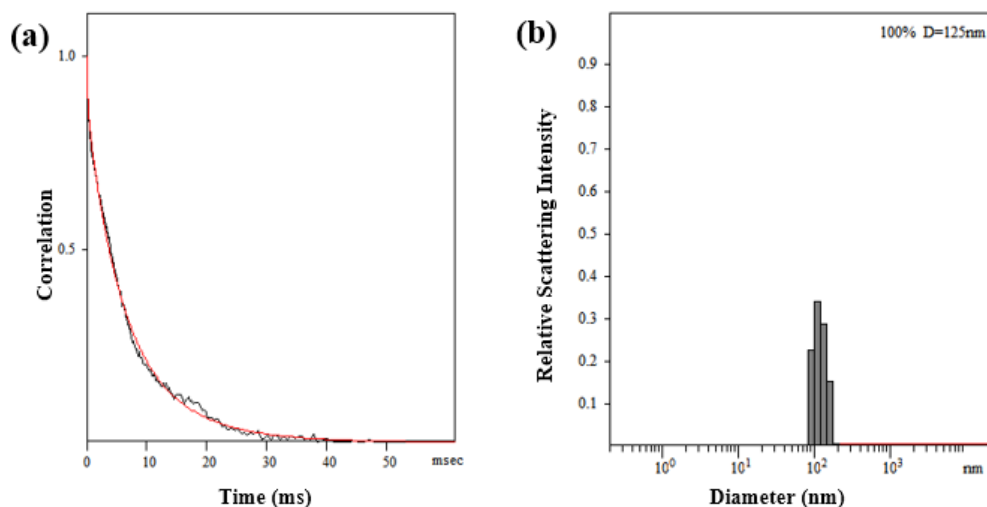
Figure 17. Representative dynamic light scattering (a) correlation curve and (b) distribution of the hydrodynamic diameter of 1a with pyrene in DCM, [1a] = 100 μM, [pyrene] = 500 μM. The diameter average from 50 raw data is 121 nm.
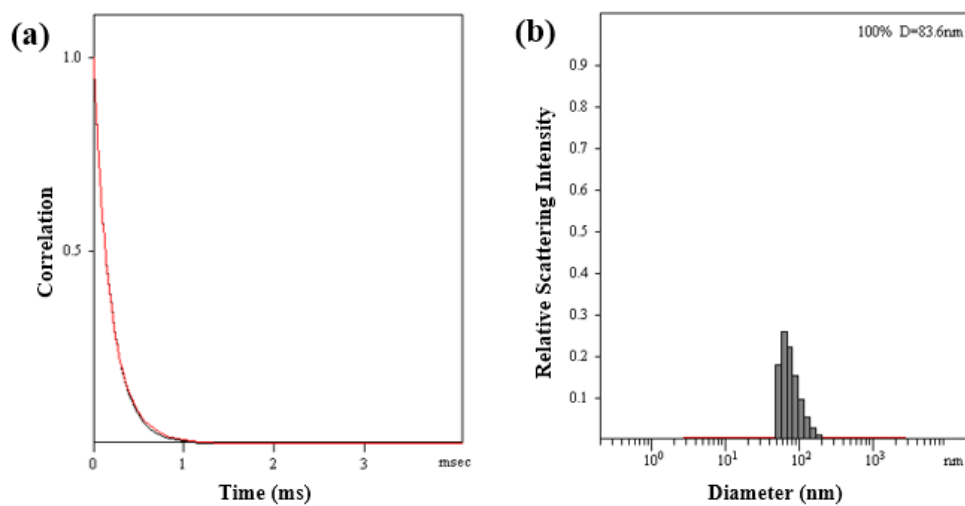
Figure 18. Representative dynamic light scattering (a) correlation curve and (b) distribution of the hydrodynamic diameter of 1a with pyrene in hexane/DCM 3/2, [1a] = 100 μM, [pyrene] = 500 μM. The diameter average from 50 raw data is 79.1 nm.
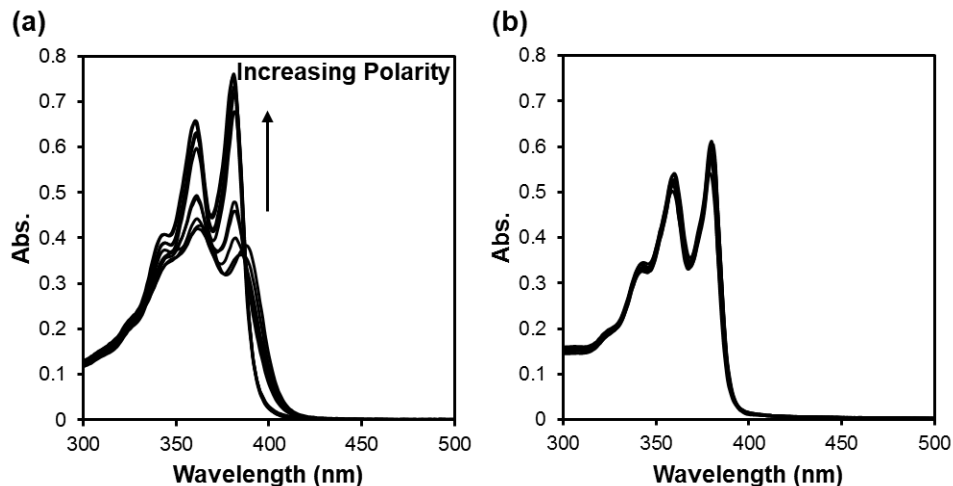
Figure 19. (a) UV-Vis spectra of compound 1a in DCM/methanol mixtures and hexane/DCM mixtures, [1a] = 15 μM. (b) UV-vis spectra of compound 1b in DCM/methanol mixtures and hexane/DCM mixtures, [1b] = 30 μM.

Table 1. Averaged hydrodynamic diameters for 1a with pyrene in DCM and 3:2 hexane/DCM from dynamic light scattering at 298 K. [1a] = 100 μM. Viscosity and refractive index of solvent mixture was approximately calculated from linear composition of volume fraction of individual solvent.

Entry	Solvent	[Pyrene] (μM)	Diameter[a] (nm)
1		0	119 ± 23
2		100	118 ± 21
3	DCM	200	134 ± 57
4		300	124 ± 27
5		400	129 ± 41
6		500	121 ± 38
7		0	85.6 ± 3.6
8		100	85.3 ± 3.4
9	3:2	200	81.6 ± 2.8
10	Hexane/DCM	300	75.1 ± 4.4
11		400	84.0 ± 3.7
12		500	79.1 ± 4.6

[a] Individual hydrodynamic diameter was generated from dynamic light scattering. Average was calculated from nearly 50 raw data, standard deviation of which was used as uncertainty.

Table 2. Binding constants of hosts 1a and 1b with guests in different solvents at 298K. All binding constants were averages of two titrations with standard error as uncertainty.

Entry	Host	Guest	Solvent(s)	K_a (M^{-1})
1[a]	**1a**	Naphthalene	Hex/DCM 3/2 (v/v)	-
2	**1a**	Naphthalene	Hex/DCM 1/4 (v/v)	$(2.2 \pm 0.1) \times 10^4$
3	**1a**	Naphthalene	DCM	$(1.0 \pm 0.3) \times 10^4$
4	**1a**	Naphthalene	DCM/MeOH 4/1 (v/v)	$(7.1 \pm 1.4) \times 10^3$
5	**1a**	Naphthalene	DCM/MeOH 1/4 (v/v)	$(2.57 \pm 0.04 \times 10^3$
6[a]	**1a**	DMN	Hex/DCM 3/2 (v/v)	-
7	**1a**	DMN	Hex/DCM 1/4 (v/v)	$(3.2 \pm 1.1) \times 10^5$
8	**1a**	DMN	DCM	$(7.4 \pm 0.8) \times 10^4$
9	**1a**	DMN	DCM/MeOH 4/1 (v/v)	$(7.8 \pm 3.4) \times 10^3$
10	**1a**	DMN	DCM/MeOH 1/4 (v/v)	$(1.3 \pm 0.8) \times 10^3$
11[a]	**1a**	Pyrene	Hex/DCM 3/2 (v/v)	-
12	**1a**	Pyrene	Hex/DCM 1/4 (v/v)	$(3.4 \pm 1.0) \times 10^5$
13	**1a**	Pyrene	DCM	$(2.4 \pm 1.4) \times 10^5$
14	**1a**	Pyrene	DCM/MeOH 4/1 (v/v)	$(2.8 \pm 1.1) \times 10^4$
15	**1a**	Pyrene	DCM/MeOH 1/4 (v/v)	$(4.0 \pm 1.6) \times 10^4$
16[a]	**1b**	DMN	Hex/DCM 1/4 (v/v)	-
17[a]	**1b**	DMN	DCM	-
18[a]	**1b**	DMN	DCM/MeOH 4/1 (v/v)	-
19[a]	**1b**	DMN	DCM/MeOH 1/4 (v/v)	-
20[a][b]	**1a**	DMN	Hex/DCM 1/4 (v/v)	-
21[a][b]	**1a**	DMN	DCM	-
22[a][b]	**1a**	DMN	DCM/MeOH 4/1 (v/v)	-
23[a][b]	**1a**	DMN	DCM/MeOH 1/4 (v/v)	-
24[a][c]	**1a**	DMN	Hex/DCM 1/4 (v/v)	-
25[a][c]	**1a**	DMN	DCM	-
26[a][c]	**1a**	DMN	DCM/MeOH 4/1 (v/v)	-
27[a][c]	**1a**	DMN	DCM/MeOH 1/4 (v/v)	-

[a] Saturation could not be reached even with high concentrations of guest. Binding was weak. [b]The binding titration were conducted after saturation with DIPEA (20-40 equiv. to **1a**). [c] The binding titration were conducted after saturation with NH$_3$ (10-20 equiv. to **1a**). (DMN: 1,5-dimethyl naphthalene)
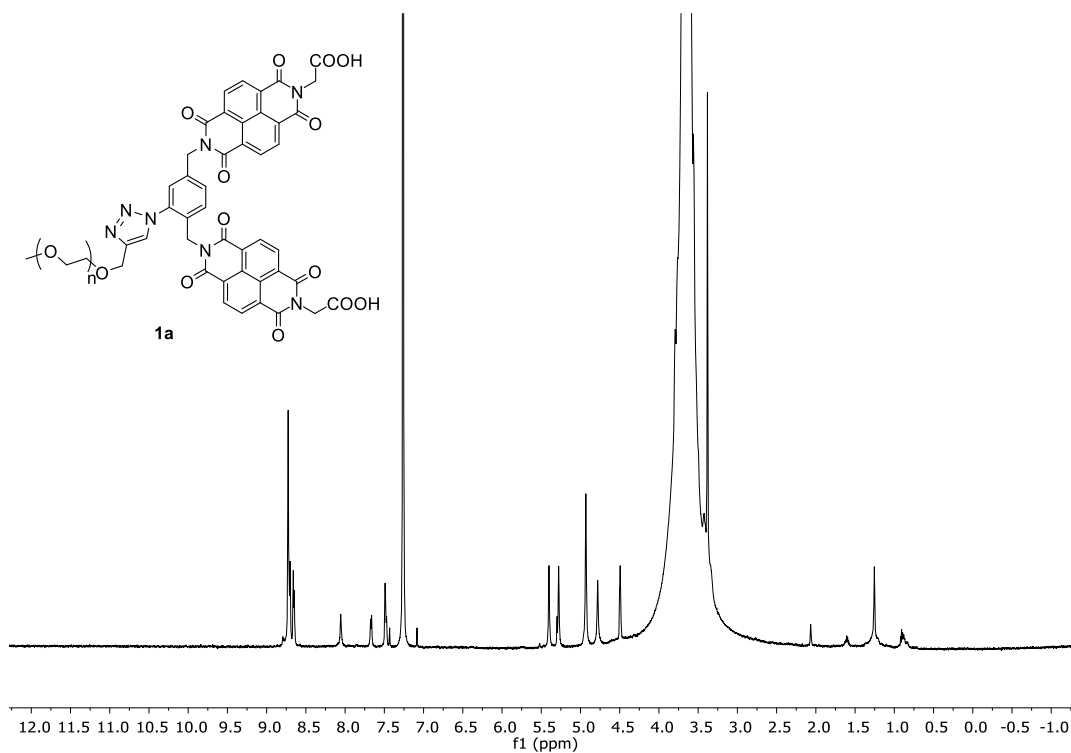
¹H and ¹³C NMR spectra
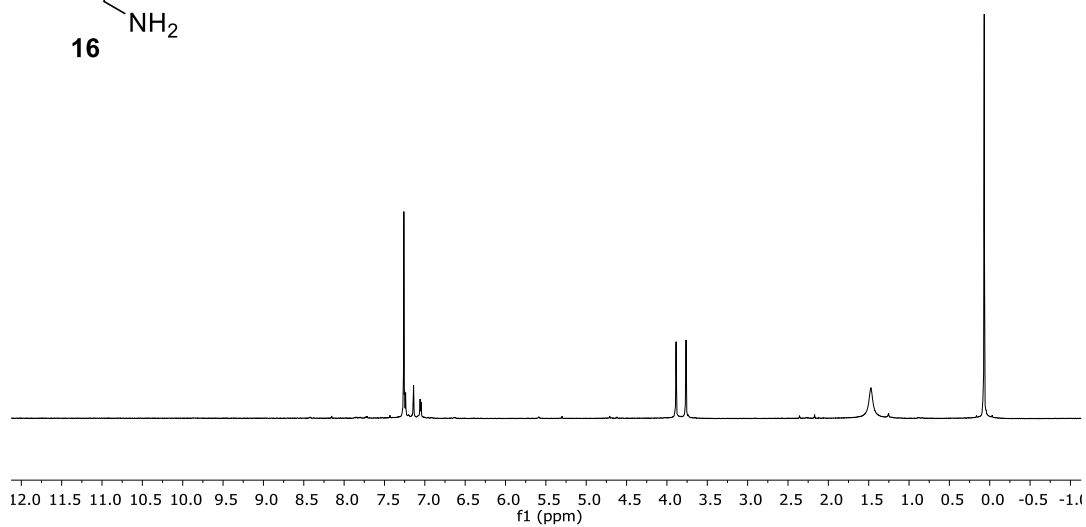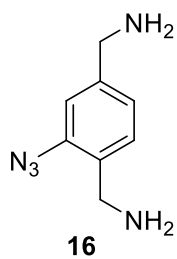
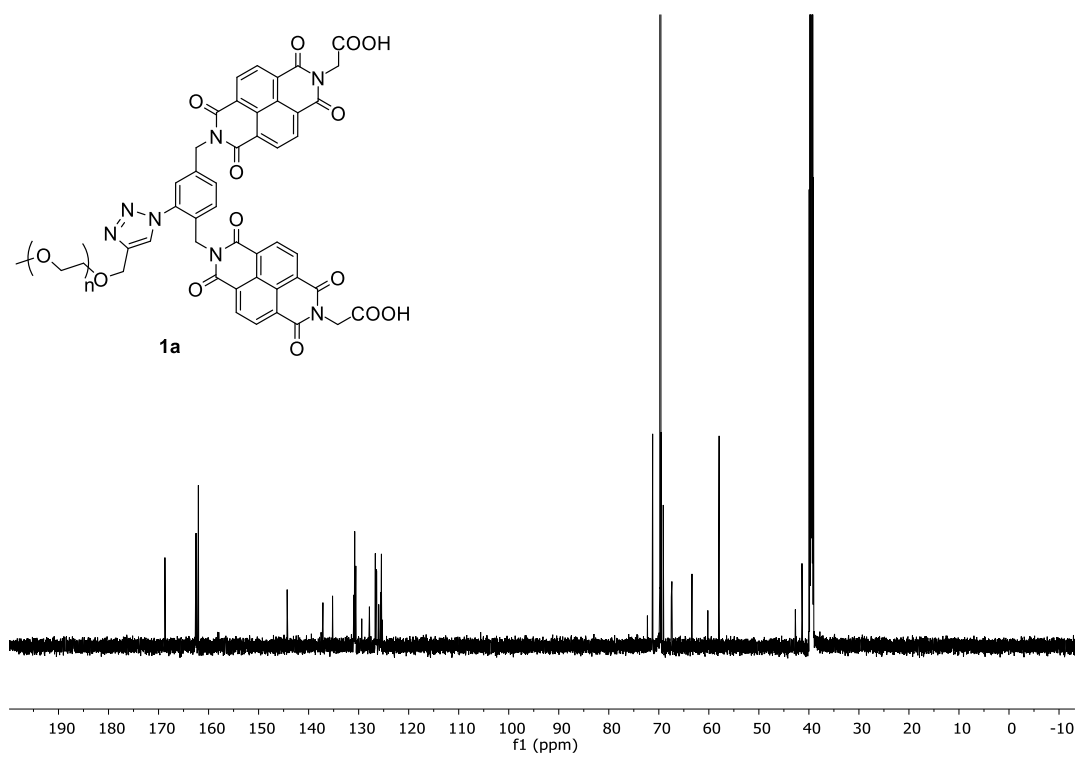**Scheme 4.** ¹H ¹³C NMR of **16**.
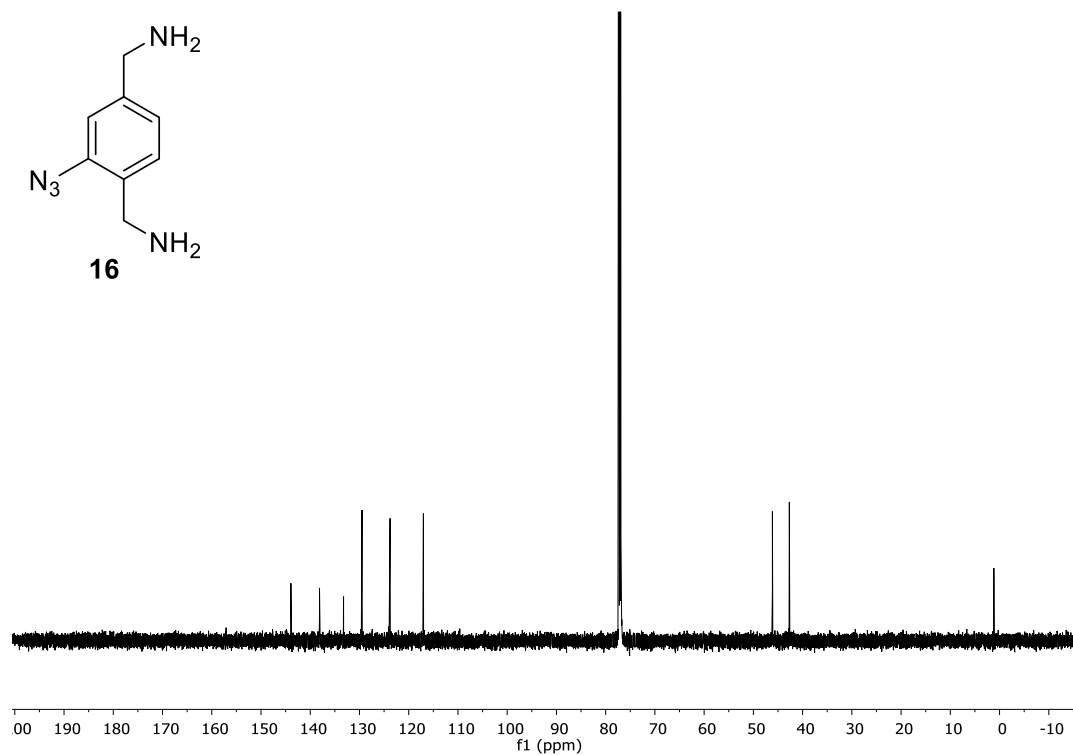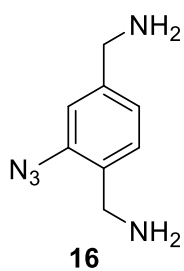
Scheme 5. ¹³C NMR of **16**.
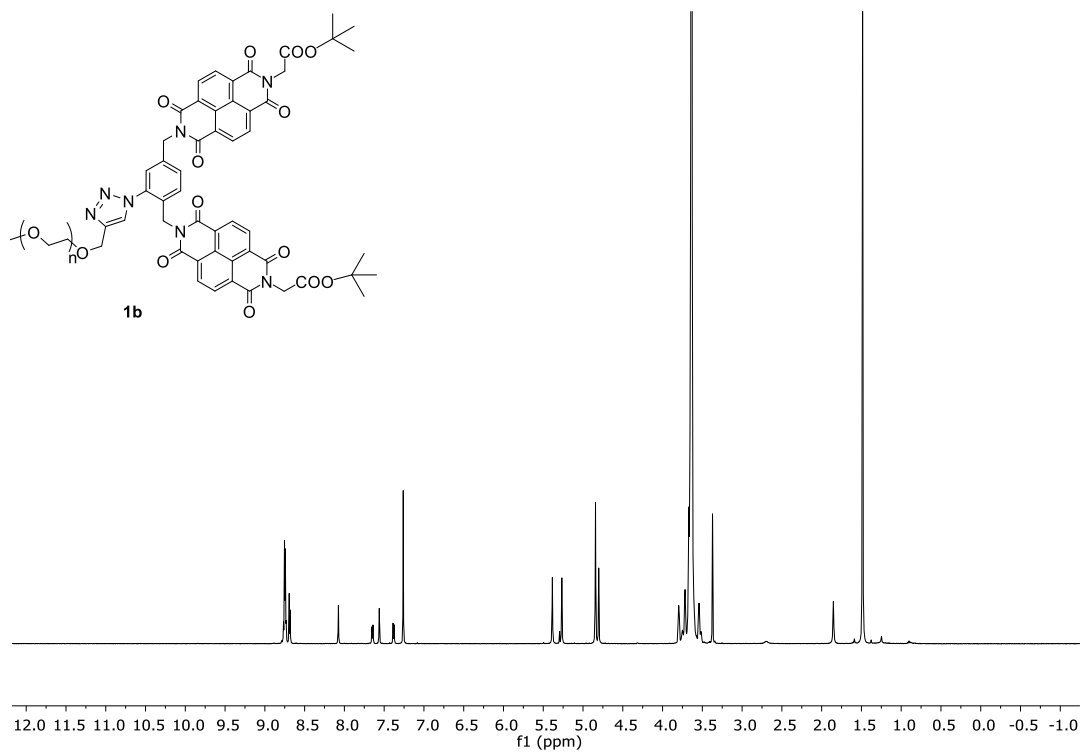
Scheme 6. ^{1}H NMR of **1b**.
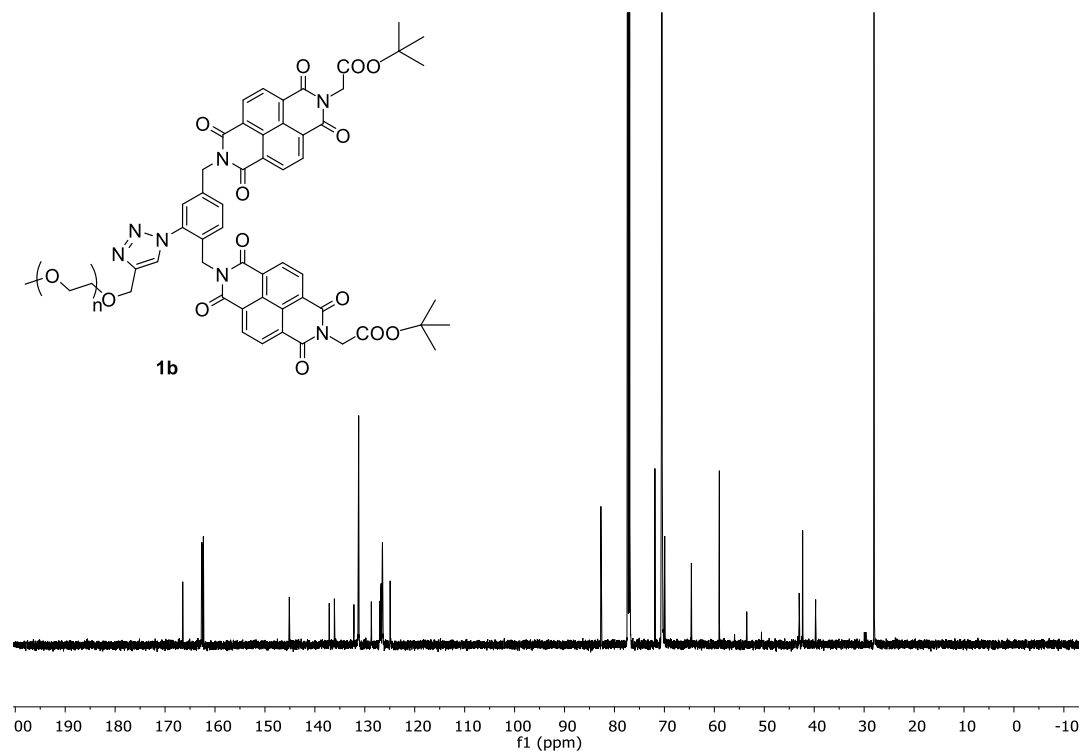
Scheme 7. ^{13}C NMR of **1b**.

Scheme 8. ^{1}H NMR of **1a**.

Scheme 9. ^{13}C NMR of **1a**.

Notes and References

(1) Chen, C. W.; Whitlock, H. W., *J. Am. Chem. Soc.* **1978,** *100*, 4921-4922.

(2) (a) Zimmerman, S. C.; VanZyl, C. M.; Hamilton, G. S., *J. Am. Chem. Soc.* **1989,** *111*, 1373-1381. (b) Zimmerman, S. C.; Mrksich, M.; Baloga, M., *J. Am. Chem. Soc.* **1989,** *111*, 8528-8530. (c) Zimmerman, S. C.; Wu, W., *J. Am. Chem. Soc.* **1989,** *111*, 8054-8055. (d) Zimmerman, S. C.; Wu, W.; Zeng, Z., *J. Am. Chem. Soc.* **1991,** *113*, 196-201.

(3) (a) Klärner, F.-G.; Benkhoff, J.; Boese, R.; Burkert, U.; Kamieth, M.; Naatz, U., *Angew. Chem. Int. Ed. Engl.* **1996,** *35*, 1130-1133. (b) Klärner, F.-G.; Kahlert, B., *Acc. Chem. Res.* **2003,** *36*, 919-932. (c) Petitjean, A.; Khoury, R. G.; Kyritsakas, N.; Lehn, J.-M., *J. Am. Chem. Soc.* **2004,** *126*, 6637-6647. (d) Harmata, M., *Acc. Chem. Res.* **2004,** *37*, 862-873. (e) Talbiersky, P.; Bastkowski, F.; Klärner, F.-G.; Schrader, T., *J. Am. Chem. Soc.* **2008,** *130*, 9824-9828. (f) Sinha, S.; Lopes, D. H. J.; Du, Z.; Pang, E. S.; Shanmugam, A.; Lomakin, A.; Talbiersky, P.; Tennstaedt, A.; McDaniel, K.; Bakshi, R.; Kuo, P.-Y.; Ehrmann, M.; Benedek, G. B.; Loo, J. A.; Klärner, F.-G.; Schrader, T.; Wang, C.; Bitan, G., *J. Am. Chem. Soc.* **2011,** *133*, 16958-16969. (g) Klärner, F.-G.; Schrader, T., *Acc. Chem. Res.* **2013,** *46*, 967-978.

(4) (a) Hunter, C. A.; Lawson, K. R.; Perkins, J.; Urch, C. J., *J. Chem. Soc. Perkin Trans. 2* **2001**, 651-669. (b) Waters, M. L., *Curr. Opin. Chem. Biol.* **2002,** *6*, 736-741. (c) Hunter, C. A.; Sanders, J. K. M., *J. Am. Chem. Soc.* **1990,** *112*, 5525-5534.

(5) Cubberley, M. S.; Iverson, B. L., *J. Am. Chem. Soc.* **2001,** *123*, 7560-7563.

(6) Reichardt, C., In *Solvents and Solvent Effects in Organic Chemistry*, 3rd ed.; Wiley-VCH: Weinheim, 2003; p 63.

(7) Smithrud, D. B.; Diederich, F., *J. Am. Chem. Soc.* **1990,** *112*, 339-343.

(8) Williams, D. H.; Stephens, E.; O'Brien, D. P.; Zhou, M., *Angew. Chem. Int. Ed.* **2004,** *43*, 6596-6616.

(9) (a) Zhao, Y., *ChemPhysChem* **2013,** *14*, 3878-3885. (b) Rodriguez-Docampo, Z.; Pascu, S. I.; Kubik, S.; Otto, S., *J. Am. Chem. Soc.* **2006,** *128*, 11206-11210. (c) Carrillo, R.; Feher-Voelger, A.; Martín, T., *Angew. Chem. Int. Ed.* **2011,** *50*, 10616-10620. (d) Carrillo, R.; Morales, E. Q.; Martín, V. S.; Martín, T., *Chem. -Eur. J.* **2013,** *19*, 7042-7048. (e) Carrillo, R.; Morales, E. Q.; Martín, V. S.; Martín, T., *J. Org. Chem.* **2013,** *78*, 7785-7795. (f) Zhong, Z.; Li, X.; Zhao, Y., *J. Am. Chem. Soc.* **2011,** *133*, 8862-8865. (g) Gunasekara, R. W.; Zhao, Y., *J. Am. Chem. Soc.* **2015,** *137*, 843-849. (h) Gunasekara, R. W.; Zhao, Y., *Chem. Commun.* **2016,** *52*, 4345-4348.

(10) The small change (~3-fold) in the diffusion coefficient of **1a** and the unchanged diffusion coefficient of **1b** upon the addition of pyrene were inconsistent with the formation of large intermolecular aggregates induced by pyrene.

(11) Greenland, B. W.; Burattini, S.; Hayes, W.; Colquhoun, H. M., *Tetrahedron* **2008,** *64*, 8346-8354.

(12) The binding constants of **1a** for **2** and **3** were only slightly weaker ($K_a = 0.3–1.1 \times 10^5$ M^{-1}, data now shown).

(13) Creighton, T. E., *Protein Structure: A Practical Approach, 2nd Ed.*; IRL Press: Oxford, 1997.

(14) (a) Nelson, J. C.; Saven, J. G.; Moore, J. S.; Wolynes, P. G., *Science* **1997,** *277*, 1793-1796. (b) Stone, M. T.; Heemstra, J. M.; Moore, J. S., *Acc. Chem. Res.* **2006,** *39*, 11-20. (c) Zhao, Y., *J. Org. Chem.* **2009,** *74*, 834-843. (d) Cho, H.; Zhao, Y., *J. Am. Chem. Soc.* **2010,** *132*, 9890-9899.

(15) Zill, A. T.; Licha, K.; Haag, R.; Zimmerman, S. C. *New J. Chem.* **2012**, *36*, 419.

(16) Giichi, S; Moriyasu, M; Kuniyoshi, N; etc. Compounds Against Helicobacter Activity. Eur. Pat. WO 03095453, Nov. 2003.

(17) Sundberg, R. J.; Suter, S. R.; Brenner, M. *J. Am. Chem. Soc.* **1972**, *94*, 513.

(18) Boyle, M. M.; Gassensmith, J. J.; Whalley, A. C.; Forgan, R. S.; Smaldone, R. A.; Hartlieb, K. J.; Blackburn, A. K.; Sauvage, J.-P.; Stoddart, J. F. *Chem.–Eur. J.* **2012**, *18*, 10312.

(19) Zhao, Y.; Zhong, Z. *J. Am. Chem. Soc.* **2005**, *127*, 17894.

(20) Schneider, H. J.; Yatsimirsky, A. K. *Principles and methods in supramolecular chemistry*; New York: J. Wiley, 2000; pp 137-146.

CHAPTER 4.
BINDING-PROMOTED CHEMICAL REACTION IN THE NANOSPACE OF A
BINDING SITE: EFFECTS OF ENVIRONMENTAL CONSTRICTION

Manuscript submitted.

Xiaoyu Xing and Yan Zhao

Abstract

Chemical reactions in confined nanospace can be very different from those in homogeneous solution. Imine formation between molecular amines and an aldehyde located inside the binding site of a nanoparticle receptor was promoted strongly by the binding. Although how well the amine fit in the binding pocket and the electronic nature of the amine both influenced the binding-normalized reactivity, the freedom of movement of the amine within the binding site was found to be the most important factor determining the reactivity.

Introduction

Molecules often behave very differently in confined nanospace than in a homogeneous solution. The steric constriction imposed on them sometimes gives rise to unusual chemical reactivity and selectivity not obtained otherwise.[1] Diel–Alder reaction, for example, could occur at the 1,4- instead of the normal 9,10-positions of anthracene.[2] Regio- and stereoselectivity of chemical reactions can be dramatically altered within self-assembled capsules.[3]

Through molecular imprinting,[4] we recently reported a method to create guest-complementary binding cavities in cross-linked micelles.[5] The resulting molecularly imprinted nanoparticles (MINPs) are protein-sized, water-soluble receptors with a tunable number of binding sites. Using a photocleavable template containing an *ortho*-nitrobenzyl ester, we could install a single carboxylic acid group inside the binding site. Because MINPs are soluble in

selected organic solvents such as DMF, we could perform chemical reactions (amide formation) inside the MINP binding pocket as well.[5c]

Although the above photocleavage and post functionalization worked well, it is difficult to obtain further insight into the reaction that occurred in the nanospace of the MINP binding site, as the heavily cross-linked micelles made it difficult to monitor the chemical reaction. Synthesis of the photocleavable templates was also quite cumbersome.[5c]

Results and Discussion

In this work, we employed an imine-based template–functional monomer (T–FM) complex to introduce an aldehyde group inside the MINP binding site. Not only was the synthesis more straightforward, importantly, the fluorescent amine used also allowed us to study the binding-promoted chemical reaction by fluorescence spectroscopy, helping us determine the important factors influencing the reaction in the confined nanospace.
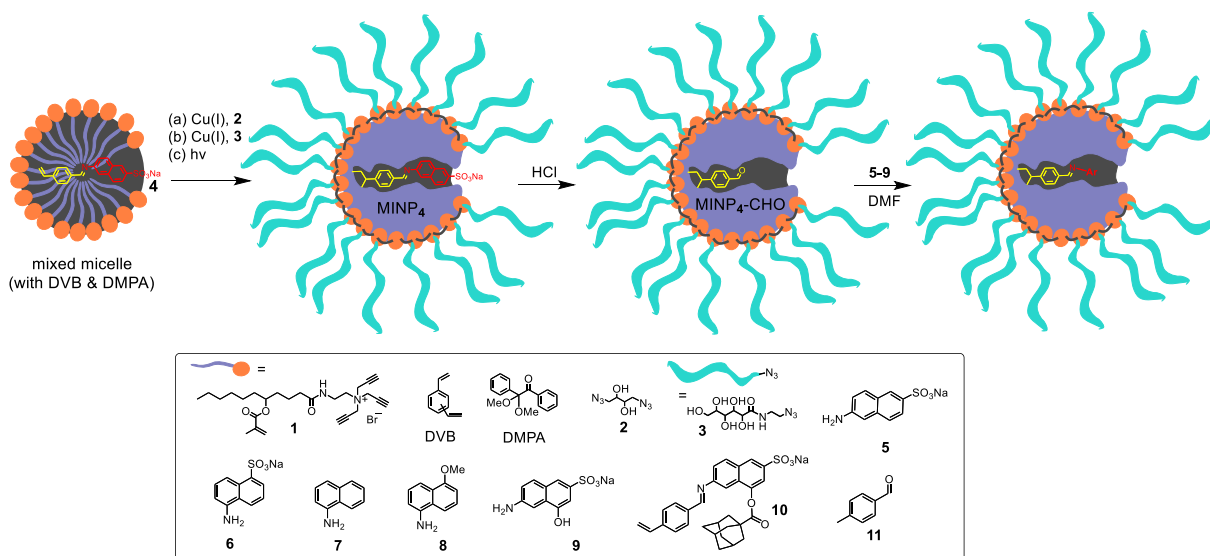
Scheme 1. Preparation of MINP-CHO by micellar covalent imprinting and hydrolysis, followed by reaction with **5**–**9** to form the imine.

The synthesis of MINP is shown in Scheme 1 (details have been reported previously[5] and are found in the experimental section). Briefly, although micelles are highly dynamic

aggregates of surfactants, by using the Cu(I)-catalyzed alkyne–azide cycloaddition, we can trap the micelles of **1** in nearly the original size using diazide **2** and decorate the surface with a layer of hydrophilic ligand **3**. The micelle normally contains a hydrophobic molecular template, a free radical cross-linker (DVB), and a photoinitiator (DMPA). UV irradiation leads to extremely efficient polymerization/cross-linking between the methacrylate of **1** and DVB inside the surface-cross-linked micelle to afford a template-complementary binding site in the doubly cross-linked micelle. MINP typically is ~5 nm in diameter, as determined by dynamic light scattering and confirmed by transmission electron microscopy (TEM).[6]

There are several considerations in the design of the T–FM complex **4**. First, imine is formed readily from the corresponding aldehyde and amine, especially with aromatic amines.[7] Second, although imine is quite stable in many solvents, its hydrolysis is easily accomplished in acidic water, meanwhile creating a template-shaped binding site with an aldehyde group at the predetermined position inside the binding site. Third, amine **5** and its analogues (**6**–**9**) are all fluorescent, allowing us to monitor both the acid-catalyzed hydrolysis (to vacate the binding site) and the re-formation of the imine in the confined nanospace of the MINP binding pocket.

Covalent imprinting in our case has the benefit of high structural fidelity, as co-polymerization/cross-linking around the T-FM complex is expected to form an complementary binding site. The question is whether one can remove the template (i.e., molecule **5**) efficiently to vacate the binding site.

We used 6 M aqueous HCl solution at 95 °C to hydrolyze the imine of MINP**4**—i.e., MINP prepared with T-FM complex **4**. As shown by Figure 1, the naphthyl group emitted at 405 nm. Upon hydrolysis, the fluorescent peak decreased gradually and retained ca 10% of the initial intensity at the end (Figure 9 in experimental section). Since the naphthyl group was the

only good fluorophore in the MINP₄, the result was interpreted as successful hydrolysis and removal of the majority of amine **5**. Meanwhile, DLS showed nearly constant particle size (~5.5 nm), suggesting the acid did not cause decomposition of the rest of the nanoparticle.

Further confirmation of the hydrolysis comes from the binding study. Once the imine is hydrolyzed, MINP₄-CHO should have a binding pocket tailored precisely for template **5**. Since the imine formation took place in DMF (vide infra), we performed the binding study first in DMF.
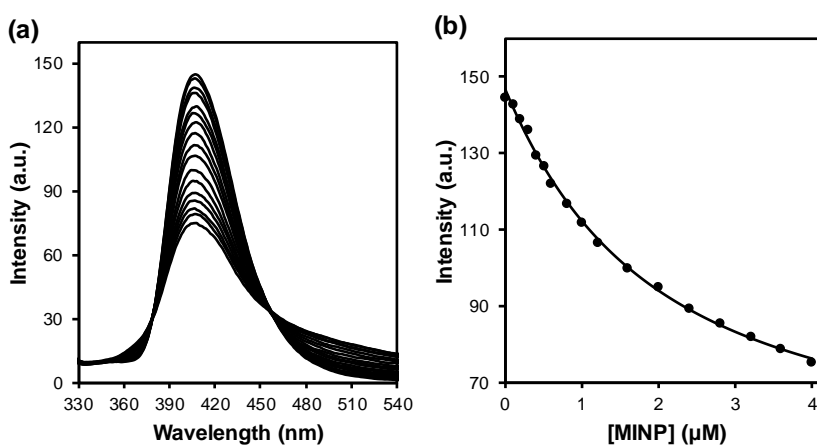
Figure 1. (a) Emission spectra of **5** upon the addition of different concentrations of MINP₄-CHO in DMF. [**5**] = 0.5 µM. λ_{ex} = 295 nm. The concentration of the MINP was calculated based on a M.W. of 50000 g/mol determined by DLS. (b) Intensity of **5** at 406 nm as a function of [MINP₄-CHO]. The smooth curve was the nonlinear least squares curve fitting of the emission intensity to a 1:1 binding isotherm.

Figure 1a shows the fluorescence spectra of **5** upon addition of different concentrations of MINP₄-CHO (i.e., the acid-hydrolyzed MINP₄). The titration partially quenched the naphthyl emission and afforded two isoemissive points, indicating a continuous transition from the free to the bound template. The fluorescence data fit well to a 1:1 binding isotherm, yielding a binding constant of $K_a = (62 \pm 5) \times 10^4 \, M^{-1}$ (Figure 1b; Table 1, entry 1).

The binding stoichiometry was verified by the Job plot, which showed a clear maximum at 0.5 molar fraction (Figure 11). Thus, the MINP receptor had on average one

binding site per nanoparticle. Our MINP is estimated to contain ~50 cross-linkable surfactants per nanoparticle by light scattering.[5a] We normally keep the surfactant/template ratio at 50:1. The single binding site on MINP$_4$-CHO is consistent with the stoichiometry and a high yielding cleavage reaction.

Table 1. Binding data for MINP-CHO and MINP-CH$_2$OH at room temperature.[a]

Entry	Host	Guest	K_a in DMF ($\times 10^4 \, M^{-1}$)
1	MINP$_4$-CHO	**5**	62 ± 5 (200 ± 30)
2	MINP$_4$-CHO	**6**	1300 ± 800 (73 ± 1)
3	MINP$_4$-CHO	**7**	62 ± 18
4	MINP$_4$-CHO	**8**	43 ± 8
5	MINP$_4$-CHO	**9**	430 ± 120
6	MINP$_4$-CH$_2$OH	**5**	50 ± 8
7	MINP$_{10}$-CHO	**5**	8.8 ± 0.8
8	MINP$_{10}$-CHO	**6**	25 ± 11
9	MINP$_{10}$-CHO	**9**	23 ± 2

[a] The titrations were generally performed in duplicates and the errors between the runs were <10%. The binding constants in parentheses were for titrations performed in 10 mM HEPES buffer (pH 7). The titration curves are found in the experimental section (Figures 12–22).

Table 1 lists the binding constants (K_a) obtained in this study. Compounds **5** and **6** differ in the substitution pattern on the naphthyl ring. As shown by the K_a values in the parentheses, MINP$_4$-CHO bound **5** (its own template) more strongly than **6** in HEPES buffer. This is the expected result from molecular imprinting and is consistent with many studies we have done using micellar imprinting.[5,8]

In DMF, however, the opposite became true, with **6** bound much more strongly than **5**. It is not exactly clear why there was such a reversal but the result suggests that hydrophobic interactions in water was essential for the excellent selectivity observed in our previous MINP bindings.[5,8] Formation of micelles and the interactions between the template and the micelle in water both have strong hydrophobic contributions. The hydrophobic interactions, however, are eliminated in DMF. Other interactions such as electrostatics (vide infra) might become more

important. Not only so, the organic solvent is expected to penetrate into the cross-linked micelle to cause it to swell. A change of the binding pocket would occur as a result. It is possible that all the above factors might have contributed to the reversed selectivity.

The binding studies in DMF showed that electrostatic interactions played an important role, as removal of the sulfonate (in **7**) and substitution of the sulfonate with a methoxy (in **8**) weakened the binding of **6** dramatically. Since MINP₄-CH₂OH, obtained by treating MINP₄-CHO with a large amount of NaBH₄, would be used as a control to study the imine formation (vide infra), we also studied the binding of **5** by MINP₄-CH₂OH. As expected, the two binding constants were fairly similar (Table 1, entries 1 and 6), suggesting that the binding interactions of an aldehyde or hydroxyl group with the amine template were not very different.

MINP₁₀-CHO were prepared similarly using template–FM complex **10**. After removal of the template, MINP₁₀-CHO is expected to have a large adamantane-shaped pocket near the binding site for the naphthyl group. We designed this template to investigate how freedom of movement of the amine in the binding pocket might influence the imine formation (vide infra). As far as the binding is concerned, all the sulfonated naphthyl amines could still be bound by this MINP but the binding constants generally decreased—a fully expected result for a less ideally fitted binding pocket (Table 1, entries 7–9).

Table 2. Kinetic data for the imine formation with MINP-CHO.[a]

Entry	Host	Guest	Temp (°C)	k_{obs} in DMF ($\times 10^{-3}$ s^{-1})	k_{obs}/K_a ($\times 10^{-9}$ M·s^{-1})
1	MINP₄-CHO	**5**	25	--[b]	--[d]
2	MINP₄-CHO	**5**	33	0.032 ± 0.002	--[d]
3	MINP₄-CHO	**5**	50	0.49 ± 0.02	0.8
4	MINP₄-CHO	**6**	50	0.85 ± 0.10	0.1
5	MINP₄-CHO	**7**	50	0.61 ± 0.01	1.0
6	MINP₄-CHO	**8**	50	0.75 ± 0.02	1.7
7	MINP₄-CHO	**9**	50	1.13 ± 0.06	0.3

Table 2. Continued.

8	**11**	**5**	50	--[c]	--[c]
9	MINP$_4$-CH$_2$OH	**5**	50	--[c]	--[c]
10	MINP$_{10}$-CHO	**5**	50	1.2 ± 0.1	14
11	MINP$_{10}$-CHO	**6**	50	1.1 ± 0.1	4
12	MINP$_{10}$-CHO	**9**	50	1.7 ± 0.2	7

[a] The reactions were generally performed in duplicates and the errors between the runs were <10%. The fluorescence spectra and the curve fittings are found in the experimental section (Figures 23–33). [b] The reaction was very slow to be measured accurately. [c] No significant change in fluorescence was observed over time.

We then studied the reaction between various amines (**5**–**9**) and the aldehyde inside the MINP binding site (Table 2). Because the reaction was too slow at 25 °C, we performed the majority of the reactions at 50°C. Two control experiments were also performed using molecular aldehyde **11** (entry 8) and MINP$_4$-CH$_2$OH (entry 9), respectively, in the reaction.
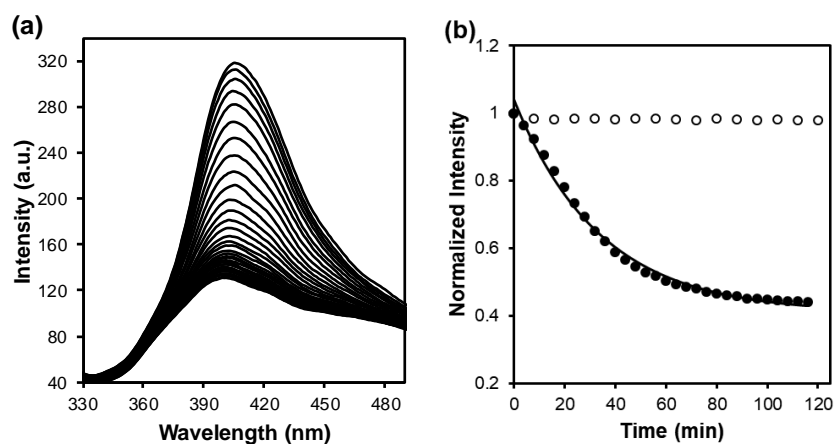
Figure 2. (a) Fluorescence spectra of **5** in the presence of 10 equiv MINP$_4$-CHO in DMF at 50 °C over time. [**5**] = 0.5 μM. λ_{ex} = 295 nm. (b) Emission intensity of **5** in the presence of 10 equiv MINP$_4$-CHO (●) and 10 equiv **11** (○), respectively. The solid line was from fitting of the data to the first-order kinetics.

For the imine formation, we normally mixed 0.5 μM **5** and 10 equiv MINP$_4$-CHO in DMF so that the change of concentration for MINP$_4$-CHO was minimal during the reaction (i.e., pseudo first order). At room temperature, the fluorescence spectrum of the mixture changed gradually (Figure 23) but, at higher temperatures (e.g., 50 °C), the emission intensity

changed more rapidly (Figure 2a). Since this large-scale decrease did not occur for any of the negative controls (Table 2, entries 8-9), we attributed the change to the imine formation. Indeed, the decrease in fluorescence intensity fit well to the pseudo first order kinetics and all the rate constants are given in Table 2.

Binding clearly promoted the imine formation, in a dramatic way. Figure 2b shows the fluorescence of **5** displayed no change under the same condition in the presence of molecular aldehyde **11** (○). Hence, without the help from the binding, imine could not form at all under our experimental conditions.

From the kinetic data in Table 2, the most surprising finding initially was the *insensitivity* of the reaction rates. Although the reaction did became faster at higher temperatures (entries 1–3), the other observed rate constants (k_{obs}) were quite similar, practically within 4–5-fold. Since binding clearly was key to the enhanced reactivity of the aldehyde group inside the MINP binding site, we listed the k_{obs}/K_a values for these reactions in Table 2 as well.

The k_{obs}/K_a value could be considered as the binding-normalized rate constant. Once the binding factor was removed, the "intrinsic reactivity" in the nanospace seems to make much sense. For example, as the amine became more electron-rich (form **6** to **7** to **8**) while their overall shape stayed very similar, the k_{obs}/K_a value showed a steady increase, from 0.1 to 1 and then to 1.7×10^{-9} M·s^{-1} (entries 4–6). This was the expected behavior from the stronger nucleophilicity of the amine. The k_{obs}/K_a value of **5** (entry 3) was 8 times as large as that of **6** (entry 4), indicating that, once the influence of the binding affinity was removed, the intrinsic reactivity of the original template was still higher than its structural analogue. As for compound **9**, its k_{obs}/K_a value was 0.3×10^{-9} M·s^{-1} (entry 7), lower than the 0.8×10^{-9} M·s^{-1} for **5** (entry 3).

It is possible that this resulted from a tradeoff between the negative effect of a less perfectly fitted shape and a positive effect of the electron-donating hydroxyl group.

The largest enhancement of the binding-normalized reactivity was observed for MINP$_{10}$-CHO, with k_{obs}/K_a 1–2 orders of magnitude higher than those for MINP$_4$-CHO. Thus, the steric effect seemed to have dominated over the "fitness" of the template and any electronic effect. We attributed this large increase in k_{obs}/K_a to the increased freedom of the amines to move inside the larger binding pocket of MINP$_{10}$-CHO. In order for the imine to form, the amine and the aldehyde groups need to approach each other in preferred angles. Whereas the optimal attacking geometry can be easily achieved in solution by random molecular collision, it could become quite challenging in a constricted nanospace. It is very possible that higher freedom of movement under such a circumstance could be far more important than other factors that tend to dominate in solution chemistry.

Conclusion

In summary, strong binding by MINP not only dramatically enhanced the reaction between a bound amine substrate and the aldehyde in the binding pocket (Figure 2b), the factors that influenced the reaction also became very different, with freedom of movement being the dominant factor in the confined nanospace. We do not think our finding is limited to a particular reaction inside the MINP binding pocket. Similar situations could occur inside a nanopore or within the enzyme active site, wherever the movement of molecules are restricted.

Acknowledgement

Experimental Section

General Method

All other reagents and solvents were of ACS-certified grade or higher, and were used as received from commercial suppliers. Routine ^{1}H and ^{13}C NMR spectra were recorded on a Bruker DRX-400, on a Bruker AV II 600 or on a Varian VXR-400 spectrometer. ESI-MS mass was recorded on Shimadzu LCMS-2010 mass spectrometer. Dynamic light scattering (DLS) data were recorded at 25 °C using PDDLS/ CoolBatch 90T with PD2000DLS instrument. Fluorescence spectra were recorded at ambient temperature on a Varian Cary Eclipse Fluorescence spectrophotometer.

Syntheses

4-vinylbenzaldehyde was synthesized following reported procedures.[9]

Scheme 2. Synthetic route for compounds **13** and **4**.
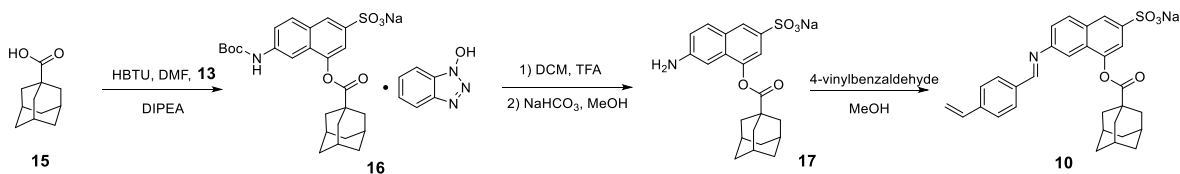
Scheme 3. Synthetic route for compounds **10**.

Compound 13. 6-Amino-4-hydroxy-2-naphthalenesulfonic acid (500 mg, 2.09 mmol), di-t-butyl dicarbonate (912 mg, 4.18 mmol), and sodium bicarbonate (351 mg, 4.18 mmol) were dissolved in a mixture of 50 mL of methanol and 2 mL of water. The reaction mixture was heated to 60 °C and stirred overnight. After the reaction mixture was concentrated by rotary evaporation, the residue was purified by flash column chromatography over silica gel

with 15:1 ethyl acetate/methanol as the eluent to give a pink powder (539 mg, 71%). ^{1}H NMR (400 MHz, CD$_3$OD, δ) 8.29 (d, J = 2.2 Hz, 1H), 7.80 – 7.74 (m, 2H), 7.55 (dd, J = 8.9, 2.2 Hz, 1H), 7.22 (d, J = 1.5 Hz, 1H), 1.55 (s, 9H). ^{13}C NMR (151 MHz, CD$_3$OD, δ) 154.0, 152.8, 140.4, 137.3, 129.9, 128.74, 126.4, 120.2, 116.1, 109.3, 104.8, 79.7, 27.4. ESI-MS (*m/z*): [M-Na] $^-$ cacld for C$_{15}$H$_{16}$NO$_6$S, 338.0704; found, 338.0706.

Compound 16. Compound **13** (27.4 mg, 0.152 mmol), HBTU (105 mg, 0.277 mmol), and DIPEA (89 mg, 0.689 mmol) were dissolved in 5 mL of DMF. After the reaction mixture as stirred for 30 min, compound **15** (50 mg, 0.138 mmol) was added. The reaction mixture was stirred at room temperature overnight. After the mixture was concentrated by rotary evaporation, the residue was purified by flash column chromatography over silica gel with 20:1 dichloromethane/methanol as the eluent to give a light-yellow powder (61.1 mg, 61%). ^{1}H NMR (400 MHz, CD$_3$OD, δ) 8.18 (s, 1H), 8.15 (s, 1H), 7.89 – 7.86 (m, 2H), 7.74 (d, J = 8.5 Hz, 1H), 7.56 – 7.44 (m, 4H), 2.26 (d, J = 2.9 Hz, 6H), 2.14 (s, 3H), 1.89 (s, 6H), 1.55 (s, 9H). ^{13}C NMR (151 MHz, CD$_3$OD, δ) 177.53, 154.82, 147.72, 141.30, 140.57, 130.93, 130.65, 129.69, 127.95, 127.04, 124.00, 121.71, 118.51, 116.96, 111.59, 108.52, 81.03, 48.43, 42.58, 40.05, 37.52, 29.48, 28.65, 19.26. ESI-MS (*m/z*): [M-HOBt-Na] $^-$ cacld for C$_{26}$H$_{30}$NO$_7$S, 500.1743; found, 500.1759.

Compound 17. Compound **16** (61.1 mg, 0.093 mmol) was dissolved in 10 mL of trifluoroacetic acid. The reaction mixture was stirred at room temperature overnight. After the reaction mixture was concentrated by rotary evaporation, the residue was re-dissolved in 25 mL methanol with sodium bicarbonate (23.4 mg, 0.279 mmol). After stirred for 30 min, the reaction mixture was concentrated by rotary evaporation and the residue was purified by flash column chromatography over silica gel with 15:1 dichloromethane/methanol as the eluent to

give a white powder (30.3 mg, 77%). ^{1}H NMR (400 MHz, CD$_3$OD, δ) 8.03 (s, 1H), 7.72 (d, J = 8.8 Hz, 1H), 7.39 (d, J = 1.6 Hz, 1H), 7.07 (dd, J = 8.8, 2.2 Hz, 1H), 6.86 (d, J = 2.2 Hz, 1H), 2.22 (d, J = 2.9 Hz, 6H), 2.14 (s, 3H), 1.87 (t, J = 3.2 Hz, 6H). ^{13}C NMR (151 MHz, CD$_3$OD, δ) 177.81, 149.60, 146.20, 131.16, 130.92, 128.52, 124.41, 120.91, 116.60, 101.60, 42.59, 40.12, 37.49, 29.43. ESI-MS (*m/z*): [M-Na] $^-$ cacld for C$_{21}$H$_{22}$NO$_5$S, 400.1219; found, 400.1218.

Compound 4. Compound **14** (0.020 mmol, 4.5 mg), 4-vinylbenzaldehyde (13.2 mg, 0.100 mmol), and sodium hydroxide (0.020 mmol, 0.8 mg) were mixed with 10 mL of ethanol. The reaction mixture was heated to reflux overnight and cooled to room temperature. Diethyl ether (40 mL) was added slowly. The precipitate formed was collected by filtration and washed with 5 mL of diethyl ether to yield a yellow powder (5.7 mg, 79.3%). The product was used in the MINP preparation without further purification. ^{1}H NMR (500 MHz, DMSO-d_6, δ) 8.78 (s, 1H), 8.17 (s, 1H), 8.03 (d, J = 8.7 Hz, 1H), 7.97 (d, J = 7.8 Hz, 2H), 7.89 (d, J = 8.6 Hz, 1H), 7.73 (d, J = 5.4 Hz, 2H), 7.65 (d, J = 7.8 Hz, 2H), 7.54 (dd, J = 8.4, 2.2 Hz, 1H), 6.83 (dd, J = 17.6, 11.0 Hz, 1H), 5.99 (d, J = 17.7 Hz, 1H), 5.40 (d, J = 10.9 Hz, 1H).

Compound 10. Compound **17** (0.020 mmol, 8.5 mg) and 4-vinylbenzaldehyde (13.2 mg, 0.100 mmol) were mixed with 10 mL of methanol. The reaction mixture was stirred overnight. Diethyl ether (40 mL) was added slowly. The precipitate formed was collected by filtration and washed with 5 mL of diethyl ether to yield a brown powder (9.8 mg, 85.4%). The product was used in the MINP preparation without further purification. ^{1}H NMR (400 MHz, DMSO-d_6, δ) 8.75 (s, 1H), 8.13 (d, J = 8.7 Hz, 1H), 8.09 (s, 1H), 7.97 (d, J = 7.1 Hz, 2H), 7.66 (d, J = 7.8 Hz, 2H), 7.60 (d, J = 8.8 Hz, 1H), 7.42 (s, 1H), 7.37 (s, 1H), 6.83 (dd, J = 17.6, 11.0

Hz, 1H), 6.00 (d, $J = 17.8$ Hz, 1H), 5.41 (d, $J = 10.9$ Hz, 1H), 2.09-2.15 (m, 9H), 1.74-1.81 (m, 6H).

Preparation of MINPs

MINPs were synthesized according to previously reported procedures.[10] To a micellar solution of **1** (10.2 mg, 0.02 mmol) in H_2O (2.0 mL), divinylbenzene (DVB, 2.8 μL, 0.02 mmol), the template–FM complex (**4** or **10**) in DMSO (0.0004 mmol), and 2,2-dimethoxy-2-phenylacetophenone (DMPA) in DMSO (10 μL of a 12.8 mg/mL, 0.0005 mmol) were added. The mixture was sonicated for 10 min. Cross-linker **2** (4.1 mg, 0.024 mmol), $CuCl_2$ in H_2O (10 μL of 6.7 mg/mL, 0.0005 mmol), and sodium ascorbate in H_2O (10 μL of 99 mg/mL, 0.005 mmol) were then added and the reaction mixture was stirred slowly at room temperature for 12 h. Compound **3** (10.6 mg, 0.04 mmol), $CuCl_2$ (10 μL of a 6.7 mg/mL solution in H_2O, 0.0005 mmol), and sodium ascorbate (10 μL of a 99 mg/mL solution in H_2O, 0.005 mmol) were then added and the solution stirred for another 6 h at room temperature. The reaction mixture was transferred to a glass vial, purged with nitrogen for 15 min, sealed with a rubber stopper, and irradiated in a Rayonet reactor for 12 h. The reaction mixture was poured into acetone (8 mL). The precipitate was collected by centrifugation and washed with a mixture of methanol/acetic acid (5 mL/0.1 mL) three times. The off-white product was dried in air to afford the final MINPs (> 80%).

Preparation of MINP-CHO

MINP$_4$ (15.2 mg) was sonicated in 2 mL of 6 M hydrochloric acid for 20 min. The resulting solution was stirred at 95 °C for 2 h and then was poured into acetone (8 mL). The precipitate formed was collected by centrifugation and washed with a mixture of acetone/water (5 mL/1 mL) three times. The off-white product was dried in air to afford the MINP$_4$-CHO (12.0 mg, 79%).

Preparation of MINP₄-CH₂OH

MINP₄-CHO (12.0 mg) were sonicated in 1 mL of anhydrous DMF for 20 min until fully dissolved. An aliquot of sodium borohydride stock solution (37.9 mg in 1 mL of anhydrous DMF) was added to the MINP₄-CHO solution. After stirred overnight, the reaction mixture was poured into acetone (8 mL). The precipitate was collected by centrifugation and washed with a mixture of acetone/water (5 mL/1 mL) three times, and then a mixture of methanol/acetic acid (5 mL/0.1 mL) three times. The off-white product was dried in air. To remove the borate ions, the MINP₄-CH₂OH was re-dissolved and stirred with 2 mL of sodium chloride solution (5000 equiv based on MINP concentration) overnight. The solution was transferred to a dialysis tube (MWCO 3.5K). The tube was placed in 2 L of deionized water with gentle stirring. The dialysis tube was sonicated and the water was changed after 2, 4, 6, and 20 h. After 48 h, the MINP solution was poured into 40 mL of acetone and the precipitate was collected by centrifugation. The precipitate was dried in air to afford MINP₄-CH₂OH (8.6 mg, 72%).

Titration by Fluorescence Spectroscopy and Data Analysis Method

A stock solution of MINP-CHO (200 μM) was prepared in 10 mM HEPES buffer (pH 7) or DMF. Stock solutions (200 μM) of the guests (**5-9**) were prepared in water. For the titrations, a typical procedure is as follows. An aliquot of the guest stock solution was added to 2.00 mL of the appropriate solvent (HEPES buffer or DMF) in a quartz cuvette. The concentration of the guest was 0.5 μM. The sample was gently vortexed for 30 s before its fluorescence spectrum was recorded. Aliquots of the MINP solution was added and the spectrum was recorded after each addition. The titration was continued until saturation was reached and the total volume of the MINP solution added was kept below 100 μL. The binding constant was obtained by nonlinear least squares curving fitting of the emission intensity to the

1:1 binding isotherm.[11] All titrations were performed at room temperature unless indicated otherwise.

Imine Formation Monitored by Fluorescence Spectroscopy

A stock solution of MINP-CHO and **11** (200 μM) was prepared in DMF. Stock solutions of the guests (**5-9**, 200 μM) were prepared in water. For the imine formation, a typical procedure is as follows. An aliquot of the amine stock solution was added to 2.00 mL of DMF in a quartz cuvette. The concentration of the amine was 0.5 μM. The sample was gently vortexed for 30 s and kept in a temperature-controlled cuvette holder for 5 min to reach the set temperature before its fluorescence spectrum was recorded. An aliquot of the MINP-CHO solution was added to the cuvette. The concentration of MINP-CHO was 5.0 μM. Fluorescence spectra were collected over time and the rate constant was obtained by nonlinear least squares curve fitting to the pseudo first-order rate law, in which F_t is the fluorescence intensity at time t, F_0 the initial intensity, and F_∞ the intensity at the completion of the reaction.

$$ln\frac{F_t - F_0}{F_0 - F_\infty} = -k_{obs}t$$

Figure 3. ^{1}H NMR spectra of (a) surfactant 1 in CDCl3, (b) surface-cross-linked micelles (SCM) in D2O, (c) surface-functionalized SCM in D2O, and (d) core-cross-linked micelles in D2O for MINP4.

Figure 4. Distribution of the hydrodynamic diameters of the nanoparticles in water as determined by DLS for (a) surface-cross-linked micelles (SCM), (b) surface-functionalized SCM, and (c) purified MINP4.

Figure 5. Distribution of the molecular weights and the correlation curve for MINP$_4$ from the DLS. The PRECISION DECONVOLVE program assumes the intensity of scattering is proportional to the mass of the particle squared. If each unit of building block for the MINP is assumed to contain one molecule of surfactant (MW = 465 g/mol), 1.2 molecules of cross linker (MW = 172 g/mol), one molecule of DVB (MW = 130 g/mol), and 0.8 molecules of sugar derivative (MW = 264 g/mol), the molecular weight of MINP translates to 51 [= 52100 / (465 + 1.2×172 + 130 + 0.8×264)] of such units.
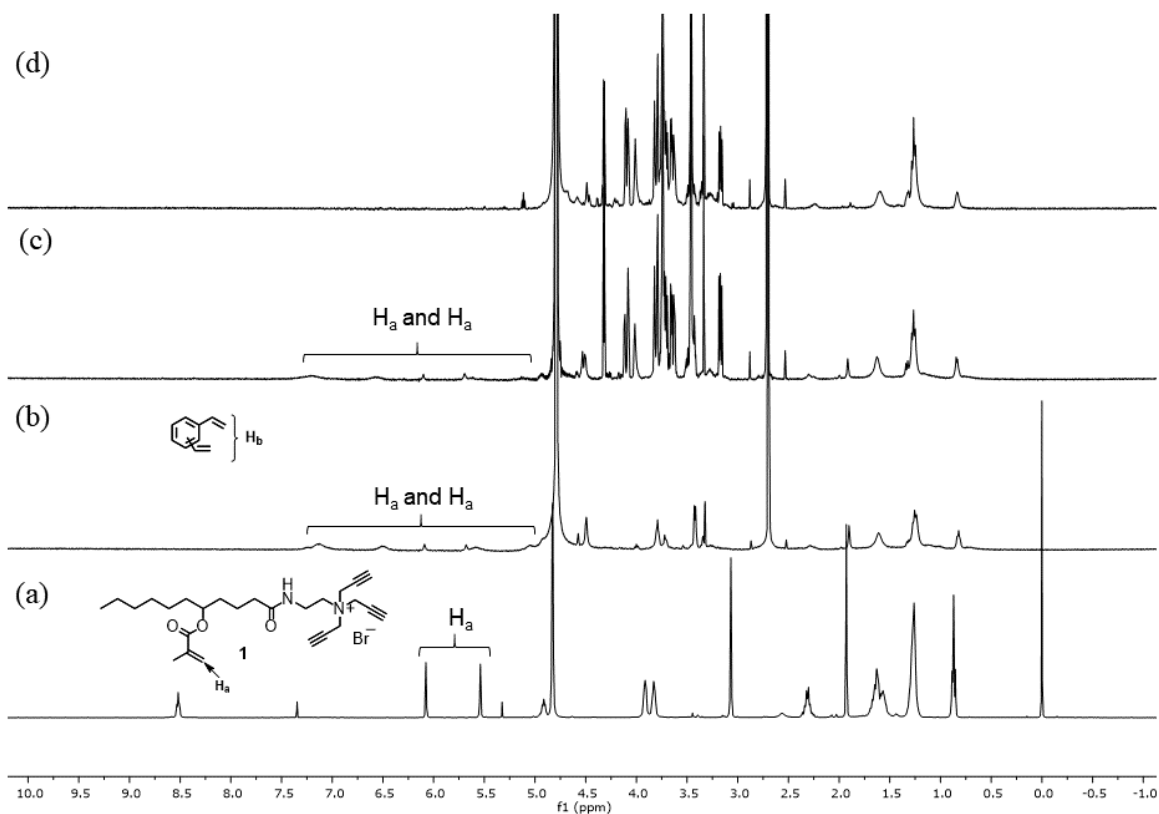
Figure 6. ^{1}H NMR spectra of (a) surfactant 1 in CDCl3, (b) surface-cross-linked micelles (SCM) in D2O, (c) surface-functionalized SCM in D2O, and (d) core-cross-linked micelles in D2O for MINP10.
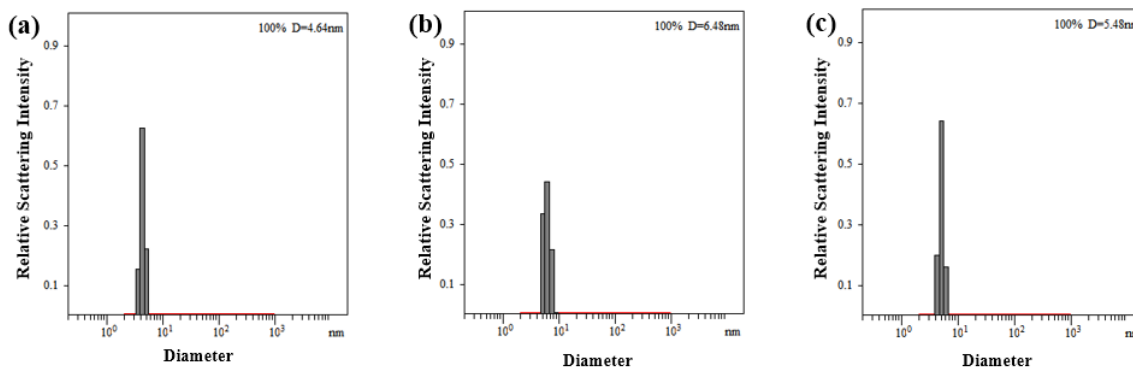
Figure 7. Distribution of the hydrodynamic diameters of the nanoparticles in water as determined by DLS for (a) surface-cross-linked micelles (SCM), (b) surface-functionalized SCM, and (c) purified MINP$_{10}$.
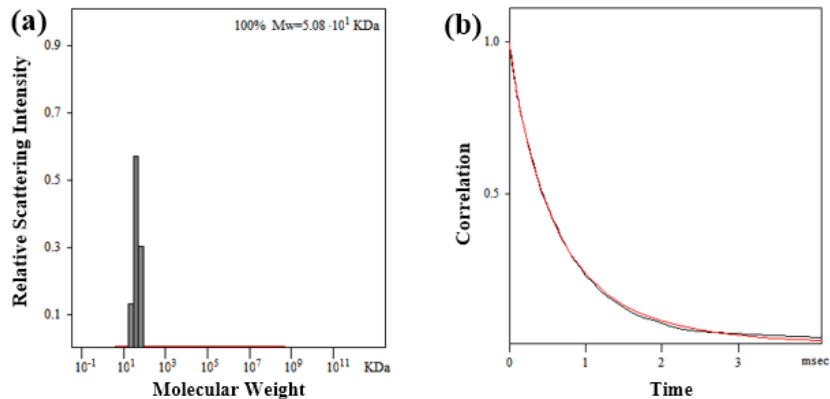
Figure 8. Distribution of the molecular weights and the correlation curve of MINP$_{10}$ from the DLS. The PRECISION DECONVOLVE program assumes the intensity of scattering is proportional to the mass of the particle squared. If each unit of building block for the MINP is assumed to contain one molecule of surfactant (MW = 465 g/mol), 1.2 molecules of cross linker (MW = 172 g/mol), one molecule of DVB (MW = 130 g/mol), and 0.8 molecules of sugar derivative (MW = 264 g/mol), the molecular weight of MINP translates to 50 [= 50800 / (465 + 1.2×172 + 130 + 0.8×264)] of such units.
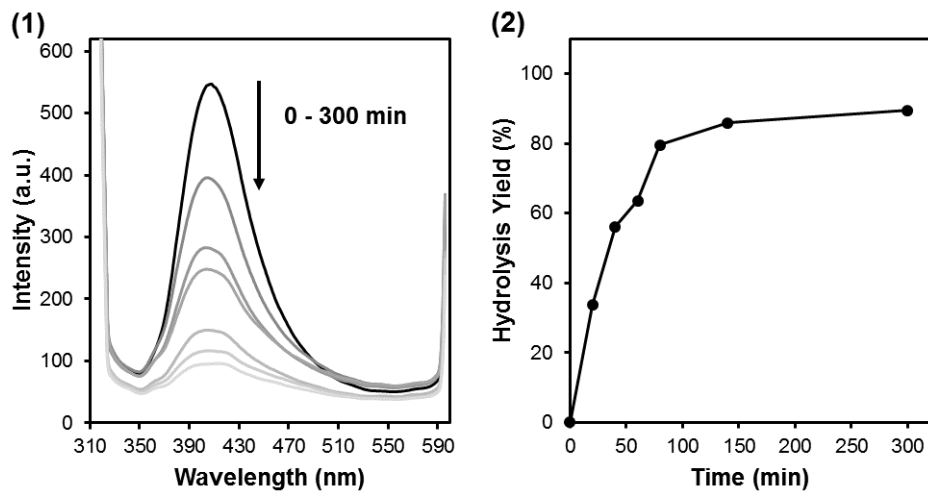
Figure 9. (1) Fluorescence spectra of MINP$_4$ during hydrolysis process. (2) Hydrolysis yield calculated based on fluorescence. To calculate the hydrolysis yield, an aliquot (40 μL) of the hydrolyzed reaction mixture was poured into acetone (10 mL). The precipitate was collected by centrifugation and washed three times with acetone (5 mL). After dried in air, the sample was dissolved in 2.00 mL of water with sonication. The fluorescence spectrum was then recorded. The hydrolysis yield was calculated based on the initial intensity.
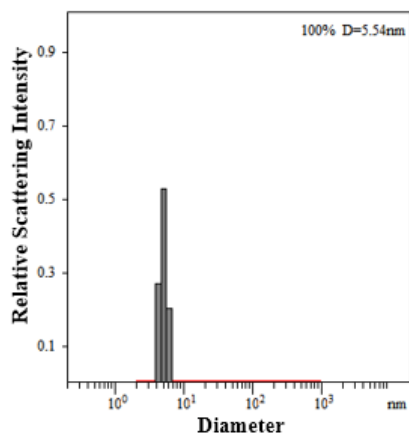
Figure 10. Distribution of the hydrodynamic diameters of the nanoparticles in water as determined by DLS for MINP₄ after HCl hydrolysis.
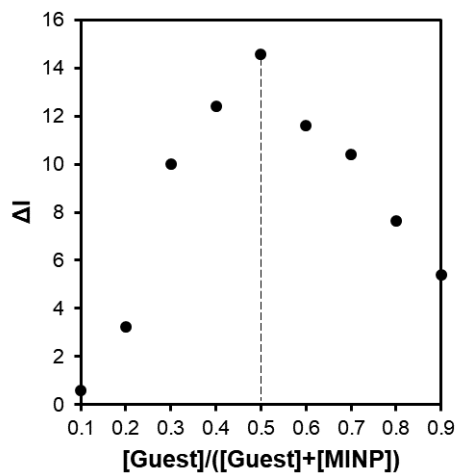
Figure 11. Job plot for MINP₄-CHO with **5** in DMF by fluorescence. The total concentration of MINP and the guest was 1.0 μM.
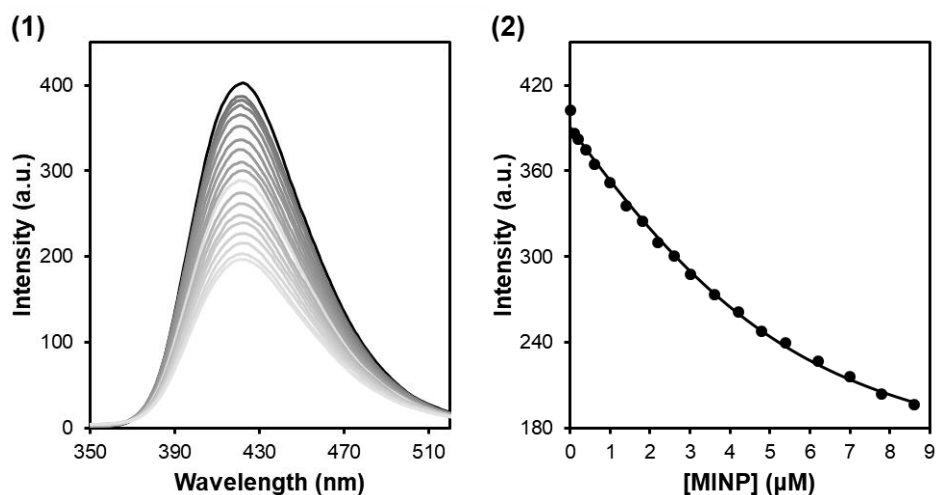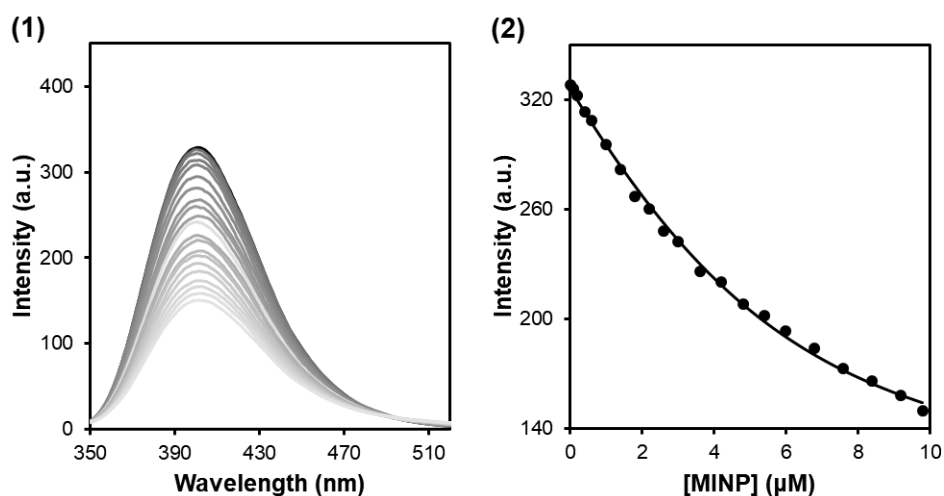
Fluorescence Titrations
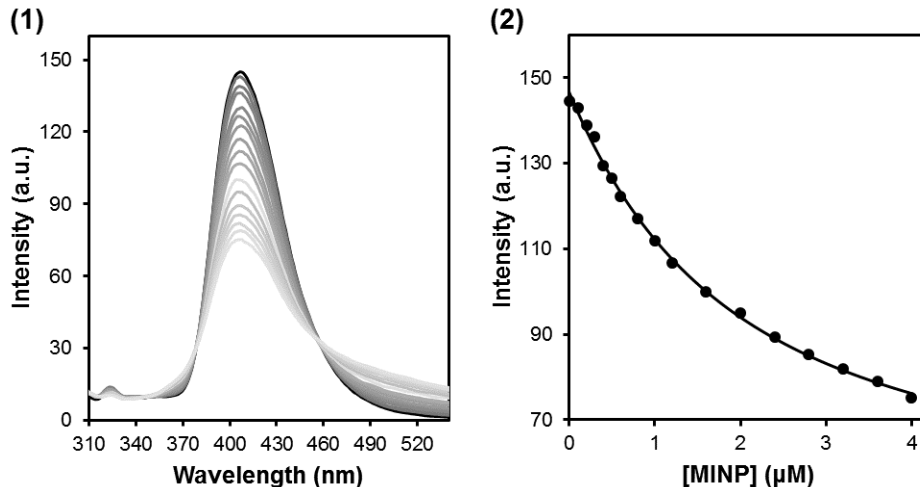
Figure 12. (1) Emission spectra of **5** upon the addition of different concentrations of MINP$_4$-CHO in DMF. [**5**] = 0.5 μM. The concentration of MINP was calculated based on an approximate M.W. of 50000 g/mol. λ_{ex} = 295 nm. (2) Plot of intensity at 406 nm with concentration of MINP and nonlinear least squares fitting of the emission intensity at 406 nm to a 1:1 binding isotherm. (Table 1, entry 1)
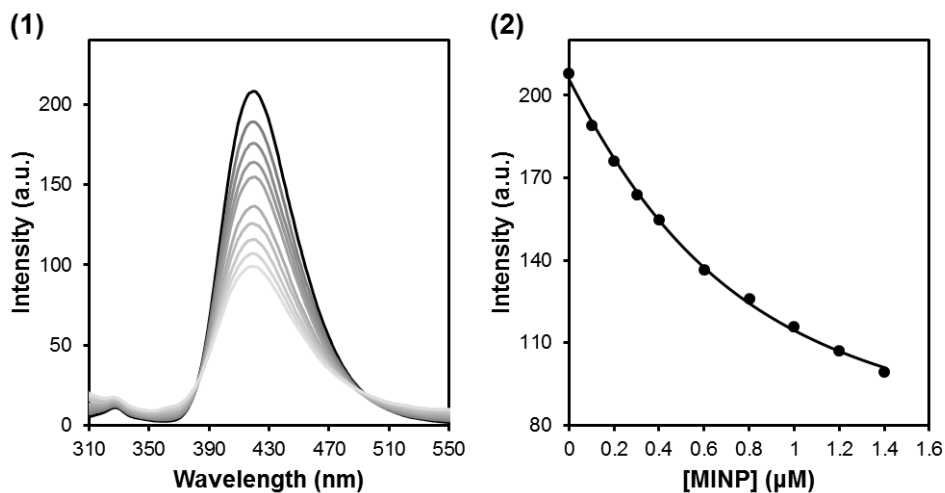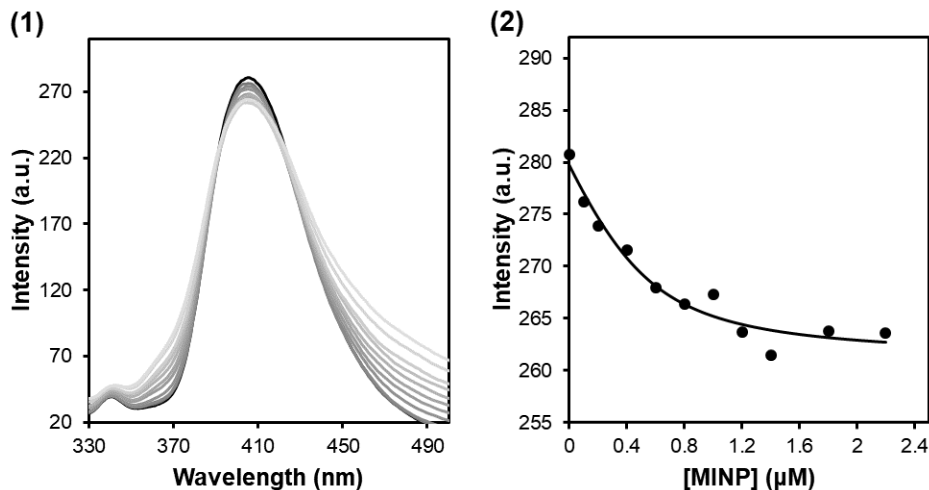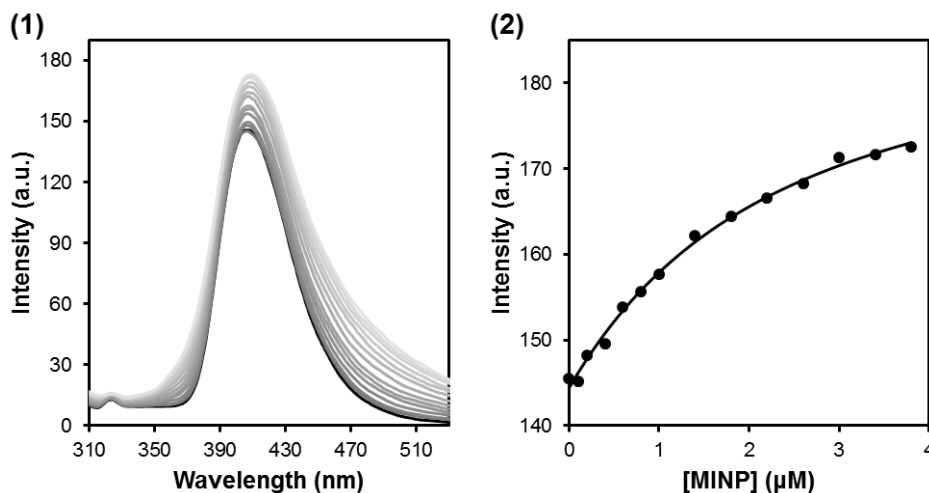

Figure 13. (1) Emission spectra of **5** upon the addition of different concentrations of MINP$_4$-CHO in 10 mM HEPES buffer pH 7.0. [**5**] = 0.5 μM. The concentration of MINP was calculated based on an approximate M.W. of 50000 g/mol. λ_{ex} = 295 nm. (2) Plot of intensity at 420 nm with concentration of MINP and nonlinear least squares fitting of the emission intensity at 420 nm to a 1:1 binding isotherm. (Table 1, entry 1 in parentheses)
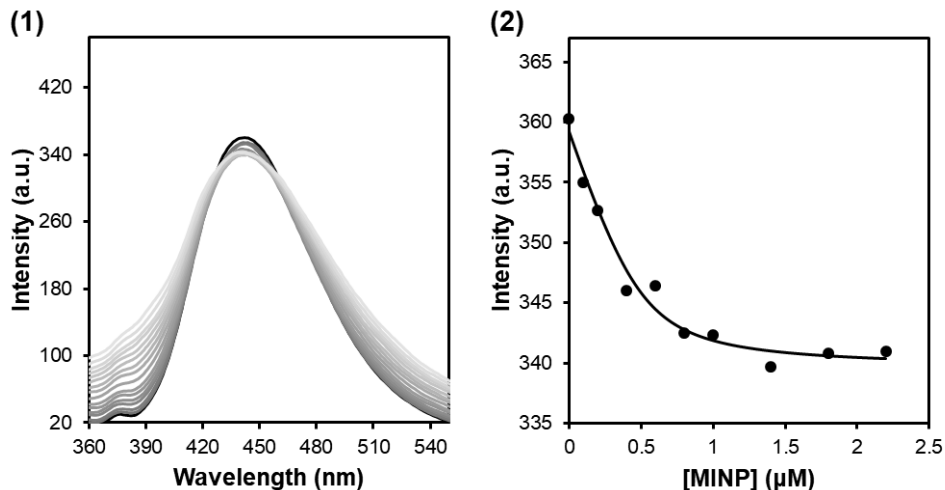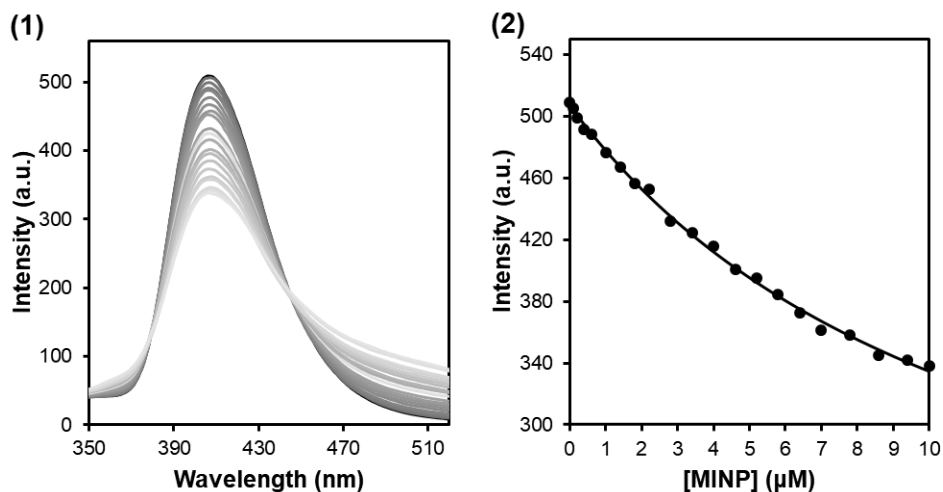
Figure 14. (1) Emission spectra of **6** upon the addition of different concentrations of MINP$_4$-CHO in DMF. [**6**] = 0.5 µM. The concentration of MINP was calculated based on an approximate M.W. of 50000 g/mol. λ_{ex} = 338 nm. (2) Plot of intensity at 440 nm with concentration of MINP and nonlinear least squares fitting of the emission intensity at 440 nm to a 1:1 binding isotherm. (Table 1, entry 2)
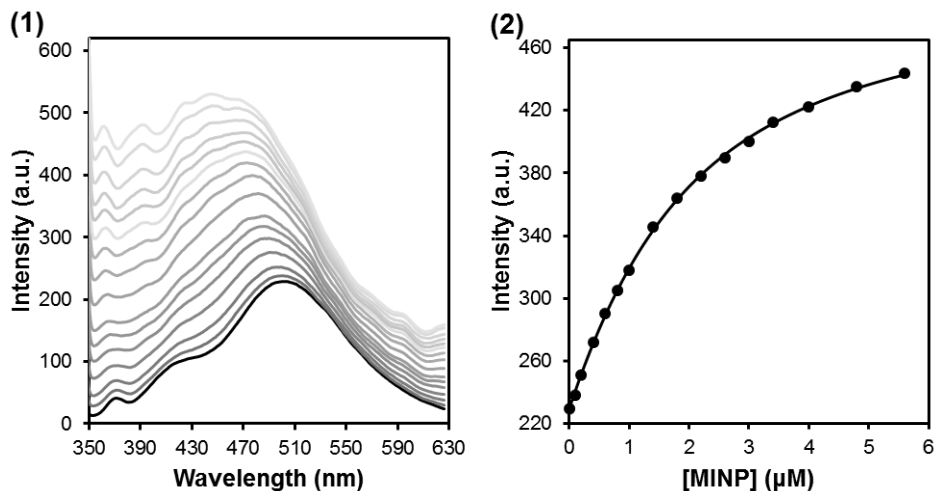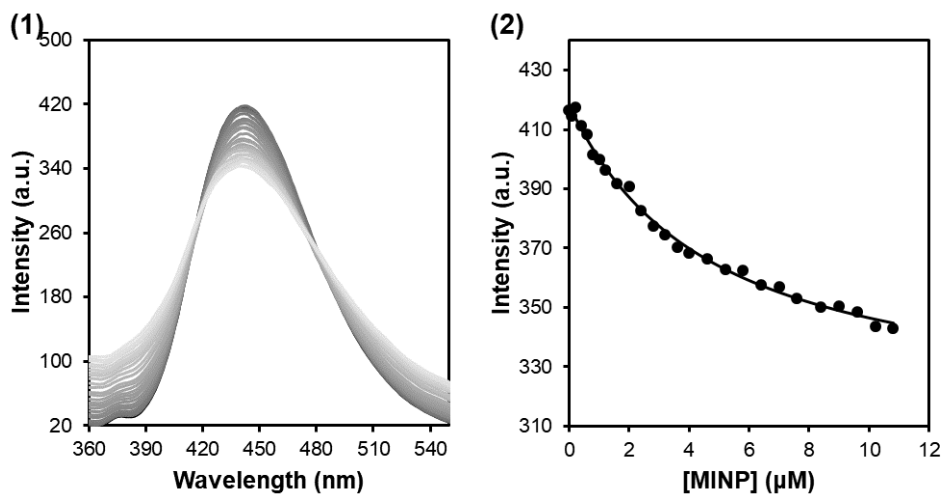

Figure 15. (1) Emission spectra of **6** upon the addition of different concentrations of MINP$_4$-CHO in 10 mM HEPES buffer pH 7.0. [**6**] = 1.0 µM. The concentration of MINP was calculated based on an approximate M.W. of 50000 g/mol. λ_{ex} = 330 nm. (2) Plot of intensity at 500 nm with concentration of MINP and nonlinear least squares fitting of the emission intensity at 500 nm to a 1:1 binding isotherm. (Table 1, entry 2 in parentheses)

Figure 16. (1) Emission spectra of **7** upon the addition of different concentrations of MINP$_4$-CHO in DMF. [**7**] = 5.0 μM. The concentration of MINP was calculated based on an approximate M.W. of 50000 g/mol. λ_{ex} = 335 nm. (2) Plot of fluorescence intensity at 420 nm with concentration of MINP and nonlinear least squares fitting of the emission intensity at 420 nm to a 1:1 binding isotherm. (Table 1, entry 3)
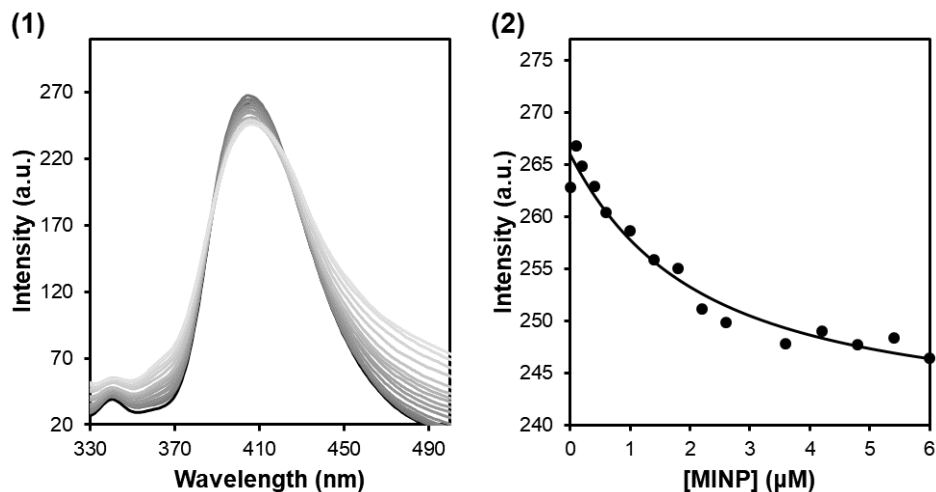

Figure 17. (1) Emission spectra of **8** upon the addition of different concentrations of MINP$_4$-CHO in DMF. [**8**] = 5.0 μM. The concentration of MINP was calculated based on an approximate M.W. of 50000 g/mol. λ_{ex} = 335 nm. (2) Plot of fluorescence intensity at 400 nm with concentration of MINP and nonlinear least squares fitting of the emission intensity at 400 nm to a 1:1 binding isotherm. (Table 1, entry 4)

**Figure 18.** (1) Emission spectra of **9** upon the addition of different concentrations of MINP$_4$-CHO in DMF. [**9**] = 0.5 μM. The concentration of MINP was calculated based on an approximate M.W. of 50000 g/mol. λ_{ex} = 309 nm. (2) Plot of fluorescence intensity at 406 nm with concentration of MINP and nonlinear least squares fitting of the emission intensity at 406 nm to a 1:1 binding isotherm. (Table 1, entry 5)

Figure 19 (1) Emission spectra of **5** upon the addition of different concentrations of MINP$_4$-CH$_2$OH (reduced by NaBH$_4$ from MINP$_4$-CHO) in DMF. [**5**] = 0.5 μM. The concentration of MINP was calculated based on an approximate M.W. of 50000 g/mol. λ_{ex} = 295 nm. (2) Plot of intensity at 406 nm with concentration of MINP and nonlinear least squares fitting of the emission intensity at 406 nm to a 1:1 binding isotherm. (Table 1, entry 6)

Figure 20. (1) Emission spectra of **5** upon the addition of different concentrations of MINP$_{10}$-CHO in DMF. [**5**] = 0.5 μM. The concentration of MINP was calculated based on an approximate M.W. of 50000 g/mol. λ_{ex} = 295 nm. (2) Plot of intensity at 406 nm with concentration of MINP and nonlinear least squares fitting of the emission intensity at 406 nm to a 1:1 binding isotherm. (Table 1, entry 7)

Figure 21. (1) Emission spectra of **6** upon the addition of different concentrations of MINP$_{10}$-CHO in DMF. [**6**] = 0.5 μM. The concentration of MINP was calculated based on an approximate M.W. of 50000 g/mol. λ_{ex} = 338 nm. (2) Plot of intensity at 440 nm with concentration of MINP and nonlinear least squares fitting of the emission intensity at 440 nm to a 1:1 binding isotherm. (Table 1, entry 8)

Figure 22. (1) Emission spectra of **9** sodium upon the addition of different concentrations of MINP$_{10}$-CHO in DMF. [**9**] = 0.5 μM. The concentration of MINP was calculated based on an approximate M.W. of 50000 g/mol. λ_{ex} = 309 nm. (2) Plot of fluorescence intensity at 406 nm with concentration of MINP and nonlinear least squares fitting of the emission intensity at 406 nm to a 1:1 binding isotherm. (Table 1, entry 9)

Imine Formation Kinetics.
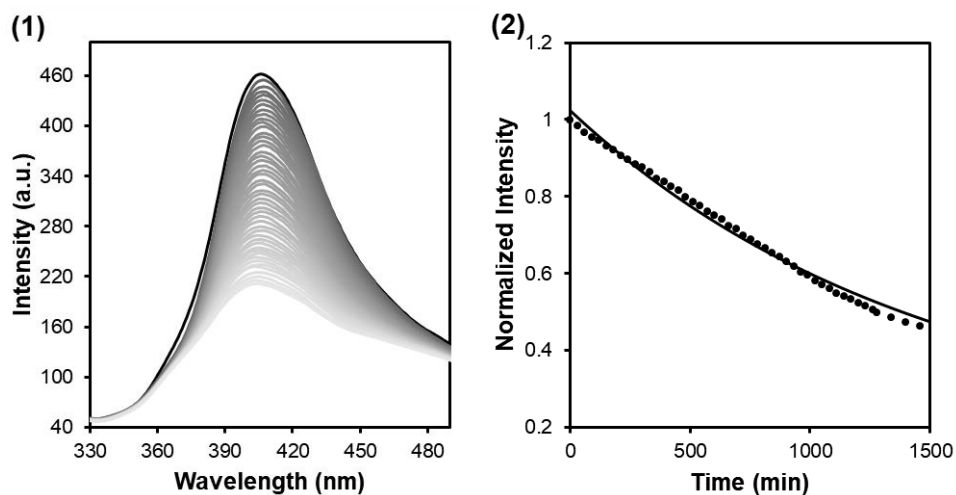
Figure 23. (1) Fluorescence spectra of **5** with 5.0 μM MINP$_4$-CHO with time in DMF at room temperature. [**5**] = 0.5 μM. λ_{ex} = 295 nm. (2) Plot of emission intensity at 406 nm of spectra in (1) and non-linear curving fitting to the first-order kinetics (Table 2, entry 1).
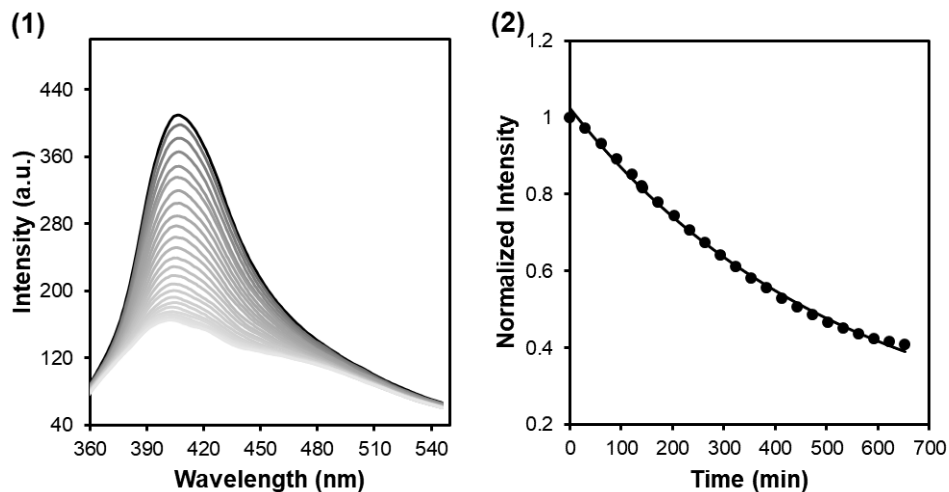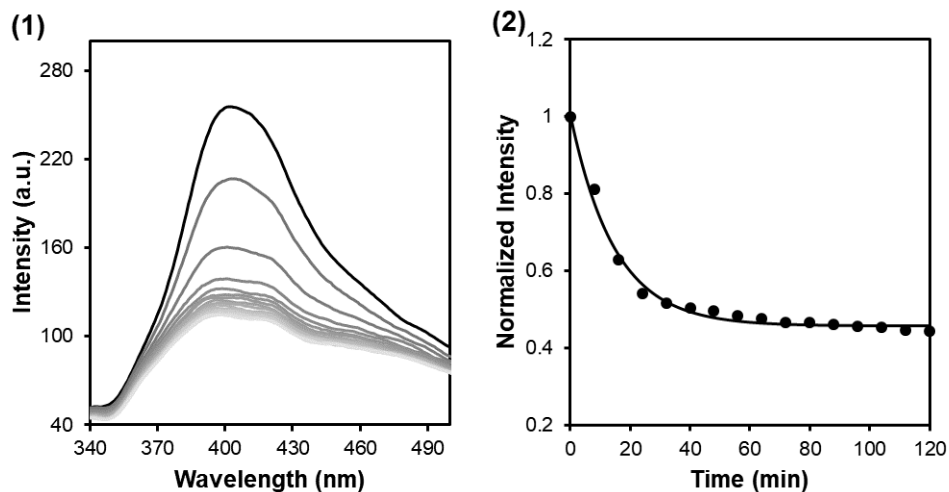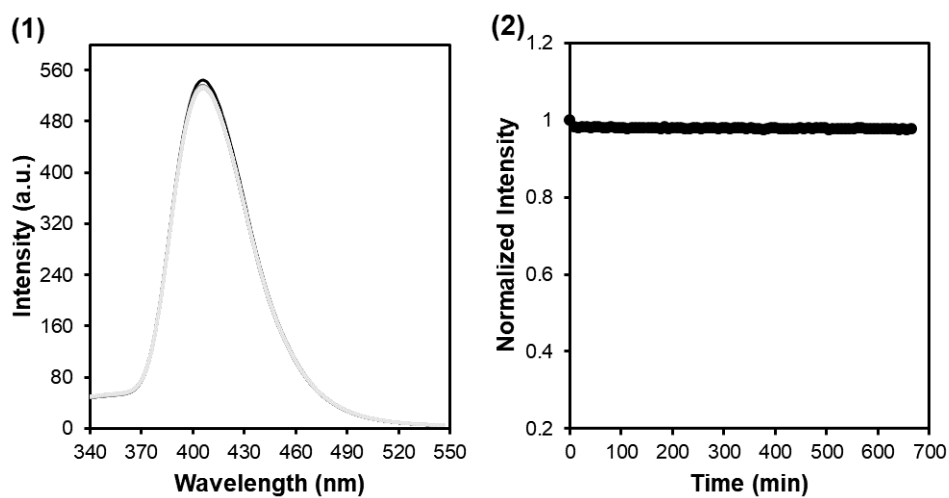
Figure 24. (1) Fluorescence spectra of **5** with 5.0 μM MINP$_4$-CHO with time in DMF at 33 °C. [**5**] = 0.5 μM. λ_{ex} = 295 nm. (2) Plot of emission intensity at 406 nm of spectra in (1) and non-linear curving fitting to the first-order kinetics (Table 2, entry 2).
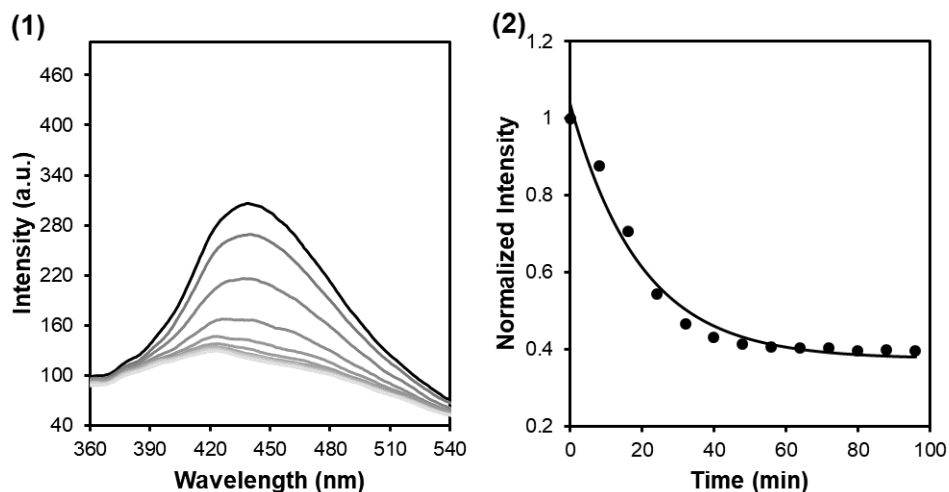
Figure 25. (1) Fluorescence spectra of **6** sodium with 5.0 μM MINP$_4$-CHO with time in DMF at 50 °C. [**6**] = 0.5 μM. λ_{ex} = 338 nm. (2) Plot of emission intensity at 439 nm of spectra in (1) and non-linear curving fitting to the first-order kinetics (Table 2, entry 4).
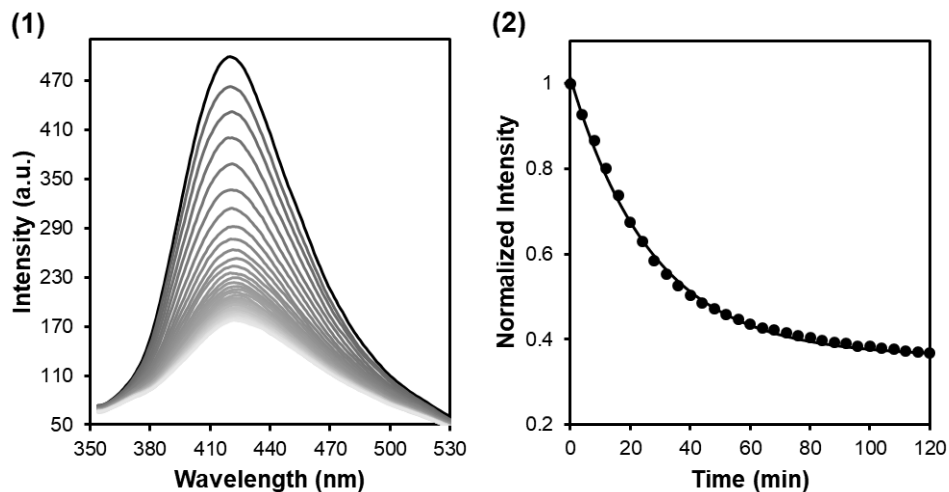
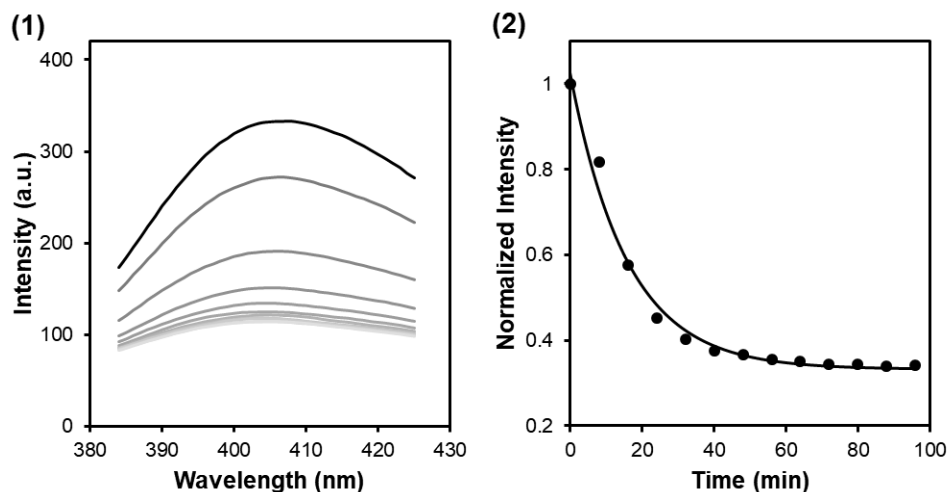**Figure 26.** (1) Fluorescence spectra of **7** with 5.0 μM MINP₄-CHO with time in DMF at 50 °C. [**7**] = 0.5 μM. λ_{ex} = 335 nm. (2) Plot of emission intensity at 420 nm of spectra in (1) and non-linear curving fitting to the first-order kinetics (Table 2, entry 5).
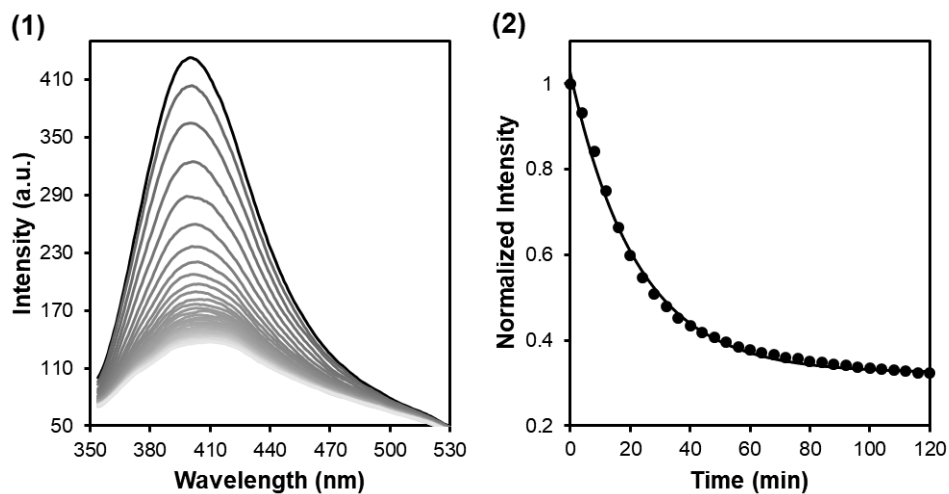
Figure 27. (1) Fluorescence spectra of **8** with 5.0 μM MINP₄-CHO with time in DMF at 50 °C. [**8**] = 0.5 μM. λ_{ex} = 335 nm. (2) Plot of emission intensity at 400 nm of spectra in (1) and non-linear curving fitting to the first-order kinetics (Table 2, entry 6).
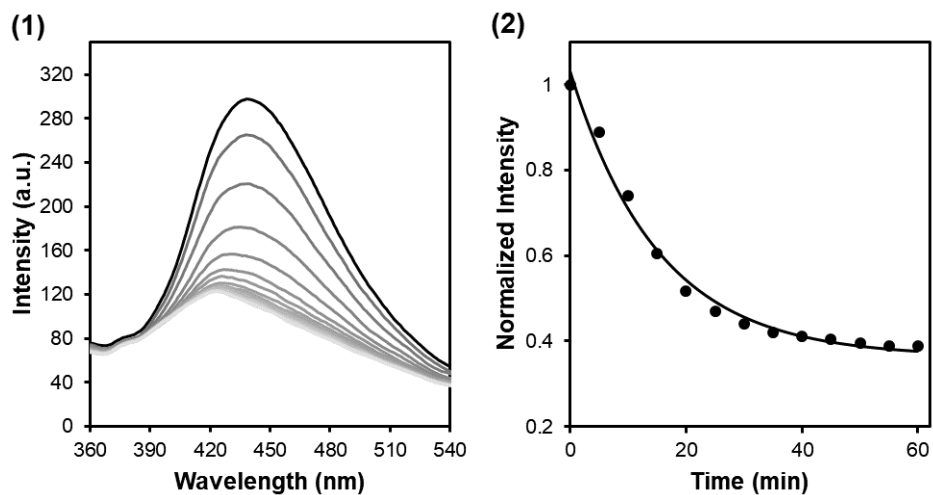
Figure 28. (1) Fluorescence spectra of **9** sodium with 5.0 μM MINP₄-CHO with time in DMF at 50 °C. [**9**] = 0.5 μM. λ_{ex} = 309 nm. (2) Plot of emission intensity at 406 nm of spectra in (1) and non-linear curving fitting to the first-order kinetics (Table 2, entry 7).
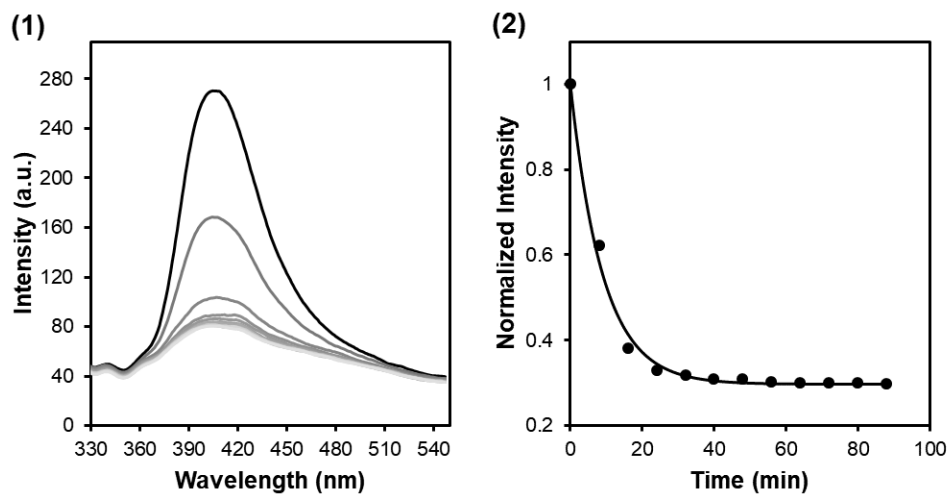

Figure 29. (1) Fluorescence spectra of **5** with 5.0 μM **11** with time in DMF at 50 °C. [**5**] = 0.5 μM. λ_{ex} = 295 nm. (2) Plot of emission intensity at 406 nm of spectra in (1) (Table 2, entry 8).
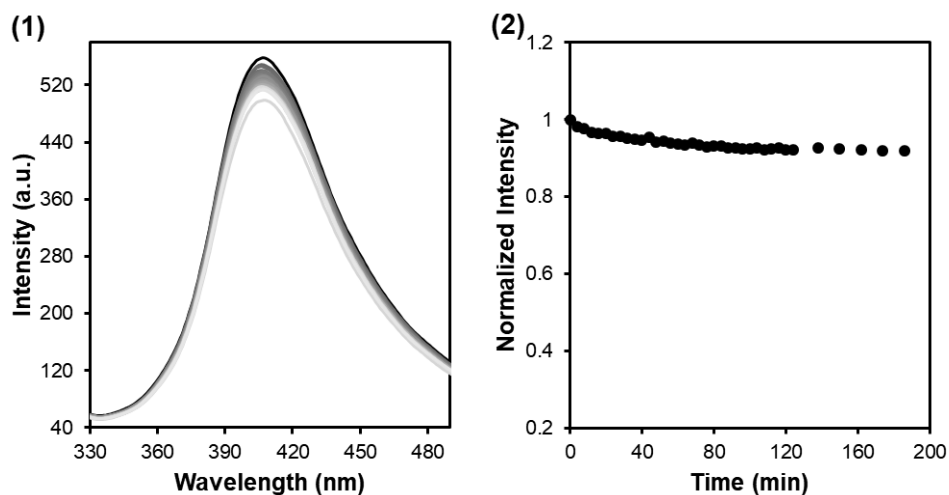
Figure 30. (1) Fluorescence spectra of **5** with 5.0 μM MINP$_4$-CH$_2$OH (reduced by NaBH$_4$ from MINP$_4$-CHO) with time in DMF at 50 °C. [**5**] = 0.5 μM. λ_{ex} = 295 nm. (2) Plot of emission intensity at 406 nm of spectra in (1) (Table 2, entry 9).

Figure 31. (1) Fluorescence spectra of **5** with 5.0 μM MINP$_{10}$-CHO with time in DMF at 50 °C. [**5**] = 0.5 μM. λ_{ex} = 295 nm. (2) Plot of emission intensity at 406 nm of spectra in (1) and non-linear curving fitting to the first-order kinetics (Table 2, entry 10).

Figure 32. (1) Fluorescence spectra of **6** with 5.0 μM MINP$_{10}$-CHO with time in DMF at 50 °C. [**6**] = 0.5 μM. λ_{ex} = 338 nm. (2) Plot of emission intensity at 439 nm of spectra in (1) and non-linear curving fitting to the first-order kinetics (Table 2, entry 11).
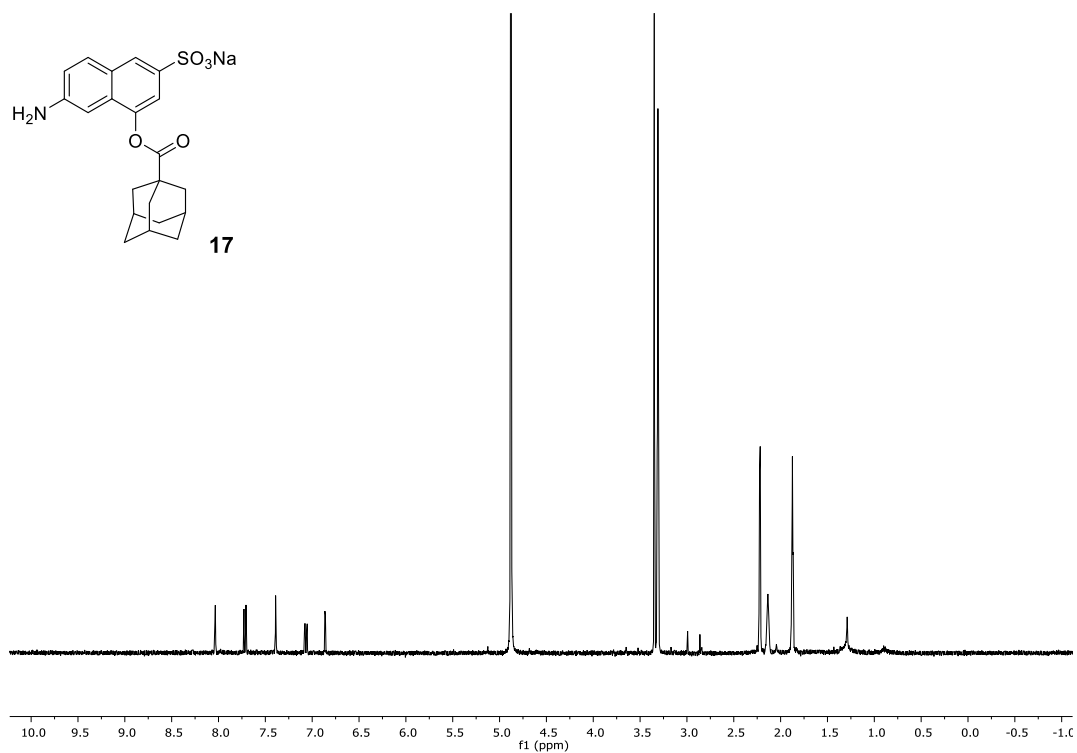

Figure 33. (1) Fluorescence spectra of **9** with 5.0 μM MINP$_{10}$-CHO with time in DMF at 50 °C. [**9**] = 0.5 μM. λ_{ex} = 309 nm. (2) Plot of emission intensity at 406 nm of spectra in (1) and non-linear curving fitting to the first-order kinetics (Table 2, entry 12).

^{1}H and ^{13}C NMR Spectra
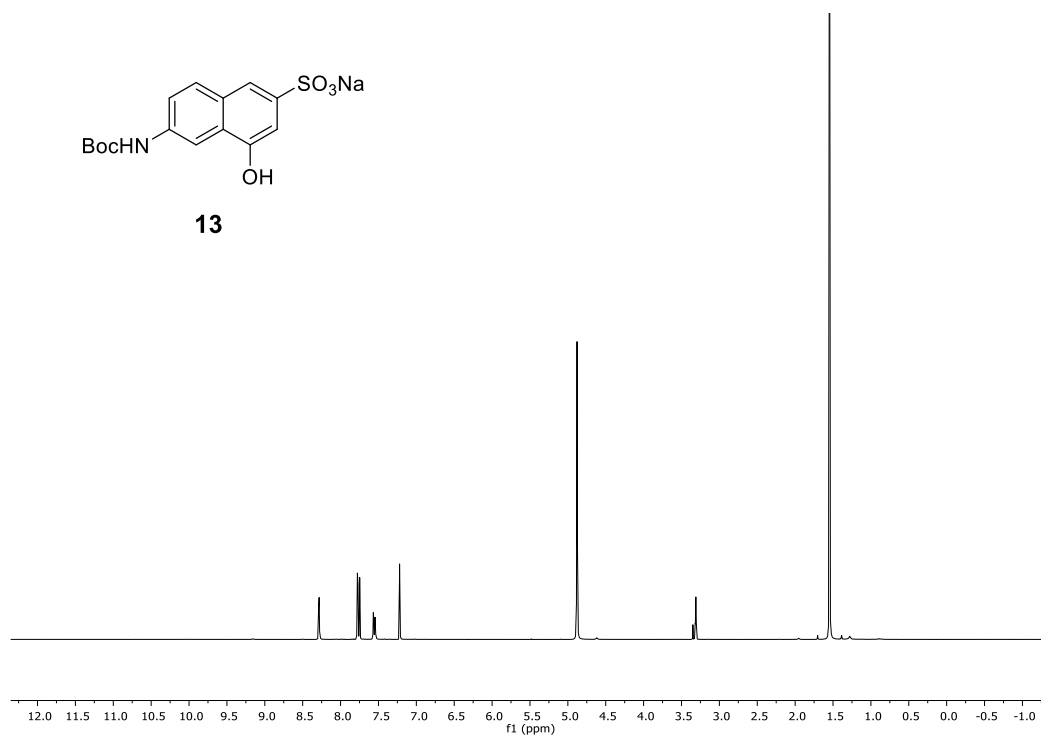
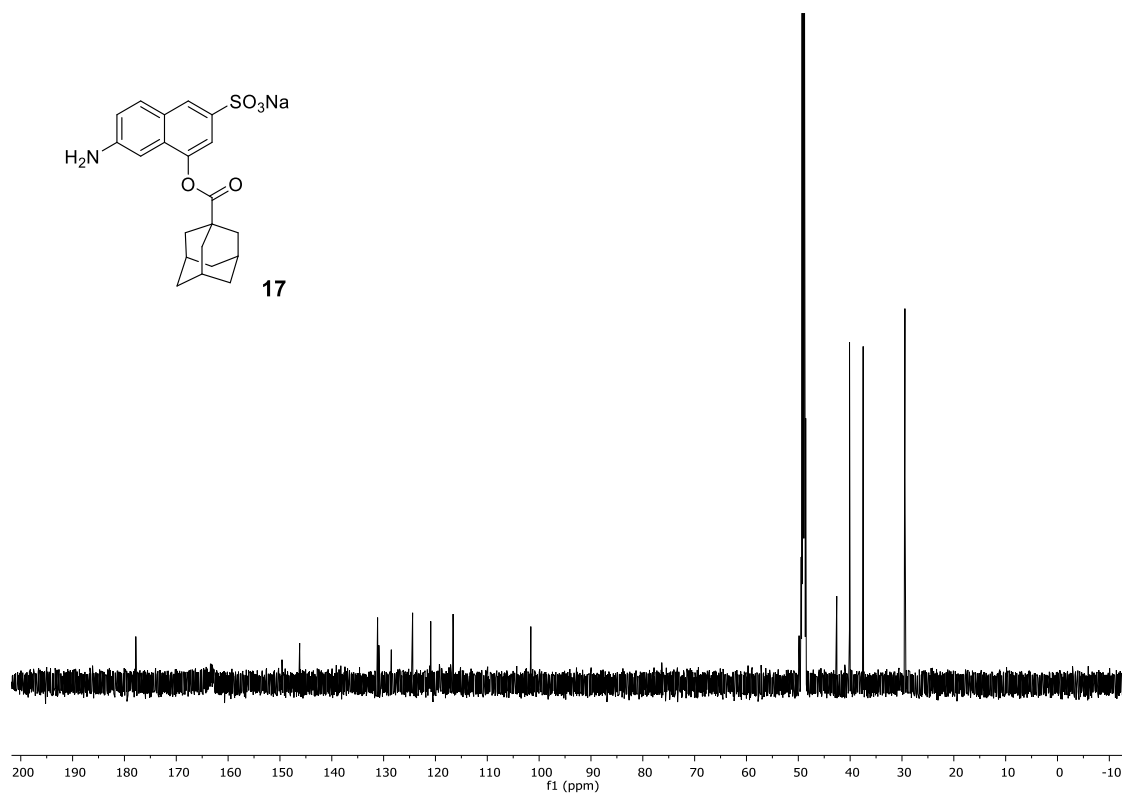**Scheme 4.** ^{1}H NMR of **13**.
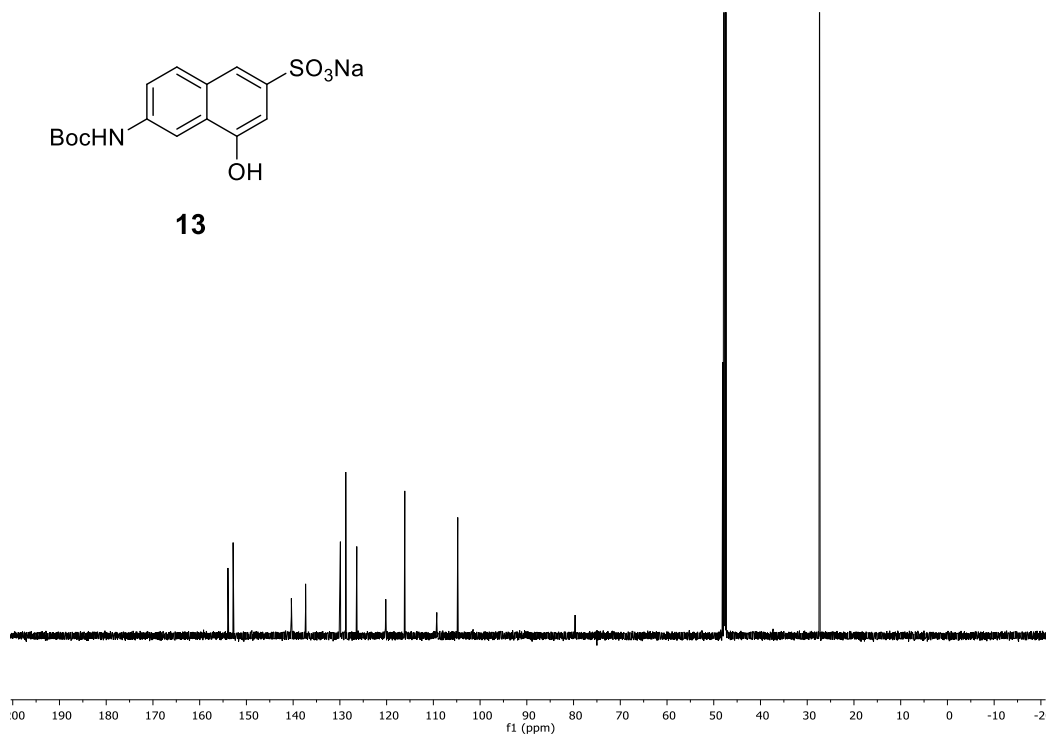
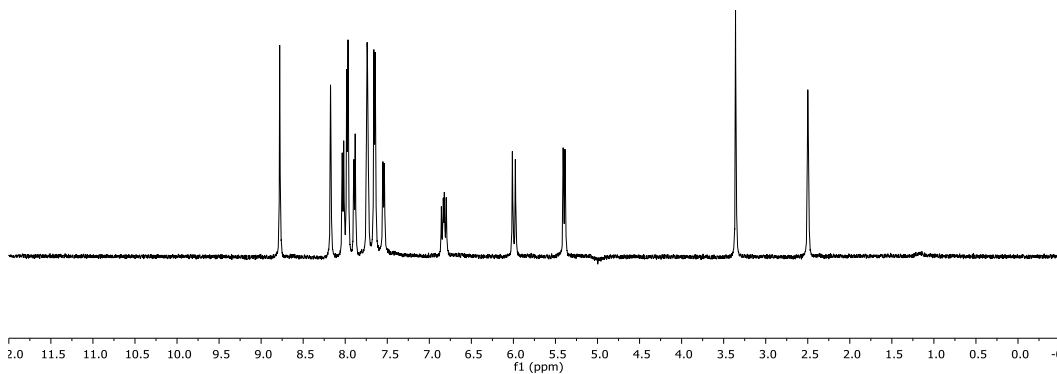**Scheme 5.** ^{13}C NMR of **13**.
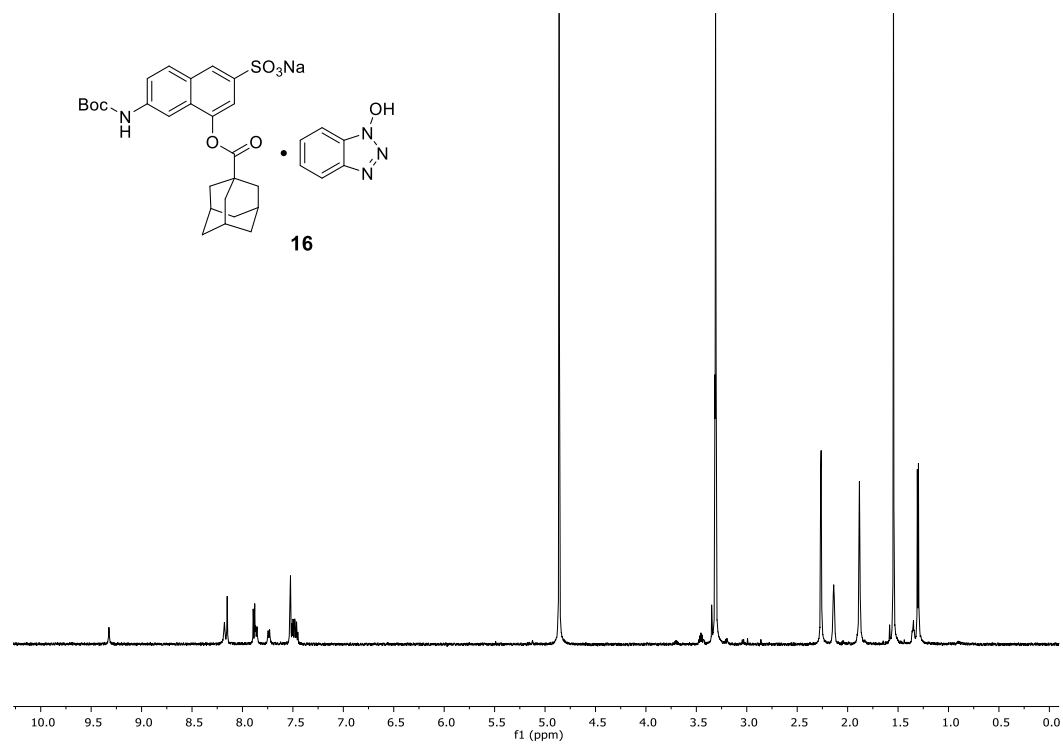
Scheme 6. ^{1}H NMR of **16**.
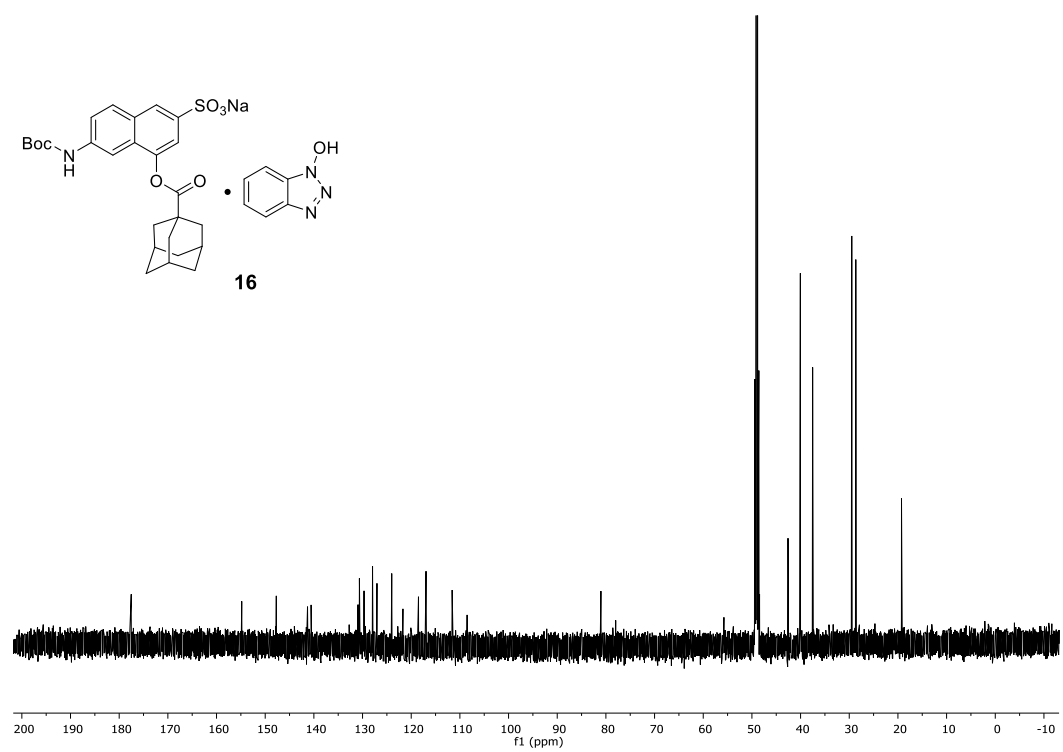
Scheme 7. ^{13}C NMR of **16**.

Scheme 8. ^{1}H NMR of **17**.

Scheme 9. ^{13}C NMR of **17**.
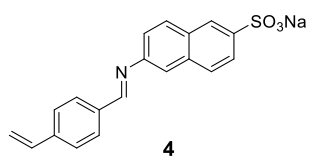
Scheme 10. ^{1}H NMR of **4**.
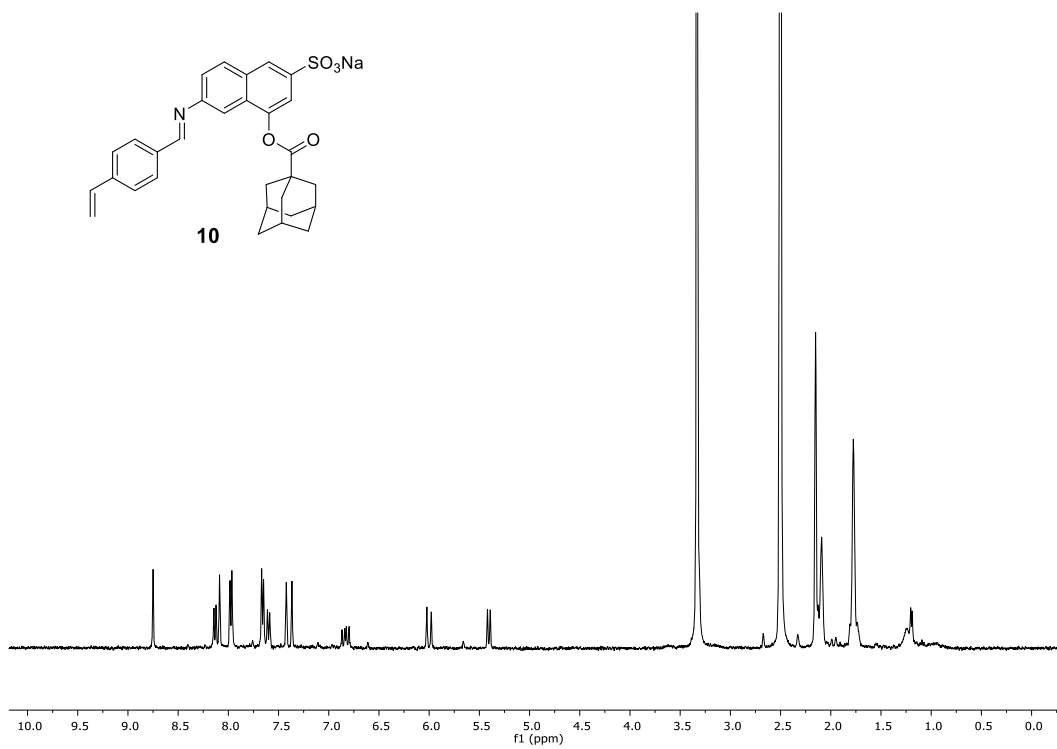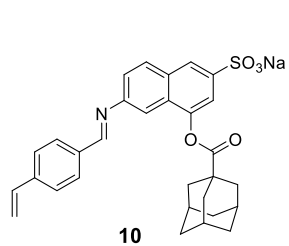
Scheme 11. ^{1}H NMR of **10**.

Notes and References

(1) (a) Hou, J.-L.; Ajami, D.; Rebek, J. Reaction of Carboxylic Acids and Isonitriles in Small Spaces. *J. Am. Chem. Soc.* **2008**, *130*, 7810-7811.(b) Kaphan, D. M.; Toste, F. D.; Bergman, R. G.; Raymond, K. N. Enabling New Modes of Reactivity Via Constrictive Binding in a Supramolecular-Assembly-Catalyzed Aza-Prins Cyclization. *J. Am. Chem. Soc.* **2015**, *137*, 9202-9205.

(2) (a) Yoshizawa, M.; Tamura, M.; Fujita, M. Diels-Alder in Aqueous Molecular Hosts: Unusual Regioselectivity and Efficient Catalysis. *Science* **2006**, *312*, 251-254.(b) Nishioka, Y.; Yamaguchi, T.; Yoshizawa, M.; Fujita, M. Unusual [2+4] and [2+2] Cycloadditions of Arenes in the Confined Cavity of Self-Assembled Cages. *J. Am. Chem. Soc.* **2007**, *129*, 7000-7001.

(3) (a) Kaanumalle, L. S.; Ramamurthy, V. Photodimerization of Acenaphthylene within a Nanocapsule: Excited State Lifetime Dependent Dimer Selectivity. *Chem. Commun.* **2007**, 1062-1064.(b) Laughrey, Z. R.; Gibb, C. L. D.; Senechal, T.; Gibb, B. C. Guest Binding and Orientation within Open Nanoscale Hosts. *Chem.-Eur. J.* **2003**, *9*, 130-139.(c) Parthasarathy, A.; Kaanumalle, L. S.; Ramamurthy, V. Controlling Photochemical Geometric Isomerization of a Stilbene and Dimerization of a Styrene Using a Confined Reaction Cavity in Water. *Org. Lett.* **2007**, *9*, 5059-5062.(d) Natarajan, A.; Kaanumalle, L. S.; Jockusch, S.; Gibb, C. L. D.; Gibb, B. C.; Turro, N. J.; Ramamurthy, V. Controlling Photoreactions with Restricted Spaces and Weak Intermolecular Forces: Exquisite Selectivity During Oxidation of Olefins by Singlet Oxygen. *J. Am. Chem. Soc.* **2007**, *129*, 4132-4133.

(4) (a) Wulff, G. Molecular Imprinting in Cross-Linked Materials with the Aid of Molecular Templates— a Way Towards Artificial Antibodies. *Angew. Chem. Int. Ed. Engl.* **1995**, *34*, 1812-1832.(b) Wulff, G. Enzyme-Like Catalysis by Molecularly Imprinted Polymers. *Chem. Rev.* **2001**, *102*, 1-28.(c) Haupt, K.; Mosbach, K. Molecularly Imprinted Polymers and Their Use in Biomimetic Sensors. *Chem. Rev.* **2000**, *100*, 2495-2504.(d) Ye, L.; Mosbach, K. Molecular Imprinting: Synthetic Materials as Substitutes for Biological Antibodies and Receptors. *Chem. Mater.* **2008**, *20*, 859-868.(e) Shea, K. J. Molecular Imprinting of Synthetic Network Polymers: The De Novo Synthesis of Macromolecular Binding and Catalytic Sites. *Trends Polym. Sci.* **1994**, *2*, 166-173.(f) Sellergren, B.: *Molecularly Imprinted Polymers: Man-Made Mimics of Antibodies and Their Applications in Analytical Chemistry*; Elsevier: Amsterdam, 2001.(g) Komiyama, M.: *Molecular Imprinting: From Fundamentals to Applications*; Wiley-VCH: Weinheim, 2003.(h) Yan, M.; Ramström, O.: *Molecularly Imprinted Materials: Science and Technology*; Marcel Dekker: New York, 2005.(i) Alexander, C.; Andersson, H. S.; Andersson, L. I.; Ansell, R. J.; Kirsch, N.; Nicholls, I. A.; O'Mahony, J.; Whitcombe, M. J. Molecular Imprinting Science and Technology: A Survey of the Literature for the Years up to and Including 2003. *J. Mol. Recognit.* **2006**, *19*, 106-180.(j) Sellergren, B.; Hall, A. J.: Molecularly Imprinted Polymers. In *Supramolecular Chemistry: From Molecules to Nanomaterials*; Steed, J. W., Gale, P. A., Eds.; Wiley: Online, 2012.(k) Haupt, K.: *Molecular Imprinting*; Springer: Heidelberg ; New York, 2012.

(5) (a) Awino, J. K.; Zhao, Y. Protein-Mimetic, Molecularly Imprinted Nanoparticles for Selective Binding of Bile Salt Derivatives in Water. *J. Am. Chem. Soc.* **2013**, *135*, 12552-12555.(b) Awino, J. K.; Zhao, Y. Molecularly Imprinted Nanoparticles as Tailor-Made Sensors for Small Fluorescent Molecules. *Chem. Commun.* **2014**, *50*, 5752-5755.(c) Awino, J. K.; Zhao, Y. Water-Soluble Molecularly Imprinted Nanoparticles (Minps) with Tailored, Functionalized, Modifiable Binding Pockets. *Chem.-Eur. J.* **2015**, *21*, 655-661.(d) Awino, J. K.; Zhao, Y. Polymeric Nanoparticle Receptors as Synthetic Antibodies for Nonsteroidal Anti-Inflammatory Drugs (Nsaids). *ACS Biomater. Sci. Eng.* **2015**, *1*, 425-430.

(6) (a) Fa, S.; Zhao, Y. Peptide-Binding Nanoparticle Materials with Tailored Recognition Sites for Basic Peptides. *Chem. Mater.* **2017**, *29*, 9284-9291.(b) Fa, S.; Zhao, Y. Water-Soluble Nanoparticle Receptors Supramolecularly Coded for Acidic Peptides. *Chem. -Eur. J.* **2018**, *24*, 150-158.

(7) Layer, R. W. The Chemistry of Imines. *Chem. Rev.* **1963**, *63*, 489-510.

(8) (a) Awino, J. K.; Hu, L.; Zhao, Y. Molecularly Responsive Binding through Co-Occupation of Binding Space: A Lock–Key Story. *Org. Lett.* **2016**, *18*, 1650-1653.(b) Awino, J. K.; Gunasekara, R. W.; Zhao, Y. Sequence-Selective Binding of Oligopeptides in Water through Hydrophobic Coding. *J. Am. Chem. Soc.* **2017**, *139*, 2188-2191.(c) Awino, J. K.; Zhao, Y. Imprinted Micelles for Chiral Recognition in Water: Shape, Depth, and Number of Recognition Sites. *Org. Biomol. Chem.* **2017**, *15*, 4851-4858.

(9) D. Song, S. Cho, Y. Han, Y. You, W. Nam, *Org. Lett.* **2013**, *15*, 3582-3585.

(10) Arifuzzaman, M. D.; Zhao, Y. *J. Org. Chem.* **2017**, *81*, 7518.

(11) Schneider, H. J.; Yatsimirsky, A. K. *Principles and methods in supramolecular chemistry*; New York: J. Wiley, 2000; pp 137-146.

CHAPTER 5.
FLUORESCENCE NANOPARTICLE SENSORS WITH TAILOR-MADE RECOGNITION UNITS AND PROXIMATE FLUORESCENT REPORTER GROUPS

Manuscript submitted.

Xiaoyu Xing and Yan Zhao

Abstract

The molecular recognition unit of a fluorescent sensor is its most cumbersome part to design and synthesize, but is key to the specificity of the sensor. Molecular imprinting within cross-linked micelles using easily synthesized modular templates allowed us to create analyte-specific binding sites with a nearby fluorescent probe. This strategy makes it straightforward to vary the recognition unit independent of the reporting unit, making the sensor potentially applicable to a wide range of molecular analytes.

Introduction

Fluorescent sensors have attracted many researchers' attention for their high sensitivity, ease of operation, and broad range of analytes that can be detected.[1-5] The general design of a fluorescent sensor consists of a recognition unit whose binding of the analyte is transduced to a nearby fluorescent probe.[6] Although different signal-transducing mechanisms such as quenching, FRET, and PET may be used, the central feature for any sensor is the selective binding of the interested analyte. With the advancement of supramolecular chemistry over the last decades, many metal-binding ligands and macrocycles have been developed and used in fluorescent sensing.[1-6] For molecular analytes, their structural diversity makes it challenging to have a common recognition motif. Generally speaking, the design and synthesis of the recognition unit in a fluorescent sensor is the most tedious part of the research and must be performed on an individual basis for each analyte.

Molecular imprinting is a technique to create analyte-specific binding sites in a polymer matrix.[7, 8] Molecularly imprinted polymers (MIPs) have been used in molecular sensing since their discovery.[9-15] Nonetheless, traditional MIPs are highly cross-linked macroscopic polymers with poor solubility and a heterogeneous distribution of binding sites. Although they can be converted into fluorescent sensors for specific molecules, their insolubility and high cross-linking density make it difficult to manipulate these materials accurately on the molecular level.

Results and Discussion
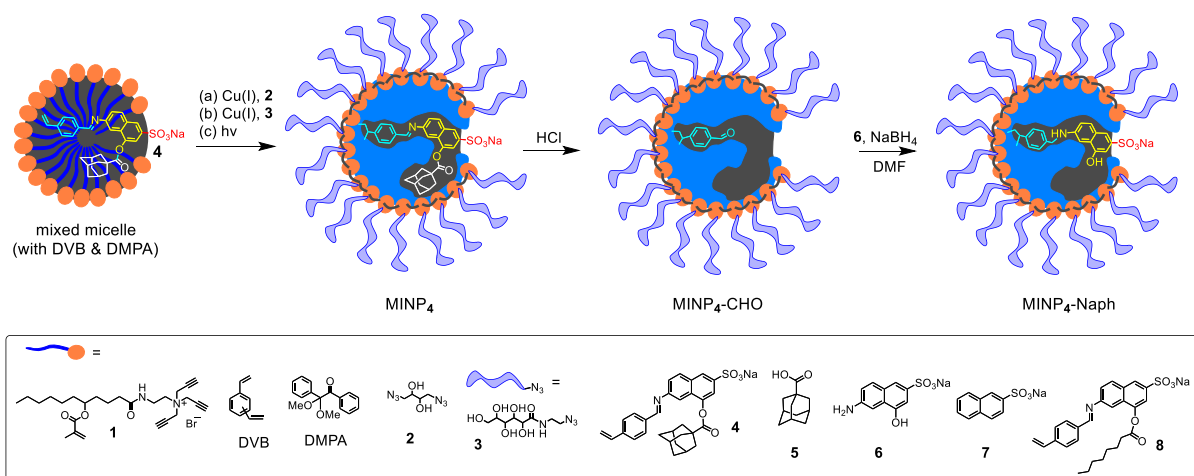
Scheme 1. Preparation of MINP-CHO by micellar covalent imprinting and hydrolysis, followed by reaction with **6** to form MINP₄-Naph.

In this work, we employed a strategy that combined covalent imprinting with post-functionalization on molecularly imprinted nanoparticles (MINPs).[16-19] The strategy was enabled by the solubility of the materials in water and selected organic solvents, the nanodimension of the materials, and the location of the template near the surface of the cross-linked nanoparticles. Our method readily afforded a tailor-made binding site for specific analytes (carboxylic acids as an example) with a nearby fluorescent reporting probe. We

believe the method represents a general way to construct molecule-specific fluorescent sensors with minimal individual design of the molecular recognition unit.

The synthesis of our fluorescent sensors is shown in Scheme 1, based on the micellar imprinting recently developed by our group.[20-23] The essence of the method is to confine the polymerization/cross-linking for the imprinting within individual micelles, a feature that has been difficult to realize. Using the highly efficient click reaction between terminal alkynes and azides, we cross-linked the micelle of surfactant **1** first on the surface using diazide **2**. Another round of click reaction with monoazide **3** decorated the surface with a layer of hydrophilic groups.

The color-coded **4** in the mixed micelle of Scheme 1 is the key to our design. The molecule contains several "modules" that could be exchanged readily. The white-colored adamantanecarboxyl moiety is used to create an analyte-specific binding site (for 1-adamantanecarboxylic acid **5**). It is linked to the yellow fluorescent reporter that has a 6-aminonaphthalene-2-sulfonate moiety, which is similar to the more popular environmentally sensitive fluorophore dansyl (1-dimethylaminonaphthalene-5-sulfonyl). The amine group is linked by an imine bond to 4-vinylbenzaldehyde (shown in cyan). Previously, we have used an *ortho*-nitrobenzyl ester-based template and, by cleaving the photocleavable group, installed a carboxylic acid group inside the MINP binding pocket.[22] We chose an imine linkage in this work because of its much easier synthesis and facile post-functionalization (vide infra). The (red) anionic sulfonate group of **4** allowed the overall hydrophobic molecule to be easily incorporated into the cationic micelle of **1** and helped the molecule stay near the surface of the micelle. This feature is important to hydrolysis of the imine and the subsequent post-functionalization (vide infra).

As shown in Scheme 1, the mixed micelle also contained divinylbenzene (DVB) and 2,2-dimethoxy-2-phenylaceto-phenone (DMPA), which allowed us to perform photopolymerization/cross-linking of the micelle core, with **4** covalently attached to the micelle in the meantime by the free radical polymerization.

The synthesis and characterizations of MINPs have been reported previously[20-23] and are found in the experimental section. The surface-cross-linking, surface-decoration, and core-cross-linking were monitored by ^{1}H NMR spectroscopy and dynamic light scattering (DLS). DLS allowed us to measure the size of the MINP (ca. 5 nm) and estimate its molecular weight (ca. 50,000–60,000). The DLS size has been confirmed by transmission electron microscopy (TEM).[24, 25]
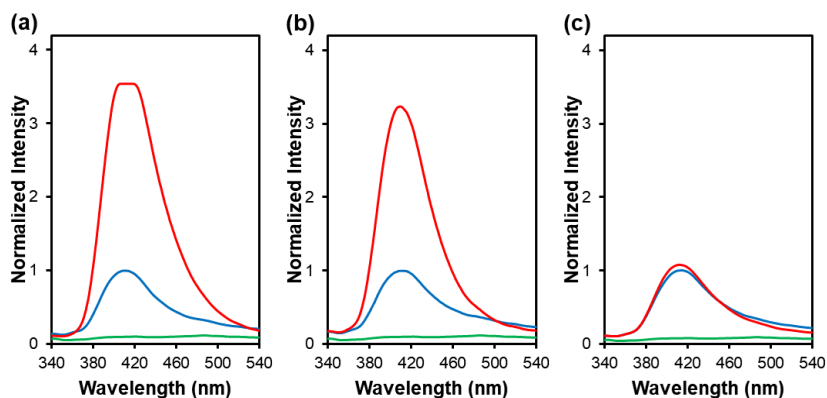
Figure 1. Normalized fluorescence spectra of MINP**4**-CHO (green), as prepared MINP**4**-C=N-Naph (blue), and MINP**4**-C=N-Naph treated with (a) 0 equiv, (b) 100 equiv, (c) 500 equiv NaBH$_4$ (red). The red spectra were taken after the aqueous sample (blue spectrum) was left standing overnight. [MINP] = 5.0 μM. λ_{ex} = 307 nm.

With MINP**4** (i.e., MINP prepared with compound **4**) in hand, we studied different methods to hydrolyze the imine bond. Although the imine was located inside the hydrophobic core of the cross-linked micelle, 6 M HCl at 95 °C was found to cleave the fluorescent naphthyl group (along with the adamantyl). The naphthyl group emitted at 405 nm (Fig. 12). Treatment

with the acid reduced the fluorescence intensity and the emission of the naphthyl disappeared nearly completely at 120 min (Fig. 1a, green spectrum).

At this point, the MINP$_4$-CHO produced is expected to contain voids left from the naphthyl and the adamantyl groups. The nanosized nanoparticle was soluble in DMF[22] and was mixed with a large excess (50 equiv) of 6-amino-4-hydroxy-2-naphthalenesulfonate **6** for 2 h. Formation of the imine bond was evident from the reappearance of the naphthyl emission after excess **6** was removed (compare the blue vs green spectra in Fig. 1a). However, the imine bond was not stable in aqueous solution, as incubation of the resulting nanoparticle (referred to as MINP$_4$-C=N-Naph) in water released **6** into the environment, which showed a stronger fluorescence (red).

Treatment of MINP$_4$-C=N-Naph with 100 equiv NaBH$_4$ increased its aqueous stability, as shown by the smaller difference between the incubated (red) and the as prepared MINP$_4$-C=N-Naph (blue) spectra in Fig. 1b. This should come from the reduction of the imine bond to amine by NaBH$_4$. Indeed, treatment of MINP$_4$-C=N-Naph with 500 equiv NaBH$_4$ led to aqueous-stable MINP$_4$-Naph that displayed little change in fluorescence after incubation in water overnight (Fig. 1c, note the nearly identical blue and red spectra).
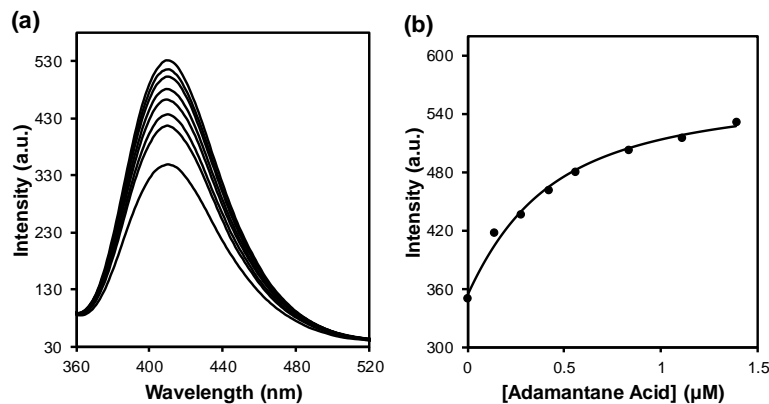
Figure 2. (a) Emission spectra of MINP$_4$-Naph upon addition of different concentrations of **5** in water. [MINP$_4$-Naph] = 1.0 μM. λ_{ex} = 307 nm. (b) Nonlinear least squares curve fitting of the fluorescence intensity at 410 nm to the 1:1 binding isotherm.

If the hydrolysis of imine and the following reductive amination worked as expected, MINP$_4$-Naph was expected to have an adamantyl-shaped binding pocket with a nearby fluorescent group (Scheme 1). It should be able to bind 1-adamantanecarboxylic acid **5** and the binding should influence the fluorescence of the nearby covalently attached 6-aminonaphthalene-2-sulfonate. Indeed, as shown in Fig. 2, addition of **5** to an aqueous solution of MINP$_4$-Naph increased the latter's emission intensity steadily. The fluorescence increase was consistent with displacement of water molecules near the probe by a more hydrophobic guest. The emission intensity fit well to a 1:1 binding isotherm, yielding a binding constant of $K_a = (48 \pm 14) \times 10^5 \, M^{-1}$ (Fig. 2b). The 1:1 binding resulted from the 50:1 ratio used between **1** and **4**, as well as the aggregation number of the surfactant in the micelle (ca. 50).[20] This feature has been verified numerous times in our previous MINPs both by fluorescence titration and isothermal titration calorimetry (ITC).[20-23]

1-Adamantanecarboxylic has poor solubility in water. Its large hydrophobic surface area gives the molecule a strong driving force to enter a hydrophobic environment. Additionally, hydrogen bonds may form between the carboxylic acid of **5** and the hydroxyl

group on the naphthyl group of MINP$_4$-Naph. The strong binding was consistent to the successful creation of the binding pocket from the covalent molecular imprinting and post treatment.

When we started the project, it was unclear to us how accessible the binding pocket would be to an externally added guest. Nonetheless, the fluorescence titration in Fig. 2 required no extra time for equilibration and the fluorescence stabilized quickly after each addition of **5**. It is possible that the binding site was quite close to the surface of the cross-linked micelle. Also, the propargyl groups of **1** and the diazide **2** suggest that over a dozen bonds exist between two cross-linked ammonium headgroups in our MINP. Molecules such as **5** with as many as five bonds in the cross-section might diffuse fairly easily across the surface cross-linkages. It is also possible that part of the binding pocket is exposed to water, resulting from the proximity of the adamantyl group to the surface and/or incomplete cross-linking around the template on the side of the micelle surface.

In our studies, we assumed the hydrolysis and reductive amination both proceeded quantitatively with the large excess of reagents used. Completion of the hydrolysis was evident from the near flat baseline of the fluorescence spectrum of MINP$_4$-CHO (Fig. 1, green spectra). The yield of the reductive amination, however, could not be determined directly. If the yield was less than quantitative, some of the binding events that occurred would not be reported by the fluorescence titration, as the fluorescent reporter would be absence in those MINPs that had not been functionalized with **6**. In such a case, the binding constant obtained from the fluorescence titration should represent the lower limit of the real value.

We are interested in detecting the acid in neutral water. When we performed the titration in 10mM HEPES buffer (pH 7.4), the binding was weaker, with $K_a = (3 \pm 0.3) \times 10^5$

M^{-1} (Fig. 15). This was a reasonable result because once the acid was deprotonated in the buffer, the ionic group would have difficulty entering a highly hydrophobic binding pocket due to the poor solvation of the carboxylate. The binding then needed to overcome an unfavorable re-protonation step, which weakens the binding.[22]

To make sure our hydrolysis and reductive amination conditions did not damage the rest of the MINP structure, at least the binding site, we prepared a MINP receptor for naphthalenesulfonate **7**. This template does not have a polymerizible group and the imprinting is thus noncovalent in nature. We have shown anionic hydrophobic guests of similar size can be used effectively to create a template-specific binding pocket.[20, 22, 23] In our hands, MINP**7** was found to bind **7** with $K_a = (6.2 \pm 0.2) \times 10^5\,M^{-1}$. After the 6M HCl treatment and "reductive amination/dialysis" (even though no imine bond was present), the MINP was found to bind **7** with $K_a = (5.7 \pm 0.6) \times 10^5\,M^{-1}$ and $(7.8 \pm 0.3) \times 10^5\,M^{-1}$, respectively (Fig. 16–18). Thus, these treatments did not alter the binding properties of amine-free MINPs, suggesting the "backbone" structure of the MINP—comprised of mainly hydrocarbon and cross-linked DVB/styrene/methacrylate—was not affected by the hydrolysis and reductive amination treatments.

Table 1. Binding data for MINP**4**-Naph and MINP**8**-Naph for different acids in water.[a]

Entry	MINP	Guest	K_a ($\times 10^5\,M^{-1}$)	K_{rel}
1	MINP**4**-Naph	**5**	48 ± 14	1
2	MINP**4**-Naph	benzoic acid	2.8 ± 0.2	0.06
3	MINP**4**-Naph	3,5-dinitrobenzoic acid	4.3 ± 1.2	0.09
4	MINP**4**-Naph	butyric acid	0.20 ± 0.07	0.004
5	MINP**4**-Naph	hexanoic acid	0.19 ± 0.05	0.004
6	MINP**4**-Naph	octanoic acid	0.173 ± 0.006	0.004
7	MINP**4**-Naph	decanoic acid	0.14 ± 0.03	0.003
8	MINP**4**-Naph	lauric acid	~0.001[b]	~0
9	MINP**8**-Naph	octanoic acid	0.84 ± 0.14	1
10	MINP**8**-Naph	acetic acid	--[c]	~0

Table 1. continued.

11	MINP$_8$-Naph	butyric acid	--[c]	~0
12	MINP$_8$-Naph	hexanoic acid	--[c]	~0
13	MINP$_8$-Naph	decanoic acid	~0.01[b]	~0.01
14	MINP$_8$-Naph	lauric acid	~0.04[b]	~0.05
15	MINP$_8$-Naph	**5**	~0.01[b]	~0.01

[a] The titrations were generally performed in duplicates and the errors between the runs were <10%. K_{rel} is the binding constant of a guest normalized to that of the targeted analyte by the same MINP receptor. [b] The titration showed very weak binding and the binding constant was estimated. [c] The fluorescence titrations showed random and negligible change.

One of the most important requirements for a sensor is its selective binding of the analyte among structural analogues. MINP$_4$-Naph showed significant selectivity for the targeted 1-adamantanecarboxylic acid. Its binding for other cyclic (benzoic and 3,5-dinitrobenzoic acid) and acyclic acids (C4–C12 linear carboxylic acids) were much lower, with the normalized binding constant (K_{rel}) ranging from 0–9% relative to that of the template itself (Table 1, entries 2–8).

The homologous C2–C12 carboxylic acids differ only in their hydrocarbon chain length but have the same functional group. Although fluorescent sensors for carboxylic acids have been reported,[26-28] distinguishing the chain length is very challenging because the carboxylic acid tends to be a better handle from the supramolecular point of view.

Our micellar molecular imprinting easily solved the above problem, using molecule **8** as the template that has an octanoate side chain.

As expected, MINP$_8$-Naph was able to bind octanoic acid, with $K_a = (0.84 \pm 0.14) \times 10^5\,M^{-1}$ (Table 1, entry 9). This value is about 1/60 of that for 1-adamantanecarboxylic acid by MINP$_4$-Naph (entry 1). The weaker binding is anticipated from the lower hydrophobicity of octanoic acid that gives a smaller driving force for the analyte to enter the MINP binding pocket.

Most importantly, MINP$_8$-Naph exhibited an excellent selectivity among the carboxylic acid homologues. The distinction of the carbon-carbon chain length was quite

remarkable, as either increasing or decreasing the carbon chain length shut off the binding nearly completely (Table 1, entries 10–14). Since the binding pocket of MINP$_8$-Naph is expected to be linearly C8-shaped, it is no surprise at all that 1-adamantanecarboxylic acid **5** could not fit in (entry 15).

The strong binding in water for the targeted hydrophobic acids (**5** and octanoic acid) translate to a fairly sensitive detection. The detection limits for the two acids were calculated to be 0.20 and 3.54 µM, respectively based on the 3δ/slope (experimental section).

Conclusion

In summary, we have demonstrated a highly modular synthesis of imprinted fluorescent sensors. Although carboxylic acids are used to prove the concept, the method is general and should be applicable to other molecular analytes. Our method allows one to create an analyte-specific binding site with a nearby environmentally sensitive fluorescent probe. The binding site was able to detect a change of two methylene groups easily among the linear carboxylic acids. Our MINPs have been shown to detect peptides with very similar side chains,[24, 25, 29] as well as mono- and oligosaccharides.[30, 31] Integration of the fluorescent sensing mechanism demonstrated in this work potentially can afford selective sensors for many important biomolecules.

Acknowledgement

Experimental Section

General Method

All other reagents and solvents were of ACS-certified grade or higher, and were used as received from commercial suppliers. Routine ^{1}H and ^{13}C NMR spectra were recorded on a

Bruker DRX-400, on a Bruker AV II 600 or on a Varian VXR-400 spectrometer. ESI-MS mass was recorded on Shimadzu LCMS-2010 mass spectrometer. Dynamic light scattering (DLS) data were recorded at 25 °C using PDDLS/ CoolBatch 90T with PD2000DLS instrument. Fluorescence spectra were recorded at ambient temperature on a Varian Cary Eclipse Fluorescence spectrophotometer.

Syntheses

4-vinylbenzaldehyde was synthesized following reported procedures.[32]

Scheme 2. Synthetic route.

Compound 10. Compound **6** (500 mg, 2.09 mmol), di-*t*-butyl dicarbonate (912 mg, 4.18 mmol), and sodium bicarbonate (351 mg, 4.18 mmol) were dissolved in 50 mL of methanol and 2 mL of water. The reaction mixture was heated to 60 °C and stirred overnight. After the reaction mixture was concentrated by rotary evaporation, the residue was purified by flash column chromatography over silica gel with 15:1 ethyl acetate/methanol as the eluent to give a pink powder (539 mg, 71%). ^{1}H NMR (400 MHz, CD$_3$OD, δ) 8.29 (d, J = 2.2 Hz, 1H), 7.80 – 7.74 (m, 2H), 7.55 (dd, J = 8.9, 2.2 Hz, 1H), 7.22 (d, J = 1.5 Hz, 1H), 1.55 (s, 9H). ^{13}C NMR (151 MHz, CD$_3$OD, δ) 154.0, 152.8, 140.4, 137.3, 129.9, 128.74, 126.4, 120.2, 116.1, 109.3, 104.8, 79.7, 27.4. ESI-MS (*m/z*): [M-Na]$^-$ cacld for C$_{15}$H$_{16}$NO$_6$S, 338.0704; found, 338.0706.

Compound 11. Compound **10** (27.4 mg, 0.152 mmol), HBTU (105 mg, 0.277 mmol), and DIPEA (89 mg, 0.689 mmol) were dissolved in 5 mL of DMF. After the mixture was stirred for 30 min, compound **5** (50 mg, 0.138 mmol) was added. The reaction mixture was stirred at room temperature overnight. After the solvent was removed by rotary evaporation, the residue was purified by flash column chromatography over silica gel with 20:1 dichloromethane/methanol as the eluent to give a light-yellow powder (61.1 mg, 61%). ^{1}H NMR (400 MHz, CD$_3$OD, δ) 8.18 (s, 1H), 8.15 (s, 1H), 7.89 – 7.86 (m, 2H), 7.74 (d, J = 8.5 Hz, 1H), 7.56 – 7.44 (m, 4H), 2.26 (d, J = 2.9 Hz, 6H), 2.14 (s, 3H), 1.89 (s, 6H), 1.55 (s, 9H). ^{13}C NMR (151 MHz, CD$_3$OD, δ) 177.53, 154.82, 147.72, 141.30, 140.57, 130.93, 130.65, 129.69, 127.95, 127.04, 124.00, 121.71, 118.51, 116.96, 111.59, 108.52, 81.03, 48.43, 42.58, 40.05, 37.52, 29.48, 28.65, 19.26. ESI-MS (*m/z*): [M-HOBt-Na] $^-$ cacld for C$_{26}$H$_{30}$NO$_7$S, 500.1743; found, 500.1759.

Compound 12. Compound **11** (61.1 mg, 0.093 mmol) was dissolved in 10 mL of trifluoroacetic acid. The reaction mixture was stirred at room temperature overnight. After trifluoroacetic acid was removed by rotary evaporation, the residue was redissolved in 25 mL of methanol with sodium bicarbonate (23.4 mg, 0.279 mmol). After stirred for 30 min, the reaction mixture was concentrated by rotary evaporation and the residue was purified by flash column chromatography over silica gel with 15:1 dichloromethane/methanol as the eluent to give a white powder (30.3 mg, 77%). ^{1}H NMR (400 MHz, CD$_3$OD, δ) 8.03 (s, 1H), 7.72 (d, J = 8.8 Hz, 1H), 7.39 (d, J = 1.6 Hz, 1H), 7.07 (dd, J = 8.8, 2.2 Hz, 1H), 6.86 (d, J = 2.2 Hz, 1H), 2.22 (d, J = 2.9 Hz, 6H), 2.14 (s, 3H), 1.87 (t, J = 3.2 Hz, 6H). ^{13}C NMR (151 MHz, CD$_3$OD, δ) 177.81, 149.60, 146.20, 131.16, 130.92, 128.52, 124.41, 120.91, 116.60, 101.60, 42.59,

40.12, 37.49, 29.43. ESI-MS (*m/z*): [M-Na] $^-$ cacld for $C_{21}H_{22}NO_5S$, 400.1219; found, 400.1218.

Compound 4. Compound **12** (0.020 mmol, 8.5 mg) and 4-vinylbenzaldehyde (13.2 mg, 0.100 mmol) were dissolved in10 mL of methanol. The reaction mixture was stirred overnight. Diethyl ether (40 mL) was added slowly. The precipitate formed was collected by filtration and washed with 5 mL of diethyl ether to yield a brown powder (9.8 mg, 85.4%). The product was used in the MINP preparation without further purification. ^{1}H NMR (400 MHz, DMSO-d_6, δ) 8.75 (s, 1H), 8.13 (d, *J* = 8.7 Hz, 1H), 8.09 (s, 1H), 7.97 (d, *J* = 7.1 Hz, 2H), 7.66 (d, *J* = 7.8 Hz, 2H), 7.60 (d, *J* = 8.8 Hz, 1H), 7.42 (s, 1H), 7.37 (s, 1H), 6.83 (dd, *J* = 17.6, 11.0 Hz, 1H), 6.00 (d, *J* = 17.8 Hz, 1H), 5.41 (d, *J* = 10.9 Hz, 1H), 2.09-2.15 (m, 9H), 1.74-1.81 (m, 6H).

Compound 14. Compound **13** (44.9 mg, 0.276 mmol), **10** (50 mg, 0.138 mmol), and triethylamine (27.9 mg, 0.276 mmol) were dissolved in 10 mL of anhydrous DMF. The reaction mixture was stirred at room temperature overnight. After the solvent was removed by rotary evaporation, the residue was purified by flash column chromatography over silica gel with 20:1 dichloromethane/methanol as the eluent to give an off-white powder (42.2 mg, 52%). ^{1}H NMR (400 MHz, CD$_3$OD, δ) 8.16 (s, 2H), 7.90 (d, J = 8.9 Hz, 1H), 7.58 (d, J = 1.6 Hz, 1H), 7.50 (dd, J = 8.9, 2.2 Hz, 1H), 3.16 (q, J = 7.3 Hz, 6H), 2.79 (t, J = 7.5 Hz, 2H), 1.88 (m, 2H), 1.55 (s, 9H), 1.53 – 1.32 (m, 8H), 1.27 (t, J = 7.3 Hz, 9H), 0.93 (t, 7.1 Hz, 3H). ^{13}C NMR (151 MHz, CD$_3$OD, δ) 172.5, 153.5, 146.3, 140.2, 139.3, 129.6, 129.4, 128.3, 122.7, 120.5, 115.8, 107.0, 79.8, 46.5, 33.8, 31.5, 29.0, 28.8, 27.4, 24.9, 22.4, 13.2, 7.8. ESI-MS (*m/z*): [M-Et$_3$N-Na] $^-$ cacld for $C_{23}H_{30}NO_7S$, 464.1743; found, 464.1757.

Compound 15. Compound **14** (41.3 mg, 0.070 mmol) was dissolved in 5 mL of trifluoroacetic acid. The reaction mixture was stirred at room temperature overnight. After trifluoroacetic acid was removed by rotary evaporation, the residue was redissolved in 25 mL of methanol with sodium bicarbonate (27.6 mg, 0.328 mmol). After stirred for 30 min, the reaction mixture was concentrated by rotary evaporation and the residue was purified by flash column chromatography over silica gel with 15:1 dichloromethane/methanol as the eluent to give a brown powder (23.0 mg, 85%). ^{1}H NMR (400 MHz, CD$_3$OD, δ) 8.04 (s, 1H), 7.73 (d, J = 8.8 Hz, 1H), 7.46 (d, J = 1.7 Hz, 1H), 7.07 (dd, J = 8.8, 2.2 Hz, 1H), 6.89 (d, J = 2.3 Hz, 1H), 2.76 (t, J = 7.5 Hz, 2H), 1.82 (m, 2H), 1.55 – 1.27 (m, 8H), 0.93 (t, 6.9 Hz, 3H). ^{13}C NMR (126 MHz, CD$_3$OD, δ) 172.7, 148.3, 144.8, 136.4, 129.8, 129.5, 127.1, 123.2, 119.5, 115.3, 100.4, 33.6, 31.5, 28.9, 28.8, 24.7, 22.3, 13.1. ESI-MS (*m/z*): [M-Na] $^-$ cacld for C$_{18}$H$_{22}$NO$_5$S, 364.1219; found, 364.1224.

Compound 8. Compound **15** (0.020 mmol, 7.8 mg) and 4-vinylbenzaldehyde (13.2 mg, 0.100 mmol) were dissolved in 10 mL of methanol. The reaction mixture was stirred overnight. Diethyl ether (40 mL) was added slowly. The precipitate formed was collected by filtration and washed with 5 mL of diethyl ether to yield a brown powder (7.2 mg, 71.7%). The product was used in the MINP preparation without further purification. ^{1}H NMR (500 MHz, DMSO-*d$_6$*, δ) 8.74 (s, 1H), 8.11 (d, *J* = 8.7 Hz, 1H), 8.08 (s, 1H), 7.97 (d, *J* = 7.7 Hz, 2H), 7.65 (d, *J* = 7.8 Hz, 2H), 7.58 (d, *J* = 8.7 Hz, 1H), 7.54 (s, 1H), 7.44 (s, 1H), 6.83 (dd, *J* = 17.6, 11.0 Hz, 1H), 6.00 (d, *J* = 17.6 Hz, 1H), 5.40 (d, *J* = 10.9 Hz, 1H), 2.81 (t, *J* = 7.2 Hz, 2H), 1.73 (m, 2H), 1.44 – 1.23 (m, 8H), 0.81 (d, *J* = 7.2 Hz, 3H).

Preparation of MINP$_4$, MINP$_7$, and MINP$_8$.

MINPs were synthesized according to previously reported procedures.[33] To a micellar solution of **1** (10.2 mg, 0.02 mmol) in H$_2$O (2.0 mL), divinylbenzene (DVB, 2.8 μL, 0.02

mmol), the template–FM complex (**4**, **7** or **8**) in DMSO (0.0004 mmol), and 2,2-dimethoxy-2-phenylacetophenone (DMPA) in DMSO (10 μL of a 12.8 mg/mL, 0.0005 mmol) were added. The mixture was sonicated for 10 min. Cross-linker **2** (4.1 mg, 0.024 mmol), $CuCl_2$ in H_2O (10 μL of 6.7 mg/mL, 0.0005 mmol), and sodium ascorbate in H_2O (10 μL of 99 mg/mL, 0.005 mmol) were then added and the reaction mixture was stirred slowly at room temperature for 12 h. Compound **3** (10.6 mg, 0.04 mmol), $CuCl_2$ (10 μL of a 6.7 mg/mL solution in H_2O, 0.0005 mmol), and sodium ascorbate (10 μL of a 99 mg/mL solution in H_2O, 0.005 mmol) were then added and the solution stirred for another 6 h at room temperature. The reaction mixture was transferred to a glass vial, purged with nitrogen for 15 min, sealed with a rubber stopper, and irradiated in a Rayonet reactor for 12 h. The reaction mixture was poured into acetone (8 mL). The precipitate was collected by centrifugation and washed with a mixture of methanol/acetic acid (5 mL/0.1 mL) three times. The off-white product was dried in air to afford the final MINPs (> 80%).

Preparation of MINP-CHO.

The appropriate MINP (MINP$_4$ or MINP$_8$) (15.2 mg) was sonicated in 2 mL of 6 M hydrochloric acid for 20 min. The resulting solution was stirred at 95 °C for 2 h. The mixture was poured into acetone (8 mL). The precipitate formed was collected by centrifugation and washed with a mixture of acetone/water (5 mL/1 mL) three times. The off-white product was dried in air to afford the corresponding MINP-CHO (12.0 mg, 79%). To monitor the hydrolysis yield, an aliquot (40 μL) of reaction mixture was taken and added to 1.5 mL of acetone. The precipitate formed was collected by centrifugation and washed by a mixture of acetone/water (1 mL/0.2 mL) three times. The dried precipitate was then dissolved in 2 mL of water to yield the MINP solution before the fluorescence spectrum was recorded. Fluorescence intensity at

405 nm was used to calculate the hydrolysis yield. The initial fluorescence intensity was used for 0% hydrolysis.

Preparation of MINP-Naph.

The appropriate MINP-CHO (12.0 mg) was sonicated in 1 mL of anhydrous DMF for 20 min until it was fully dissolved. An aliquot (150 μL) of a stock solution of **6** (23.9 mg in 1 mL DMSO) was added. The reaction mixture was stirred for 2 h at room temperature. An aliquot of sodium borohydride stock solution (37.9 mg in 1 mL anhydrous DMF) was added. After stirred overnight, the reaction mixture was poured into acetone (8 mL). The precipitate formed was collected by centrifugation and washed with a mixture of acetone/water (5 mL/1 mL) three times and a mixture of methanol/acetic acid (5 mL/0.1 mL) three times. The off-white powdery product was dried in air. To remove the borate ions, the above product was re-dissolved in 2 mL of sodium chloride solution (5000 equiv to the concentration of MINP) overnight. The solution was transferred to a dialysis tube (MWCO 3.5K). The tube was placed in 2 L of deionized water with gentle stirring. The dialysis tube was sonicated and the water was changed after 2, 4, 6, and 20 h. After 48 h, the MINP solution was poured into 40 mL of acetone and the precipitate was collected by centrifugation. The precipitate was dried in air to yield MINP$_4$-Naph or MINP$_8$-Naph (8.6 mg, 72%).

Titration by Fluorescence Spectroscopy and Data Analysis Method

A stock solution of MINP (200 μM) was prepared in 10 mM HEPES buffer (pH 7.4) or water. Stock solutions (200 μM) of the guests were prepared in water. (For acids such as **5** that had low solubility in water, extensive sonication of the sample was used in the preparation of the stock solution.) For the titrations, a typical procedure is as follows. An aliquot (5–10 μL) of the guest stock solution was added to 2.00 mL of the appropriate solvent (HEPES buffer or water) in a quartz cuvette. The concentration of the guest was 1.0 μM. The sample was gently

vortexed for 30 s before its fluorescence spectrum was recorded. Aliquots of the MINP solution was added and the spectrum was recorded after each addition. The titration was continued until saturation was reached and the total volume of the MINP solution added was kept below 100 μL. The binding constant was obtained by nonlinear least squares curving fitting of the emission intensity to the 1:1 binding isotherm.[34] All titrations were performed at room temperature.

Limit of Detection.

For adamantane carboxylic acid, blank fluorescence is 180.638 ± 3.834. Limit of detection, calculated by 3δ/slope, was 0.20 μM. δ was the standard deviation of six blank samples and the slope was from the fluorescence titration at low guest concentrations. For octanoic acid, blank fluorescence is 187.422 ± 2.584. Limit of detection, calculated by 3δ/slope, was 3.54 μM. δ is the standard deviation of six blank samples and the slope was from the fluorescence titration at low guest concentrations.

Figure 3. ^{1}H NMR spectra of (a) surfactant **1** in CDCl$_3$, (b) surface-cross-linked micelles (SCM) in D$_2$O, (c) surface-functionalized SCM in D$_2$O, and (d) core-cross-linked micelles in D$_2$O for MINP$_4$.
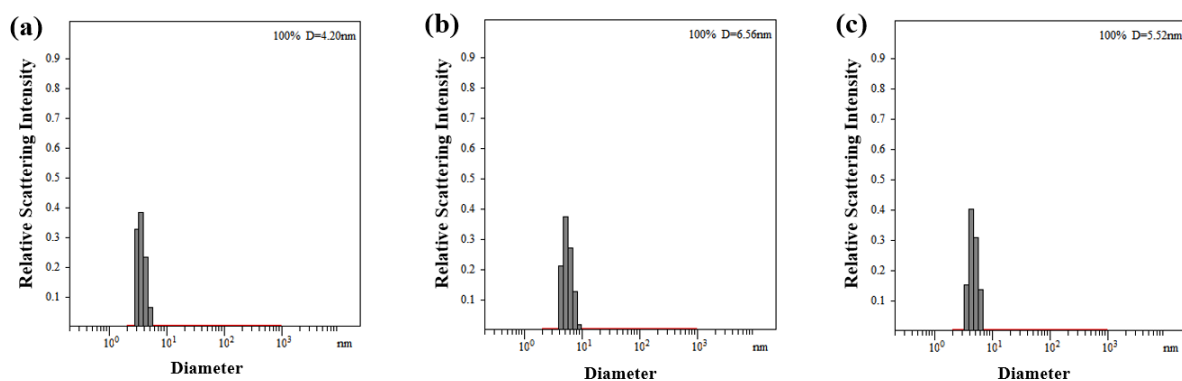

Figure 4. Distribution of the hydrodynamic diameters of the nanoparticles in water as determined by DLS for (a) surface-cross-linked micelles (SCM), (b) surface-functionalized SCM, and (c) purified MINP$_4$.
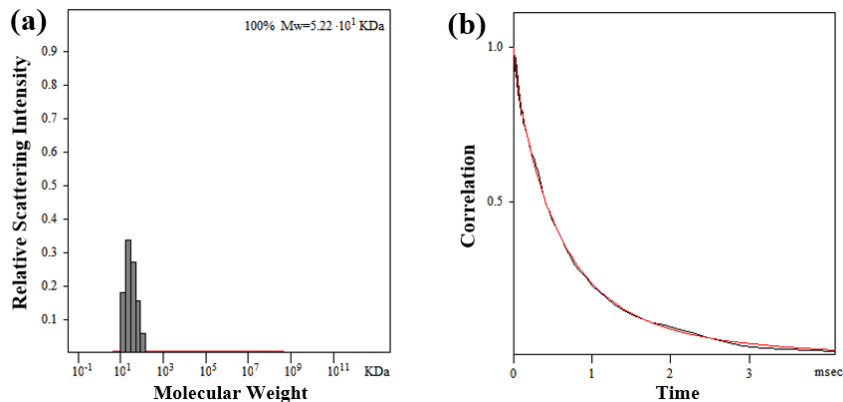
Figure 5. Distribution of the molecular weights and the correlation curve for MINP₄ from the DLS. The PRECISION DECONVOLVE program assumes the intensity of scattering is proportional to the mass of the particle squared. If each unit of building block for the MINP is assumed to contain one molecule of surfactant (MW = 465 g/mol), 1.2 molecules of cross linker (MW = 172 g/mol), one molecule of DVB (MW = 130 g/mol), and 0.8 molecules of sugar derivative (MW = 264 g/mol), the molecular weight of MINP translates to 51 [= 51300 / (465 + 1.2×172 + 130 + 0.8×264)] of such units.
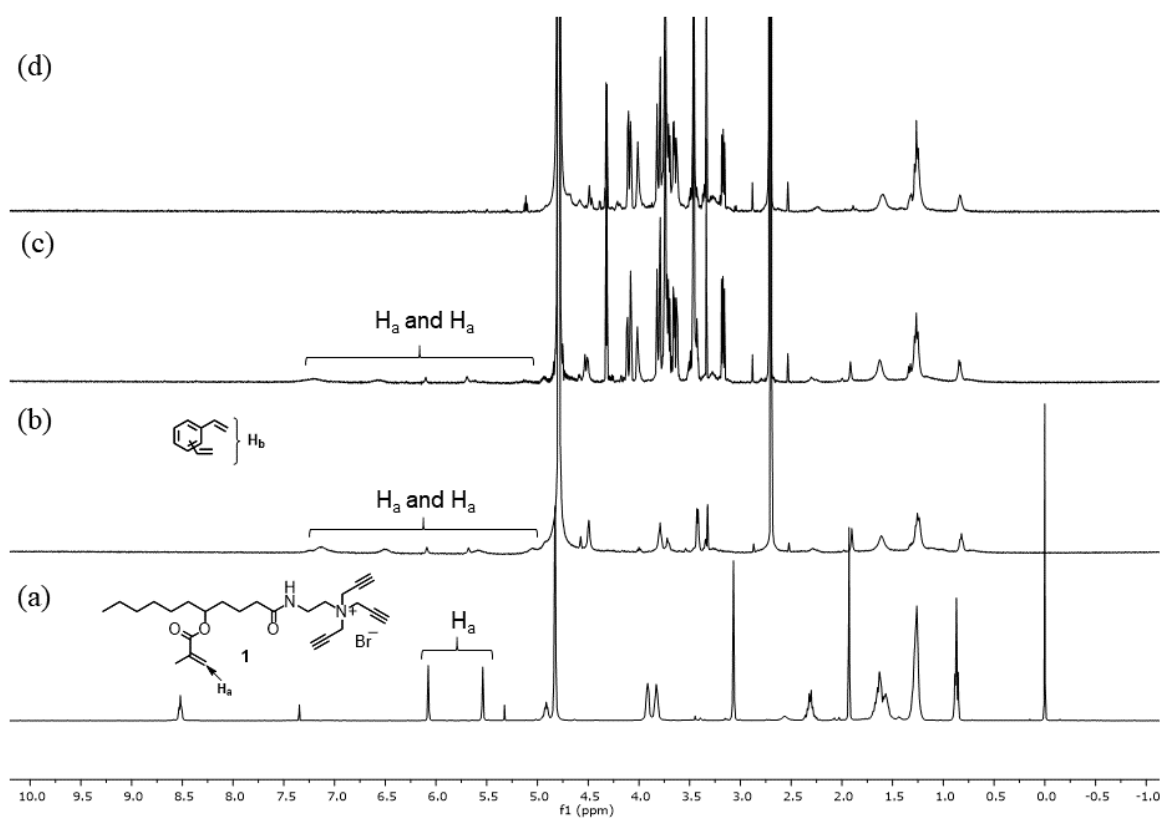
Figure 6. ^{1}H NMR spectra of (a) surfactant **1** in CDCl$_3$, (b) surface-cross-linked micelles (SCM) in D$_2$O, (c) surface-functionalized SCM in D$_2$O, and (d) core-cross-linked micelles in D$_2$O for MINP$_7$.
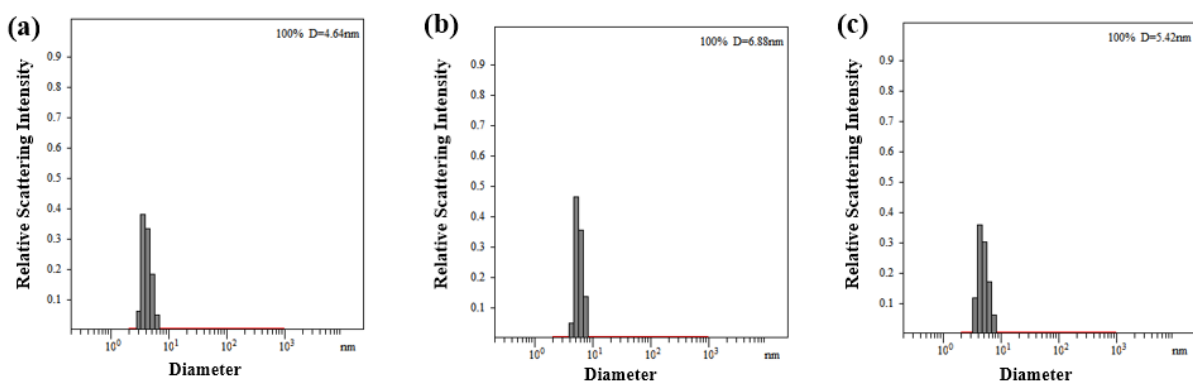
Figure 7. Distribution of the hydrodynamic diameters of the nanoparticles in water as determined by DLS for (a) surface-cross-linked micelles (SCM), (b) surface-functionalized SCM, and (c) purified MINP$_7$.
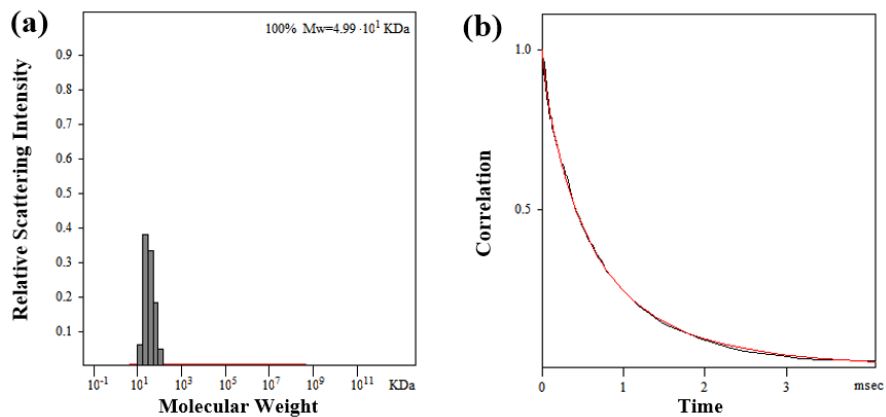
Figure 8. Distribution of the molecular weights and the correlation curve of MINP$_7$ from the DLS. The PRECISION DECONVOLVE program assumes the intensity of scattering is proportional to the mass of the particle squared. If each unit of building block for the MINP is assumed to contain one molecule of surfactant (MW = 465 g/mol), 1.2 molecules of cross linker (MW = 172 g/mol), one molecule of DVB (MW = 130 g/mol), and 0.8 molecules of sugar derivative (MW = 264 g/mol), the molecular weight of MINP translates to 49 [= 49900 / (465 + 1.2×172 + 130 + 0.8×264)] of such units.
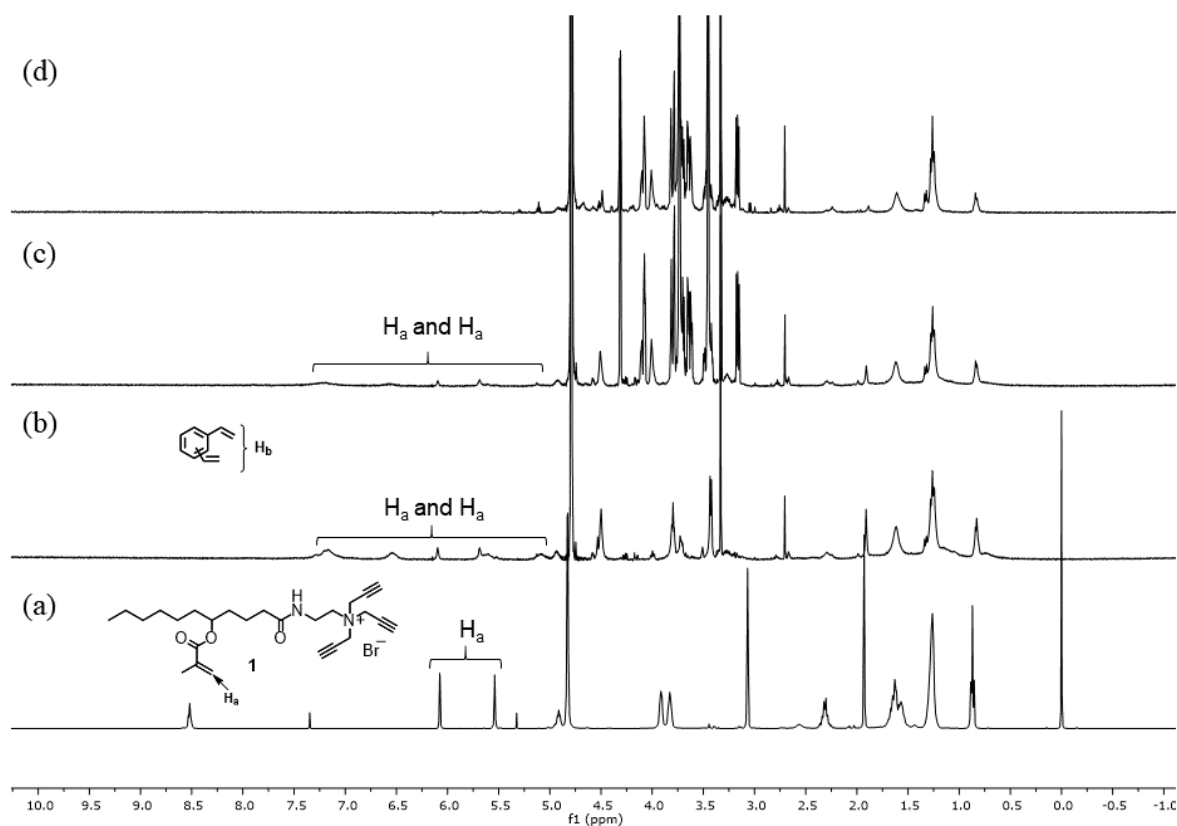
Figure 9. ^{1}H NMR spectra of (a) surfactant **1** in CDCl$_3$, (b) surface-cross-linked micelles (SCM) in D$_2$O, (c) surface-functionalized SCM in D$_2$O, and (d) core-cross-linked micelles in D$_2$O for MINP$_8$.

Figure 10. Distribution of the hydrodynamic diameters of the nanoparticles in water as determined by DLS for (a) surface-cross-linked micelles (SCM), (b) surface-functionalized SCM, and (c) purified MINP$_8$.

Figure 11. Distribution of the molecular weights and the correlation curve of MINP$_8$ from the DLS. The PRECISION DECONVOLVE program assumes the intensity of scattering is proportional to the mass of the particle squared. If each unit of building block for the MINP is assumed to contain one molecule of surfactant (MW = 465 g/mol), 1.2 molecules of cross linker (MW = 172 g/mol), one molecule of DVB (MW = 130 g/mol), and 0.8 molecules of sugar derivative (MW = 264 g/mol), the molecular weight of MINP translates to 51 [= 52200 / (465 + 1.2×172 + 130 + 0.8×264)] of such units.
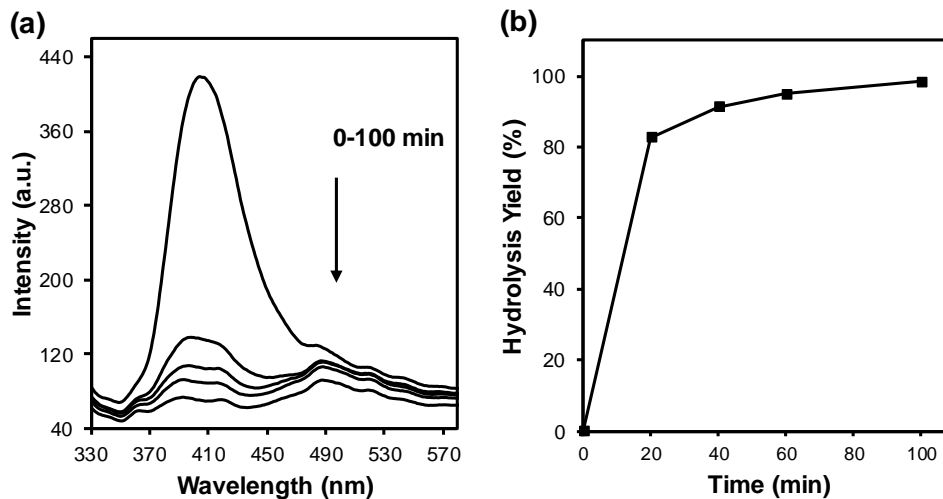
Figure 12. (a) Fluorescence spectra of MINP$_4$ hydrolysis. λ_{ex} = 307 nm. (b) Hydrolysis yield calculated based on fluorescence intensity at 405 nm. Fluorescence before heating was used for 0% hydrolysis.
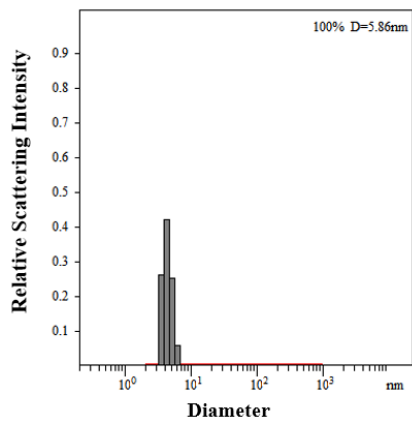
Figure 13. Distribution of the hydrodynamic diameters of the MINP4-CHO in water as determined by DLS for MINP after HCl hydrolysis.
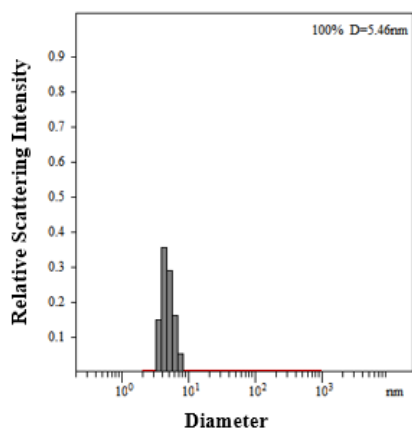
Figure 14. Distribution of the hydrodynamic diameters of the nanoparticles in 10 mM HEPES buffer (pH = 7.4) as determined by DLS for MINP4-Naph after dialysis.
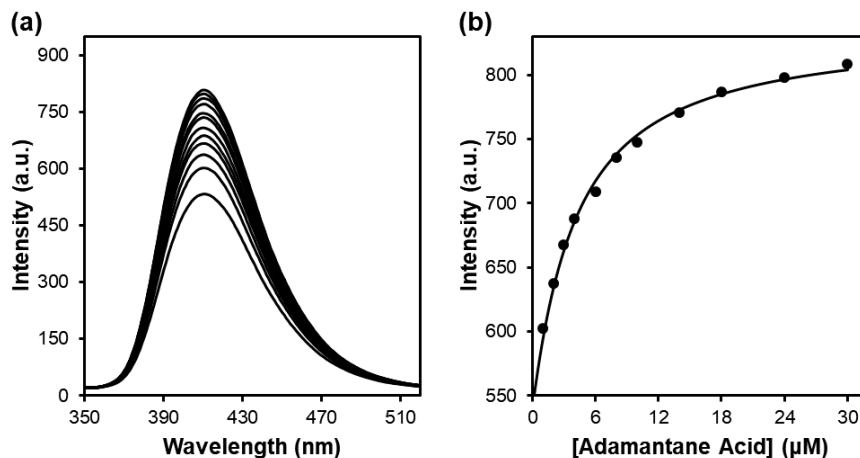
Figure 15. (a) Emission spectra of MINP4-Naph upon the addition of different concentrations of **5** in 10 mM HEPES buffer (pH = 7.4). [MINP4-Naph] = 1.0 μM, The concentration of MINP was calculated based on an approximate M.W. of 50000 g/mol. (b) Nonlinear least squares fitting of the emission intensity at 410 nm to a 1:1 binding isotherm.
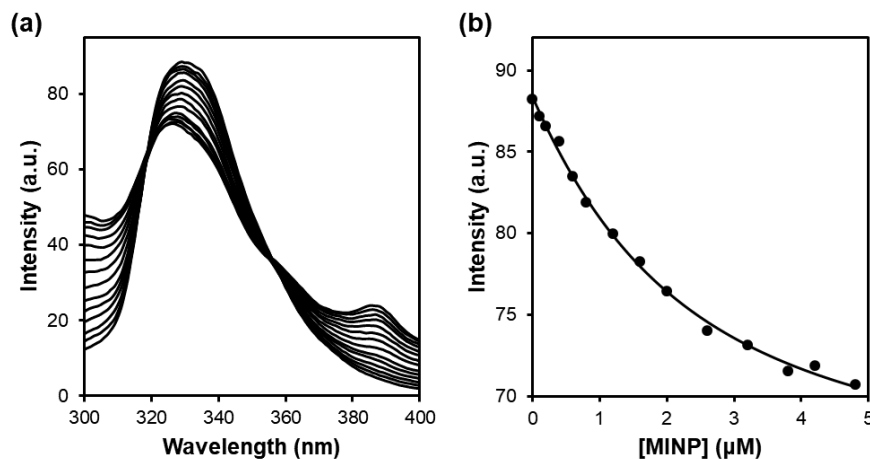
Figure 16. (a) Emission spectra of **7** upon the addition of different concentrations of MINP7 unhydrolyzed in 1 M HCl solution. [**7**] = 1.0 μM. The concentration of MINP was calculated based on an approximate M.W. of 50000 g/mol. (b) Plot of intensity at 330 nm with concentration of MINP and the nonlinear least squares fitting of the emission intensity at 330 nm to a 1:1 binding isotherm.
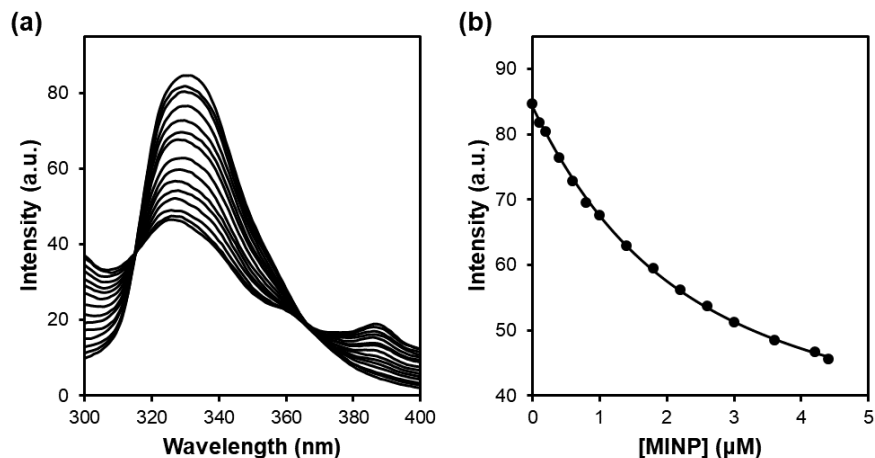
Figure 17. (a) Emission spectra of **7** upon the addition of different concentrations of MINP**7** after hydrolysis in 1 M HCl solution. [**7**] = 1.0 μM. The concentration of MINP was calculated based on an approximate M.W. of 50000 g/mol. (b) Plot of intensity at 330 nm with concentration of MINP and nonlinear least squares fitting of the emission intensity at 330 nm to a 1:1 binding isotherm.
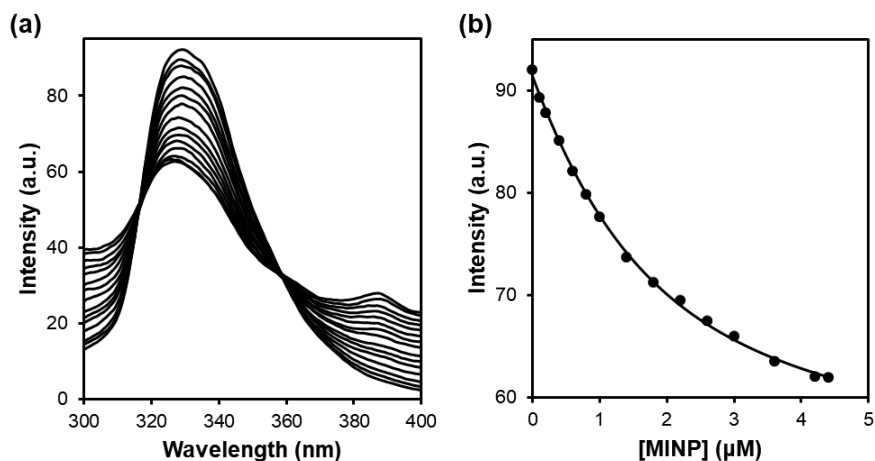
Figure 18. (a) Emission spectra of **7** upon the addition of different concentrations of MINP**7** after reductive amination in 1 M HCl solution, [**7**] = 1.0 μM. The concentration of MINP was calculated based on an approximate M.W. of 50000 g/mol. (b) Plot of intensity at 330 nm with concentration of MINP and nonlinear least squares fitting of the emission intensity at 330 nm to a 1:1 binding isotherm.
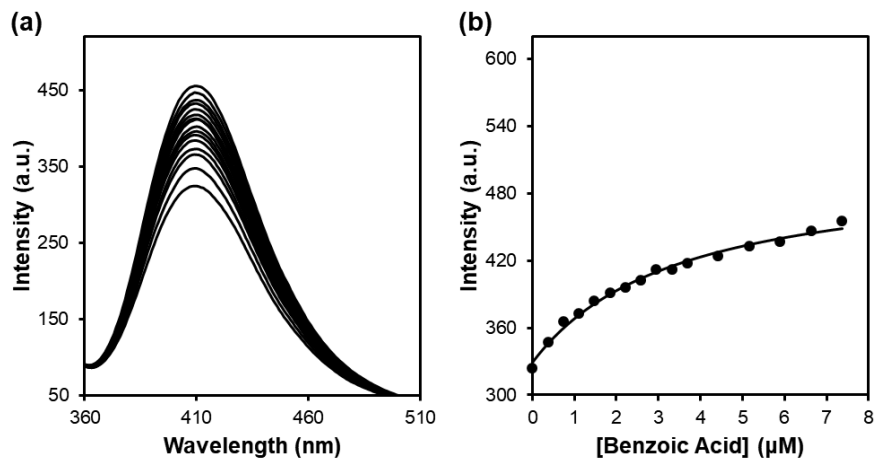
Figure 19. (a) Emission spectra of MINP$_4$-Naph upon the addition of different concentrations of benzoic acid in H$_2$O. [MINP$_4$-Naph] = 0.2 µM. The concentration of MINP was calculated based on an approximate M.W. of 50000 g/mol. (b) Nonlinear least squares fitting of the emission intensity at 410 nm to a 1:1 binding isotherm. The data correspond to entry 2 of Table 1.
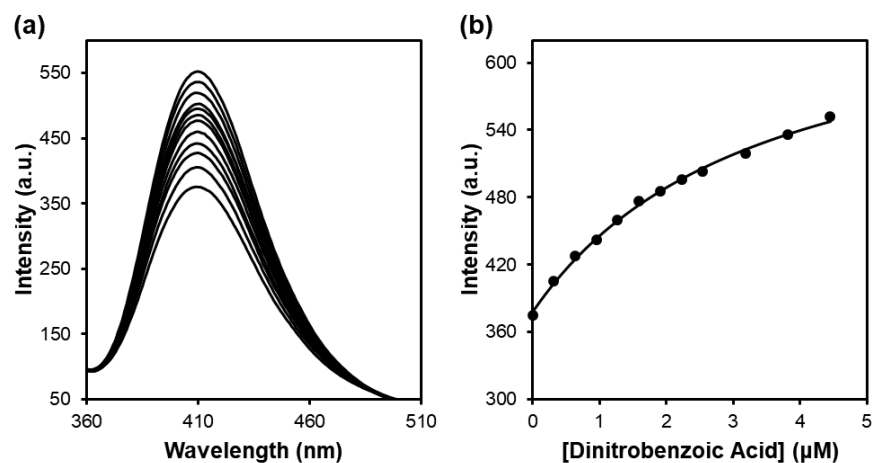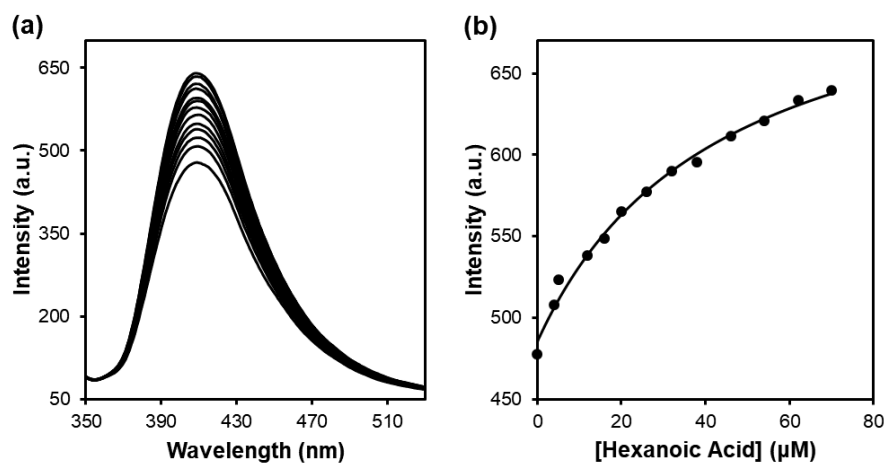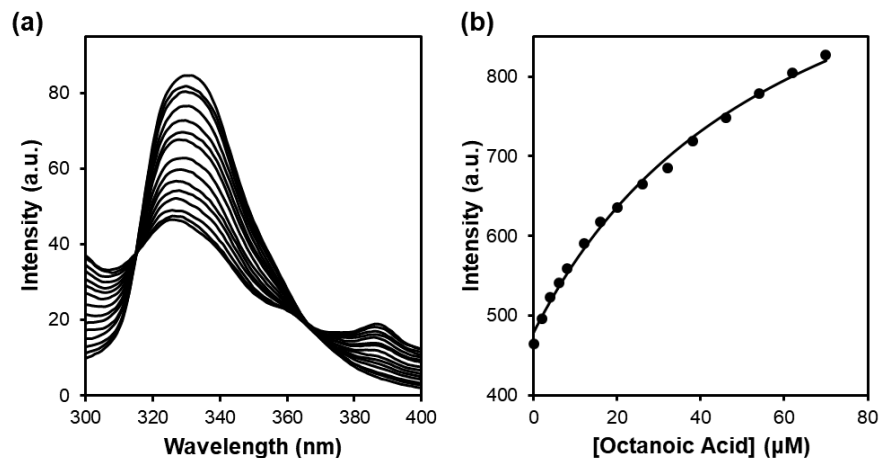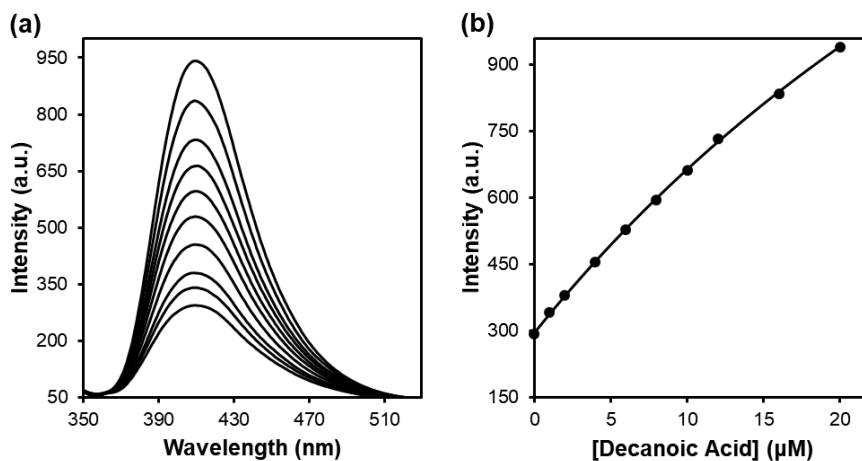

Figure 20. (a) Emission spectra of MINP$_4$-Naph upon the addition of different concentrations of 3,5-dinitrobenzoic acid in H$_2$O. [MINP$_4$-Naph] = 0.2 µM. The concentration of MINP was calculated based on an approximate M.W. of 50000 g/mol. (b) Nonlinear least squares fitting of the emission intensity at 410 nm to a 1:1 binding isotherm. The data correspond to entry 3 of Table 1.
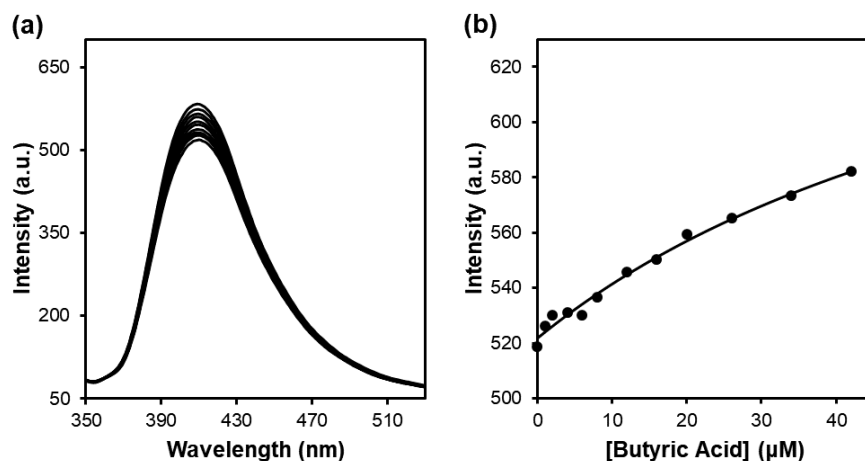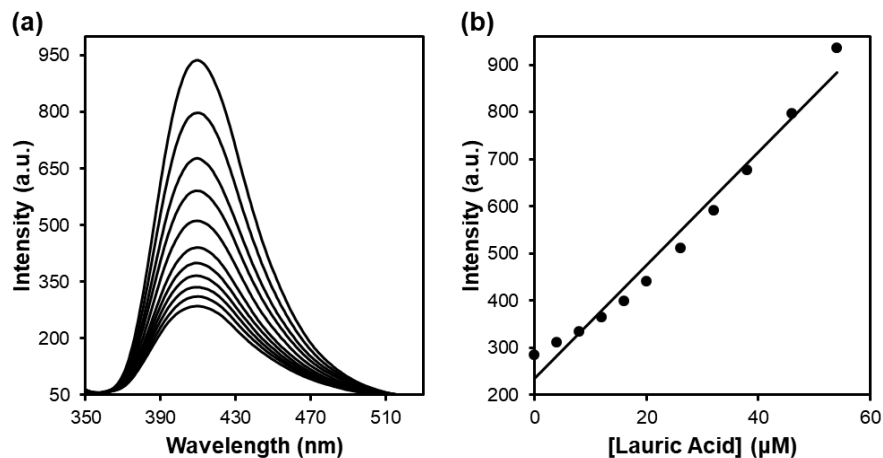
Figure 21. (a) Emission spectra of MINP₄-Naph upon the addition of different concentrations of butyric acid in H$_2$O. [MINP₄-Naph] = 1.0 μM. The concentration of MINP was calculated based on an approximate M.W. of 50000 g/mol. (b) Nonlinear least squares fitting of the emission intensity at 410 nm to a 1:1 binding isotherm. The data correspond to entry 4 of Table 1.
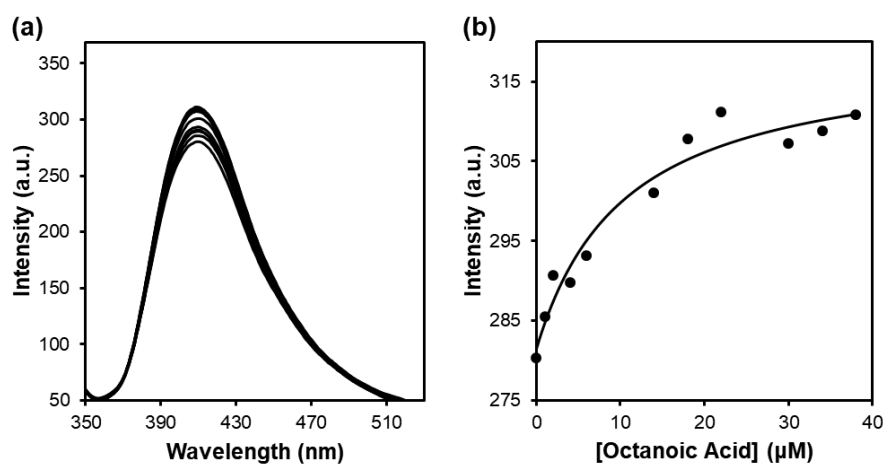

Figure 22. (a) Emission spectra of MINP₄-Naph upon the addition of different concentrations of hexanoic acid in H$_2$O, [MINP₄-Naph] = 1.0 μM. The concentration of MINP was calculated based on an approximate M.W. of 50000 g/mol. (b) Nonlinear least squares fitting of the emission intensity at 410 nm to a 1:1 binding isotherm. The data correspond to entry 5 of Table 1.

Figure 23. (a) Emission spectra of MINP4-Naph upon the addition of different concentrations of octanoic acid in H_2O. [MINP4-Naph] = 1.0 μM. The concentration of MINP was calculated based on an approximate M.W. of 50000 g/mol. (b) Nonlinear least squares fitting of the emission intensity at 410 nm to a 1:1 binding isotherm. The data correspond to entry 6 of Table 1.
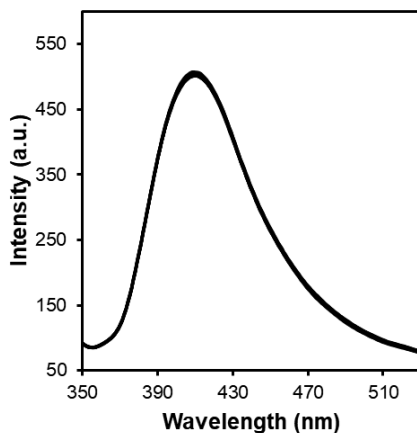

Figure 24. (a) Emission spectra of MINP4-Naph upon the addition of different concentrations of decanoic acid in H_2O, [MINP4-Naph] = 0.5 μM. The concentration of MINP was calculated based on an approximate M.W. of 50000 g/mol. (b) Nonlinear least squares fitting of the emission intensity at 410 nm to a 1:1 binding isotherm. The data correspond to entry 7 of Table 1.

Figure 25. (a) Emission spectra of MINP$_4$-Naph upon the addition of different concentrations of lauric acid in H$_2$O, [MINP$_4$-Naph] = 0.5 μM. The concentration of MINP was calculated based on an approximate M.W. of 50000 g/mol. (b) Nonlinear least squares fitting of the emission intensity at 410 nm to a 1:1 binding isotherm. The data correspond to entry 8 of Table 1.

Figure 26. (a) Emission spectra of MINP$_8$-Naph upon the addition of different concentrations of octanoic acid in H$_2$O. [MINP$_8$-Naph] = 1.0 μM. The concentration of MINP was calculated based on an approximate M.W. of 50000 g/mol. (b) Nonlinear least squares fitting of the emission intensity at 410 nm to a 1:1 binding isotherm. The data correspond to entry 9 of Table 1.

Figure 27. Emission spectra of MINP$_8$-Naph upon the addition of 0–50 μM of acetic acid in H$_2$O. [MINP$_8$-Naph] = 1.0 μM. The concentration of MINP was calculated based on an approximate M.W. of 50000 g/mol. The data correspond to entry 10 of Table 1.
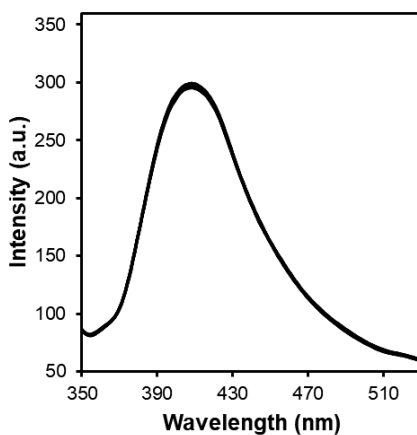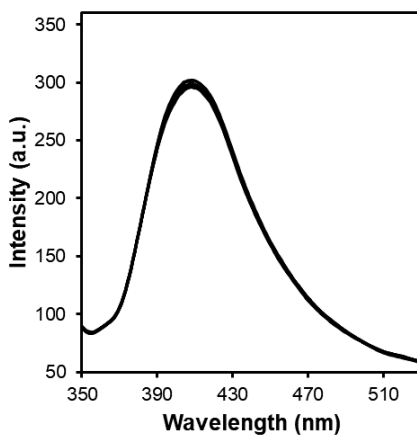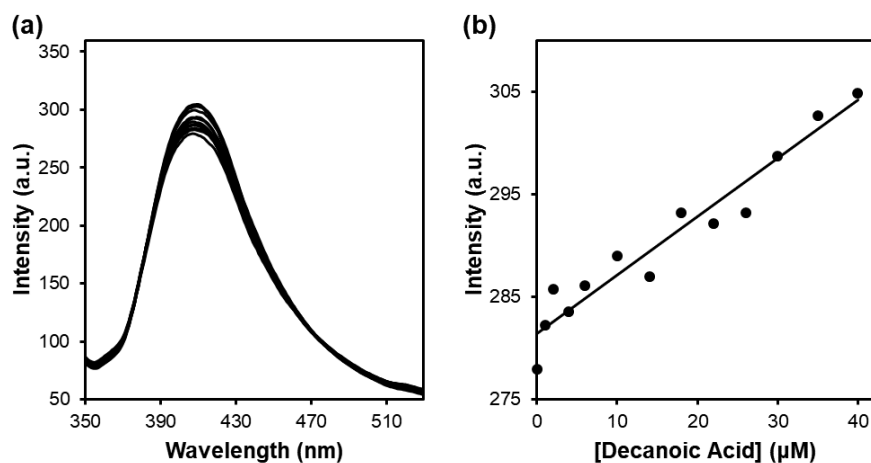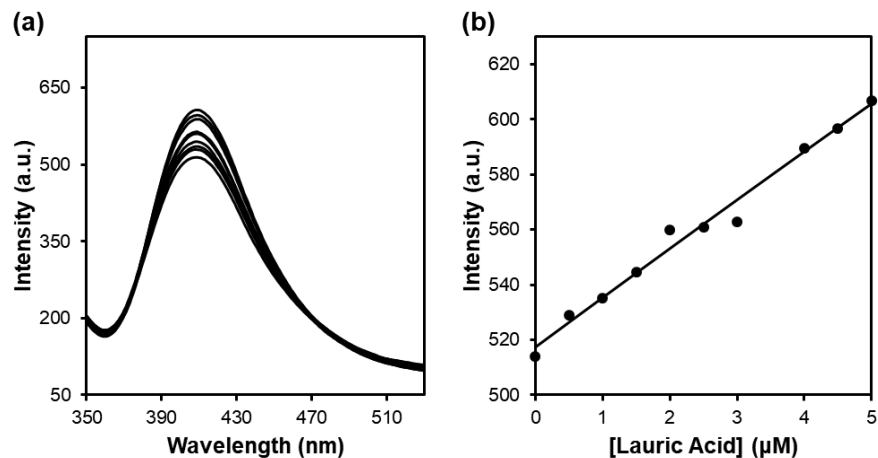

Figure 28. Emission spectra of MINP$_8$-Naph upon the addition of 0–50 μM of butyric acid in H$_2$O. [MINP$_8$-Naph] = 1.0 μM. The concentration of MINP was calculated based on an approximate M.W. of 50000 g/mol. The data correspond to entry 11 of Table 1.

Figure 29. Emission spectra of MINP$_8$-Naph upon the addition of 0–50 μM of hexanoic acid in H$_2$O. [MINP$_8$-Naph] = 1.0 μM. The concentration of MINP was calculated based on an approximate M.W. of 50000 g/mol. The data correspond to entry 12 of Table 1.

Figure 30. (a) Emission spectra of MINP$_8$-Naph upon the addition of different concentrations of decanoic acid at H$_2$O, [MINP$_8$-Naph] = 1.0 μM. The concentration of MINP was calculated based on an approximate M.W. of 50000 g/mol. (b) Nonlinear least squares fitting of the emission intensity at 410 nm to a 1:1 binding isotherm. The data correspond to entry 13 of Table 1.
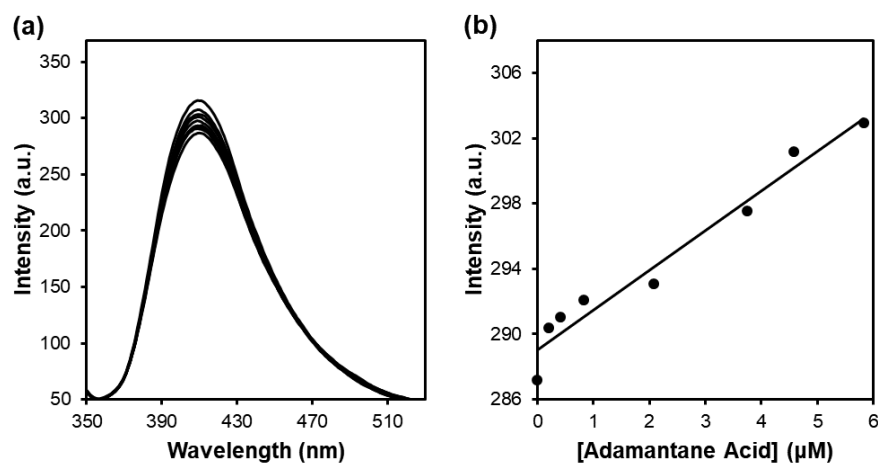
Figure 31. (a) Emission spectra of MINP$_8$-Naph upon the addition of different concentrations of lauric acid in H$_2$O, [MINP$_8$-Naph] = 0.5 μM. The concentration of MINP was calculated based on an approximate M.W. of 50000 g/mol. (b) Nonlinear least squares fitting of the emission intensity at 410 nm to a 1:1 binding isotherm. The data correspond to entry 14 of Table 1.

Figure 32. (a) Emission spectra of MINP$_8$-Naph upon the addition of different concentrations of **5** in H$_2$O. [MINP$_8$-Naph] = 0.5 μM. The concentration of MINP was calculated based on an approximate M.W. of 50000 g/mol. (b) Nonlinear least squares fitting of the emission intensity at 410 nm to a 1:1 binding isotherm. The data correspond to entry 15 of Table 1.
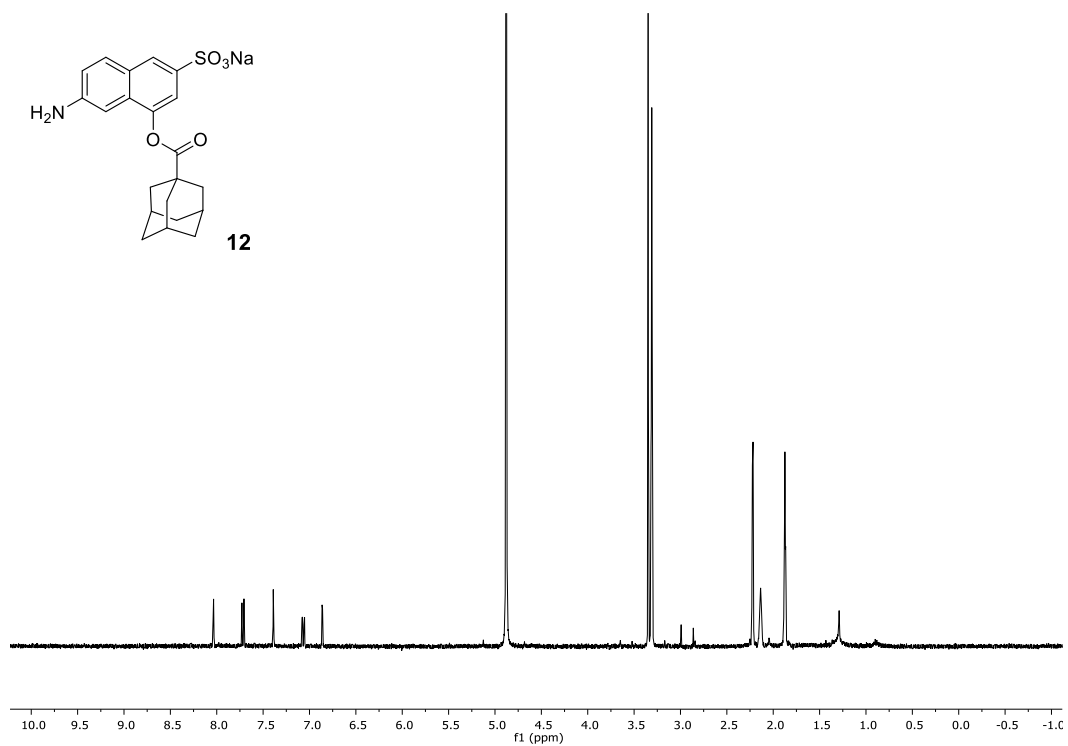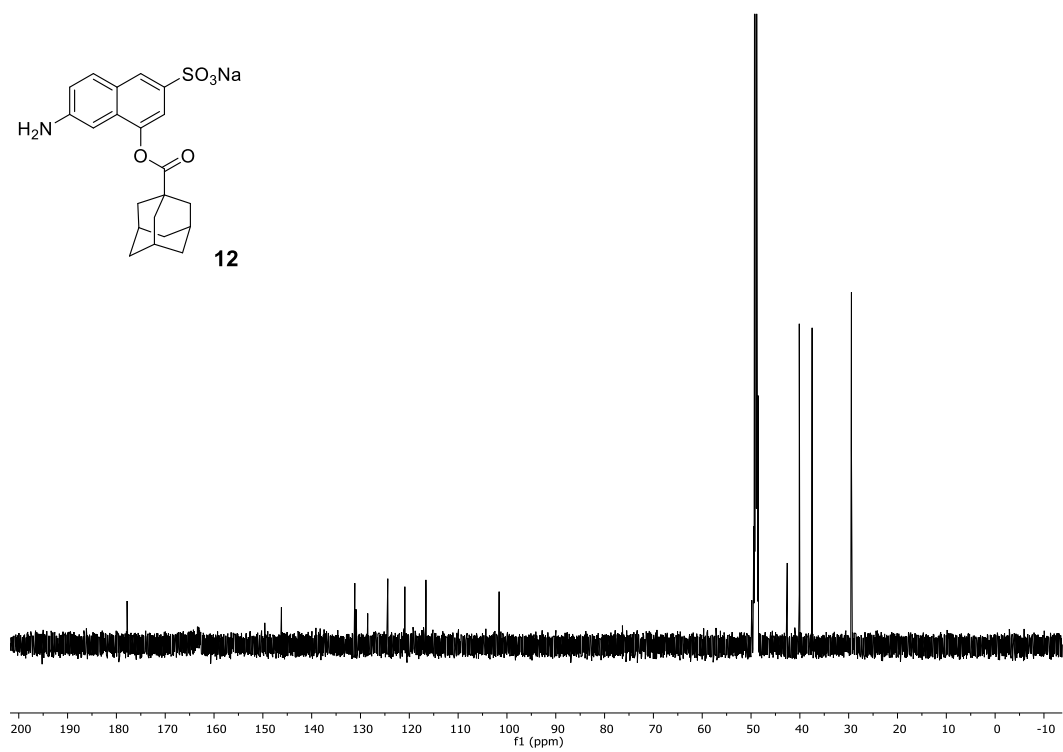
¹H and ¹³C NMR Spectra
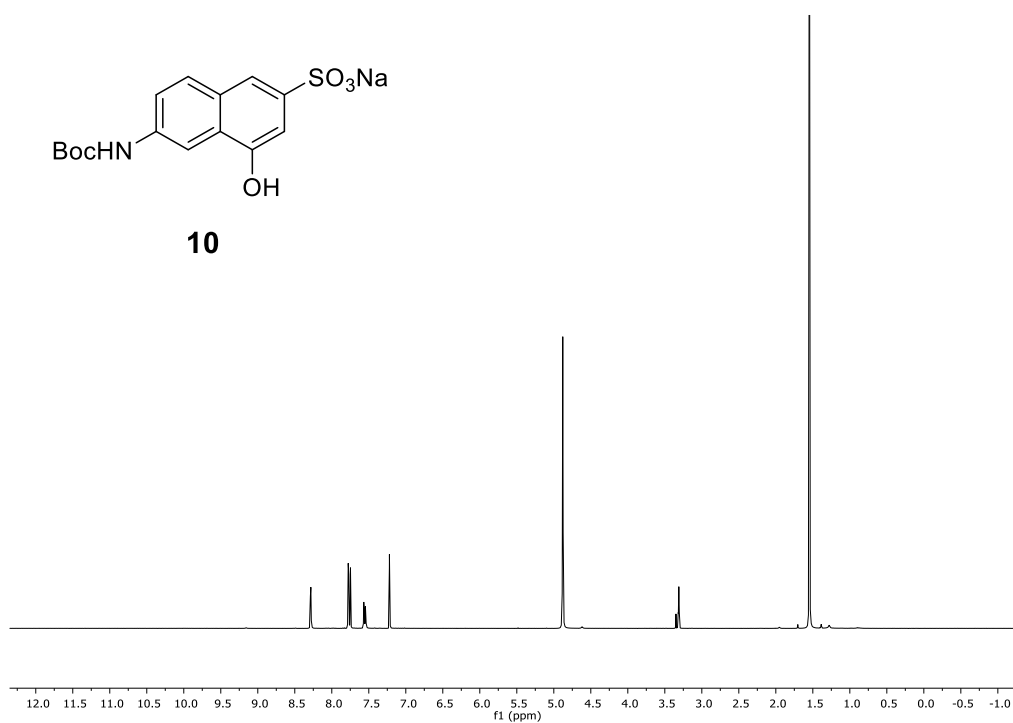
Scheme 3. ¹H NMR of **10**.
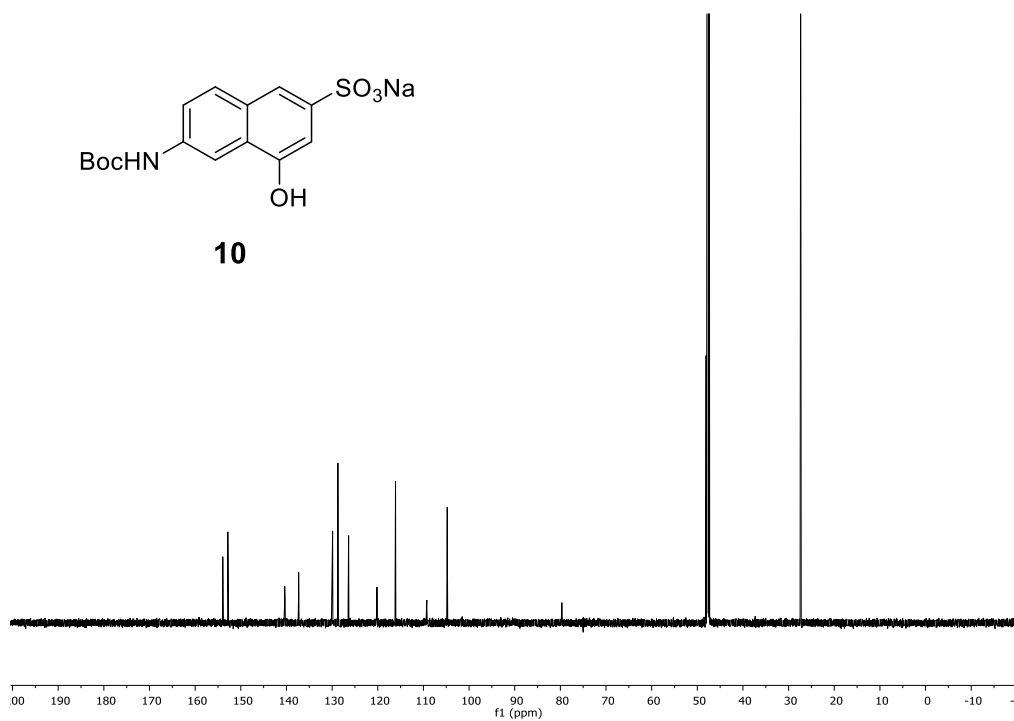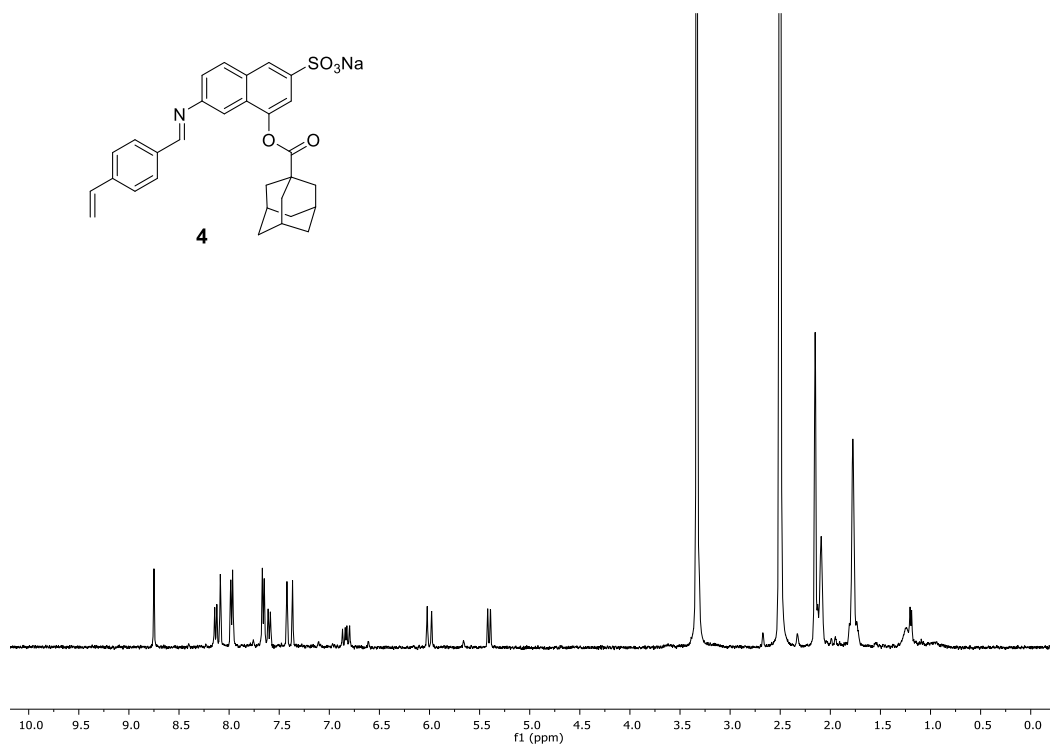

Scheme 4. ¹³C NMR of **10**.
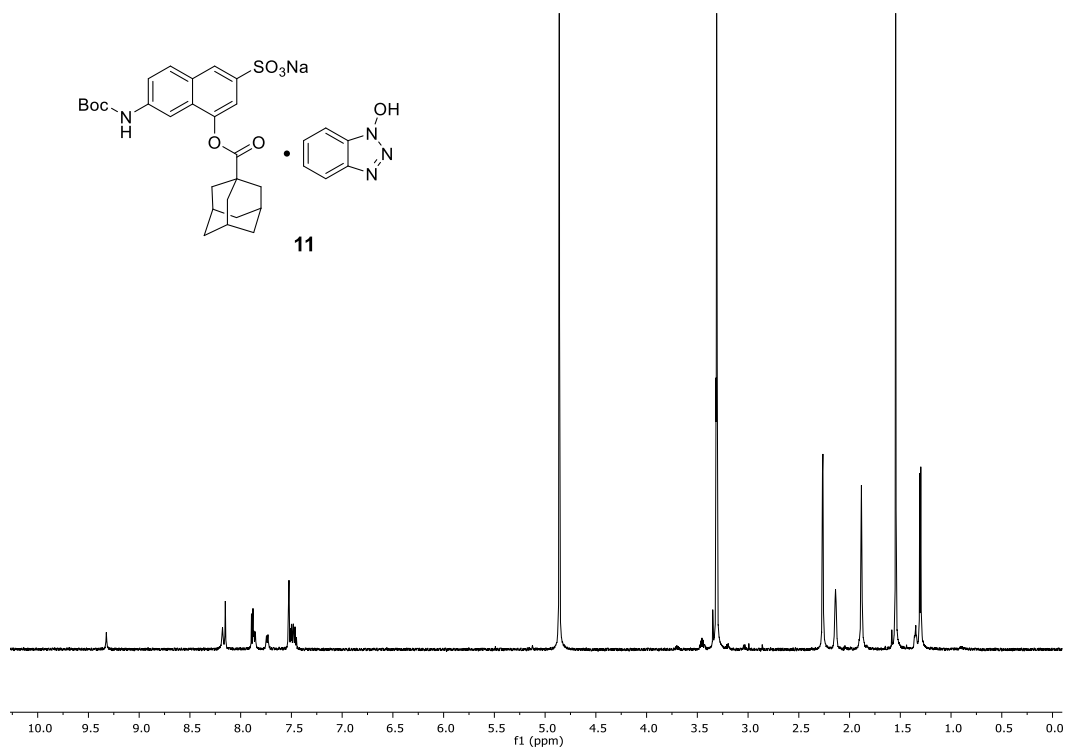
Scheme 5. ^{1}H NMR of **11**.
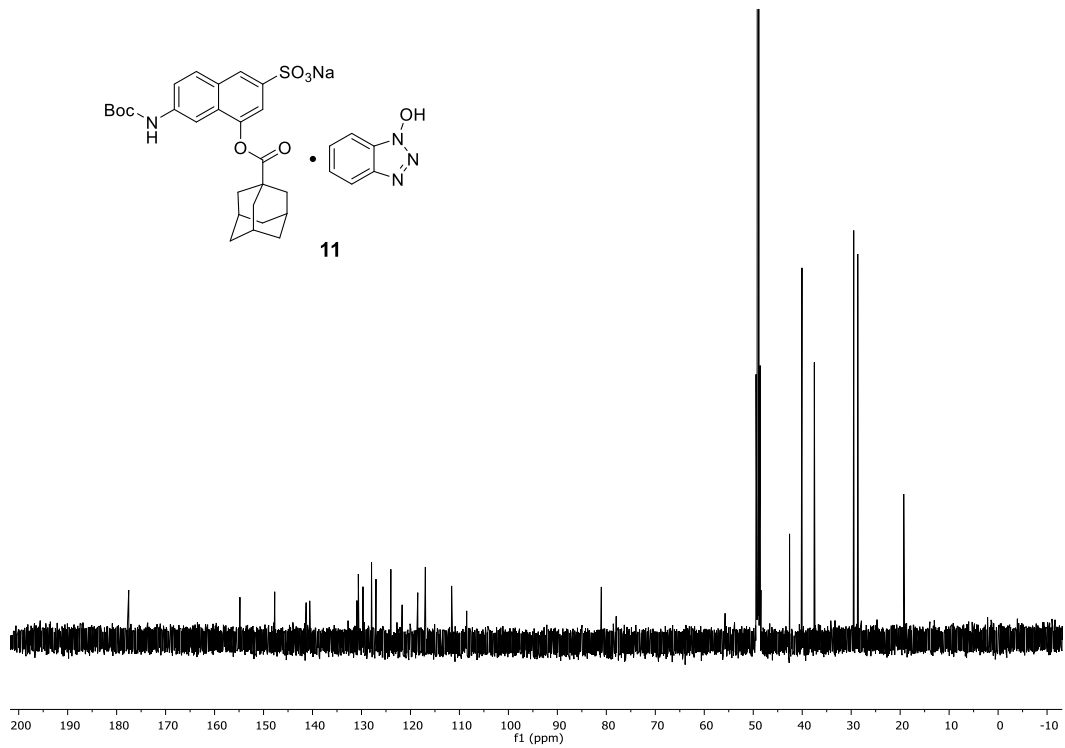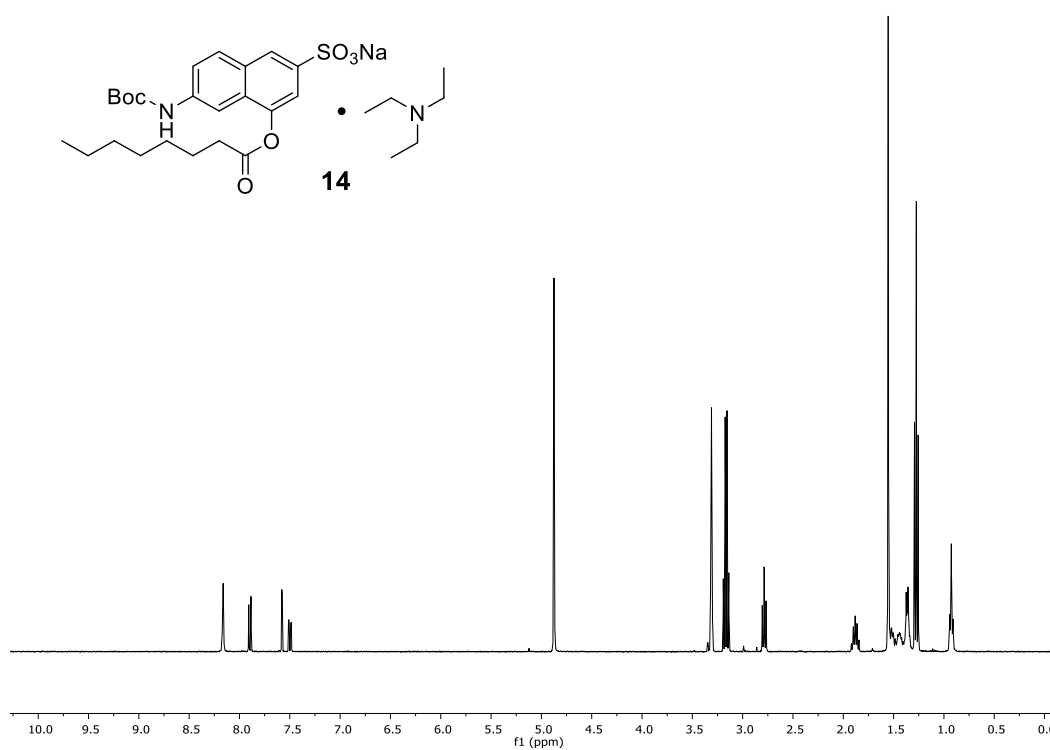

Scheme 6. ^{13}C NMR of **11**.
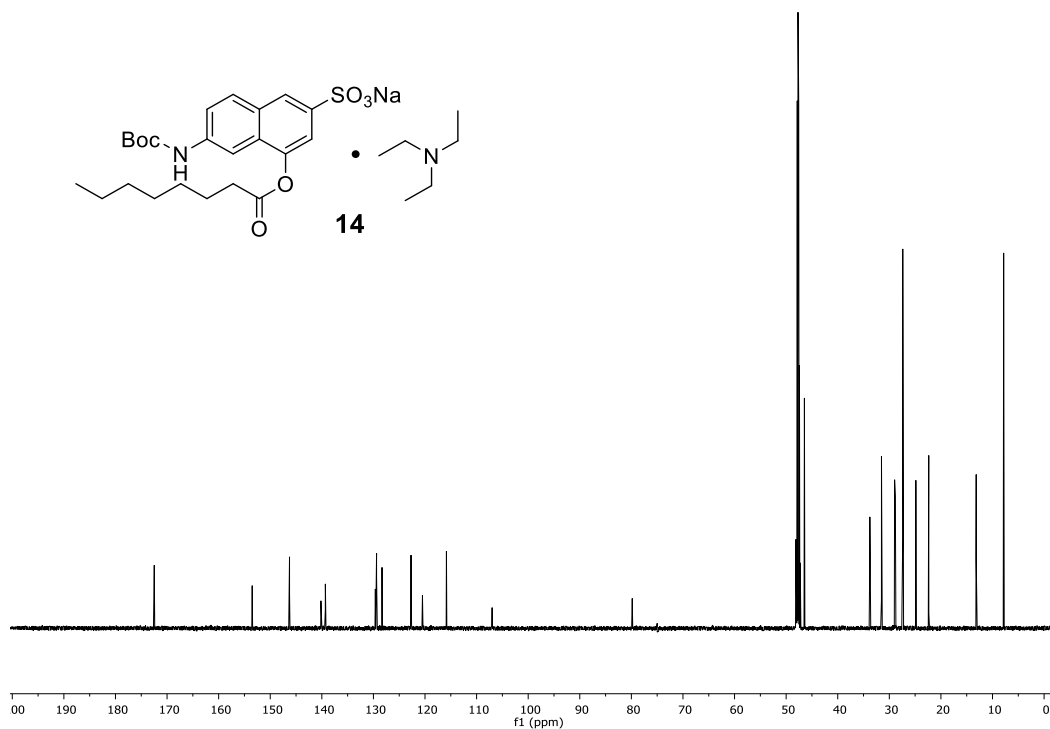
Scheme 7. ^{1}H NMR of **12**.
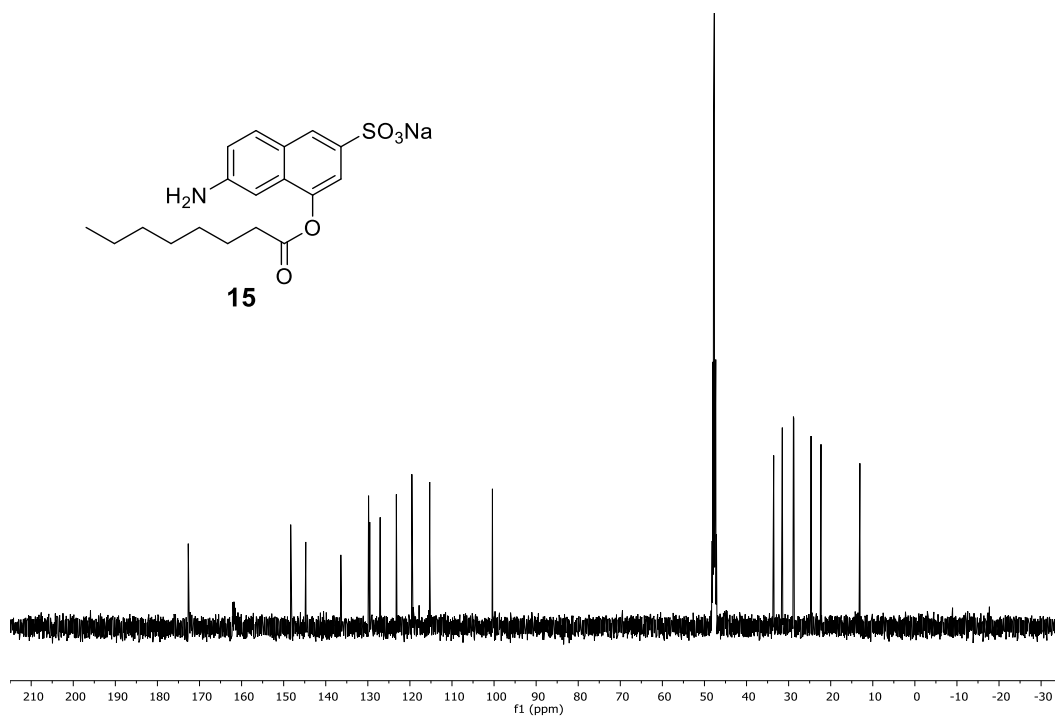

Scheme 8. ^{13}C NMR of **12**.
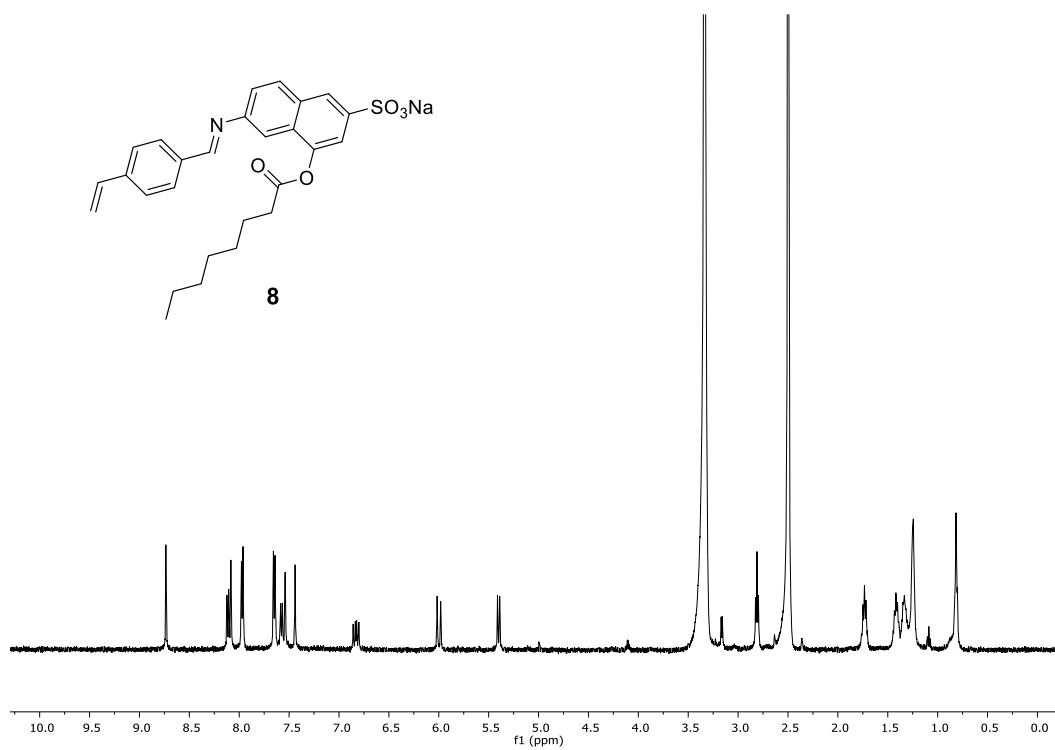
Scheme 9. ^{1}H NMR of **4**.

Scheme 10. ^{1}H NMR of **14**.

Scheme 11. ^{13}C NMR of **14**.
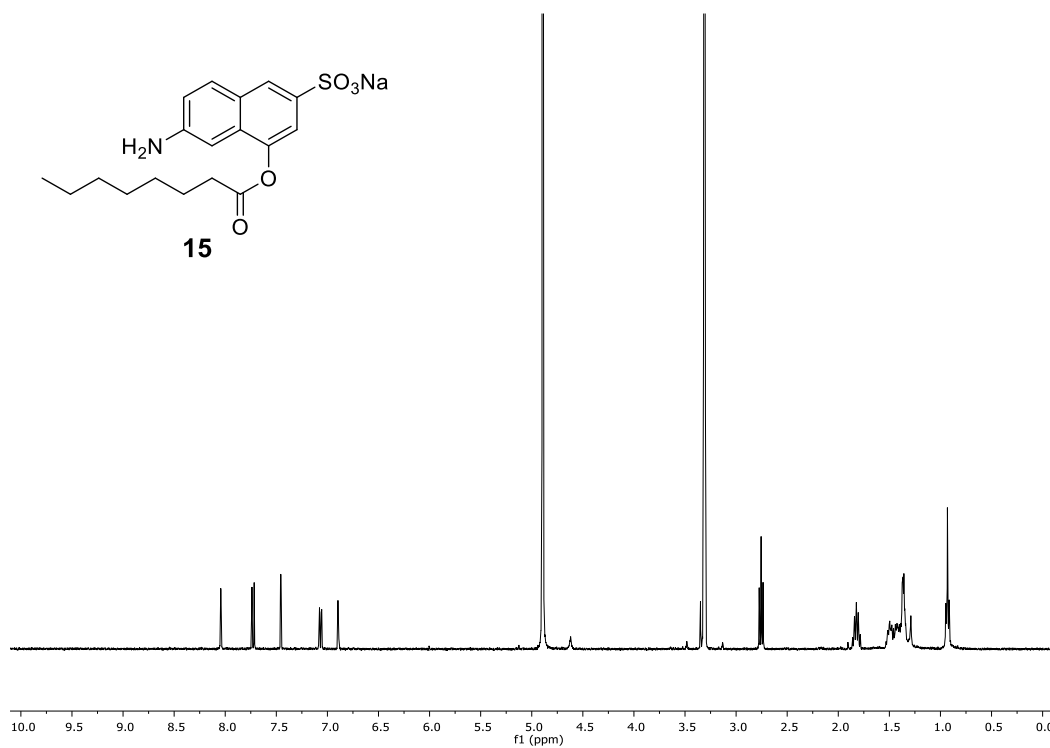
Scheme 12. ^{1}H NMR of **15**.

Scheme 13. ^{13}C NMR of **15**.

Scheme 14. ^{1}H NMR of **8**.

Notes and References

1.   B. Wang and E. V. Anslyn, *Chemosensors : principles, strategies, and applications*, Wiley, Hoboken, N.J., 2011.

2.   V. M. Mirsky and A. K. Yatsimirsky, *Artificial receptors for chemical sensors*, Wiley-VCH Verlag, Weinheim, Germany, 2011.

3.   E. M. Nolan and S. J. Lippard, *Chem. Rev.*, 2008, **108**, 3443-3480.

4.   E. L. Que, D. W. Domaille and C. J. Chang, *Chem. Rev.*, 2008, **108**, 1517-1549.

5.   K. P. Carter, A. M. Young and A. E. Palmer, *Chem. Rev.*, 2014, **114**, 4564-4601.

6.   A. P. de Silva, H. Q. N. Gunaratne, T. Gunnlaugsson, A. J. M. Huxley, C. P. McCoy, J. T. Rademacher and T. E. Rice, *Chem. Rev.*, 1997, **97**, 1515-1566.

7.   G. Wulff, *Chem. Rev.*, 2001, **102**, 1-28.

8.   L. Ye and K. Mosbach, *Chem. Mater.*, 2008, **20**, 859-868.

9.   K. Haupt and K. Mosbach, *Chem. Rev.*, 2000, **100**, 2495-2504.

10.   A. Kugimiya and T. Takeuchi, *Biosens. Bioelectron.*, 2001, **16**, 1059-1062.

11.   L. Ye and K. Haupt, *Anal. Bioanal. Chem.*, 2004, **378**, 1887-1897.

12.   K. D. Shimizu and C. J. Stephenson, *Curr. Opin. Chem. Biol.*, 2010, **14**, 743-750.

13.   P. Turkewitsch, B. Wandelt, G. D. Darling and W. S. Powell, *Anal. Chem.*, 1998, **70**, 2025-2030.

14.   M. J. Whitcombe, I. Chianella, L. Larcombe, S. A. Piletsky, J. Noble, R. Porter and A. Horgan, *Chem. Soc. Rev.*, 2011, **40**, 1547-1571.

15.   S. Shinde, Z. El-Schich, A. Malakpour, W. Wan, N. Dizeyi, R. Mohammadi, K. Rurack, A. Gjörloff Wingren and B. Sellergren, *J. Am. Chem. Soc.*, 2015, **137**, 13908-13912.

16.   K. Takeda, A. Kuwahara, K. Ohmori and T. Takeuchi, *J. Am. Chem. Soc.*, 2009, **131**, 8833-8838.

17.   T. Takeuchi, T. Mori, A. Kuwahara, T. Ohta, A. Oshita, H. Sunayama, Y. Kitayama and T. Ooya, *Angew. Chem. Int. Ed.*, 2014, **53**, 12765-12770.

18.   R. Horikawa, H. Sunayama, Y. Kitayama, E. Takano and T. Takeuchi, *Angew. Chem. Int. Ed.*, 2016, **55**, 13023-13027.

19.   G. Wulff, *Angew. Chem. Int. Ed. Engl.*, 1995, **34**, 1812-1832.

20.   J. K. Awino and Y. Zhao, *J. Am. Chem. Soc.*, 2013, **135**, 12552-12555.

21.   J. K. Awino and Y. Zhao, *Chem. Commun.*, 2014, **50**, 5752-5755.

22.   J. K. Awino and Y. Zhao, *Chem.-Eur. J.*, 2015, **21**, 655-661.

23.   J. K. Awino and Y. Zhao, *ACS Biomater. Sci. Eng.*, 2015, **1**, 425-430.

24.   S. Fa and Y. Zhao, *Chem. Mater.*, 2017, **29**, 9284-9291.

25.   S. Fa and Y. Zhao, *Chem. -Eur. J.*, 2018, **24**, 150-158.

26.   P. A. Gale, *Coord. Chem. Rev.*, 2003, **240**, 191-221.

27.   R. Martínez-Máñez and F. Sancenón, *Chem. Rev.*, 2003, **103**, 4419-4476.

28.   S. Goswami, A. Hazra, R. Chakrabarty and H.-K. Fun, *Org. Lett.*, 2009, **11**, 4350-4353.

29.   J. K. Awino, R. W. Gunasekara and Y. Zhao, *J. Am. Chem. Soc.*, 2017, **139**, 2188-2191.

30.   J. K. Awino, R. W. Gunasekara and Y. Zhao, *J. Am. Chem. Soc.*, 2016, **138**, 9759-9762.

31.   R. W. Gunasekara and Y. Zhao, *J. Am. Chem. Soc.*, 2017, **139**, 829-835.

32.   D. Song, S. Cho, Y. Han, Y. You, W. Nam, *Org. Lett.* **2013**, *15*, 3582-3585.

33.   Arifuzzaman, M. D.; Zhao, Y. *J. Org. Chem.* **2017**, *81*, 7518.

34.   Schneider, H. J.; Yatsimirsky, A. K. *Principles and methods in supramolecular chemistry*; New York: J. Wiley, 2000; pp 137-146.

CHAPTER 6.
CONCLUSIONS

This dissertation illustrated 1) how the intramolecular binding site helped the host-guest binding, 2) how water-soluble molecularly imprinted nanoparticles were readily functionalized by imine bond as well as its reaction kinetics and application as a fluorescent sensor.

A rationally designed host with intramolecular enhancement had an operating window of a strong and selective binding even in unfavorable solvents. As chapter 2 showed, polar solvents weakened the primary binding of **1**, i.e., the electrostatic interaction, but favored hydrophobic interaction. The overall binding constant peaked in methanol. In chapter 3, non-polar solvents weakened the primary binding of **1a**, i.e., the hydrophobic interaction, but favored the hydrogen bonds. The complex became most stable at 2:3 hexane/DCM. These results indicated a new approach, in addition to the preorganization principle, to design synthetic receptors.

MINPs preparation (including template synthesis and functionalization) became easier with a reversible imine bond as a part of the template, compared with the photo-cleavable motif. The imine bond formation was discussed in chapter 4. The binding affinity and freedom of movement became key factors affecting the imine formation in a confined reaction space. MINPs prepared in chapter 5 was an application as a fluorescence sensor, which showed surprising binding affinity and selectivity. There is great potential for further applications to take advantage of the readily formed imine linkage in a template.